Sparse Representations and Harmonic Wavelets for Stochastic Modeling and Analysis of Diverse Structural Systems and Related Excitations

Von der Fakultät für Bauingenieurwesen und Geodäsie

der Gottfried Wilhelm Leibniz Universität Hannover

zur Erlangung des Grades

Doktor der Ingenieurwissenschaften

Dr.-Ing.

genehmigte Dissertation

von

George D. Pasparakis

Referent: Prof. Dr.-Ing. Michael Beer

Korreferent: Prof. Antonina Pirrotta

Mitglied der Kommission: Prof. Dr.-Ing. habil. Christian Heipke

Tag der Promotion: 21.11.2022

Erklärung

Ich erkläre hiermit, dass die in dieser Dissertaion vorgestellten Ergebnisse auf meiner eigenen Arbeit beruhen und dass ich keine Arbeiten andere Personen vorgelegt habe und dass ich in allen Fällen, in denen ich auf Arbeiten anderer Personen Bezug genommen habe, diese in vollem Umfang und in angemessener Weise angegeben habe.

George D. Pasparakis

Oktober 2022

Kurzfassung

In dieser Dissertation werden neuartige analytische/rechnerische Ansätze vorgeschlagen, um verschiedene Themen im Bereich stochastischer Schwingungen zu behandeln. Das erste Thema betrifft die Bestimmung der stochastischen Systemantwort mit singulären Parametermatrizen. Solche Systeme erscheinen als Anhaltspunkt, wenn ein redundantes Schema zur Modellierung von Koordinaten verwendet wird. Dies ist oft mit einem rechnerisch kosteneffizienten Lösungskonzept und einer flexiblen Modellierung zur Behandlung komplexer Systeme verbunden. Ferner sind Strukturen Umweltanregungen ausgesetzt, wie etwa Bodenbewegungen, die typischerweise nichtstationäre Eigenschaften aufweisen.

In diesem Zusammenhang wird im Rahmen der Verbund-Zeit-Frequenz-Analyse ein kürzlich entwickeltes Generalized-Harmonic-Wavelet (GHW)-basiertes Lösungsverfahren in Verbindung mit Methoden aus der Generalized-Matrix-Inverse-Theorie eingesetzt. Dies führt zu einer Verallgemeinerung früherer Anregungs-Antwort-Beziehungen der stochastischen Schwingungstheorie, um Systeme mit singulären Matrizen zu berücksichtigen. Auf harmonischen Wavelets basierende statistische Linearisierungstechniken werden auch auf den Fall von nichtlinearen Multi-Degree-of-Freedom (MDOF)-Systemen mit singulären Matrizen ausgedehnt. Die Genauigkeit des vorgeschlagenen Schemas wird weiter verbessert, indem frühere Annahmen zur „lokalen Stationarität“ über die Antwort umgangen werden. Darüber hinaus wird das Verfahren allgemein durch die Berücksichtigung von Gleichungen unter Zwangsbedingungen verbessert. Hierdurch können generell beschränkte System mit singulären Matrizen behandelt werden. Dazu gehören beispielhaft gekoppelte elektromechanische Gleichungen, wie sie in der Energiegewinnung vorkommen, und Oszillatoren, die nicht-weißen Anregungen unterliegen, welche über Hilfsfiltergleichungen modelliert

werden.

Das zweite Thema betrifft die probabilistische Modellierung von Anregungsprozessen bei fehlenden Daten. In diesem Zusammenhang wird eine Compressive-Sampling-Methodik zur unvollständigen Rekonstruktion und Extrapolation von Windzeitverläufen in einer einzigen räumlichen Dimension sowie die damit verbundene statistische Schätzung stochastischer Felder entwickelt. Als nächstes wird ein alternatives Verfahren entwickelt, dass auf Matrizen mit einem niedrigen Rang und der Nuclear-Norm-Minimierung für die Windfeldextrapolation in zwei räumlichen Dimensionen basiert. Das vorgeschlagene Framework kann für die Überwachung von Windenergieanlagen unter Verwendung von Informationen aus wenigen gemessenen Standorten sowie im Zusammenhang mit der leistungsbasierten Entwurfsoptimierung von Struktursystemen eingesetzt werden.

Das dritte Thema beschäftigt sich mit datengetriebenen Sparse-Identification-Methoden der nichtlinearen Dynamik. Insbesondere wird eine Bayesian-Compressive-Sampling Technik unter Verwendung gemessener Antworten entwickelt, um die maßgeblichen Gleichungen von stochastisch angeregten strukturellen Systemen zu bestimmen. Diese weisen verschieden nichtlineare Verhaltensweisen auf und/oder sind ausgestattet mit Elementen von fraktionaler Ableitungen. Verglichen mit alternativen Schemata, die dem Stand der Technik entsprechen und deterministische Schätzungen für ein identifiziertes Modell liefern, weist die hier entwickelte Methodik weitere Eigenschaften für dünne Besetzungen auf und ist in der Lage, die mit der Modellschätzung verbundene Unsicherheit zu quantifizieren. Dies bietet ein quantifizierbares Maß an Konfidenz bei der Verwendung des vorgeschlagenen Frameworks als Vorhersageinstrument.

Schlagwörter: stochastische Schwingungen, singuläre Parametermatrize, stochastische Dynamik, Harmonic-Wavelet, Moore–Penrose inverse, probabilistische Modell, Stochastisches Feld, Compressive -Sampling, Nuclear-Norm-Minimierung, Windfeldextrapolation, Energiegewinnung.

Abstract

In this thesis, novel analytical and computational approaches are proposed for addressing several topics in the field of random vibration. The first topic pertains to the stochastic response determination of systems with singular parameter matrices. Such systems appear, indicatively, when a redundant coordinate modeling scheme is adopted. This is often associated with computational cost-efficient solution frameworks and modeling flexibility for treating complex systems.

Further, structures are subject to environmental excitations, such as ground motions, that typically exhibit non-stationary characteristics. In this regard, aiming at a joint time-frequency analysis of the system response a recently developed generalized harmonic wavelet (GHW)-based solution framework is employed in conjunction with tools originated form the generalized matrix inverse theory. This leads to a generalization of earlier excitation-response relationships of random vibration theory to account for systems with singular matrices. Harmonic wavelet-based statistical linearization techniques are also extended to nonlinear multi-degree-of-freedom (MDOF) systems with singular matrices.

The accuracy of the herein proposed framework is further improved by circumventing previous "local stationarity" assumptions about the response. Furthermore, the applicability of the method is extended beyond redundant coordinate modeling applications. This is achieved by a formulation which accounts for generally constrained equations of motion pertaining to diverse engineering applications. These include, indicatively, energy harvesters with coupled electromechanical equations and oscillators subject to non-white excitations modeled via auxiliary filter equations.

The second topic relates to the probabilistic modeling of excitation processes in the presence of missing data. In this regard, a compressive sampling methodology is developed for incomplete

wind time-histories reconstruction and extrapolation in a single spatial dimension, as well as for related stochastic field statistics estimation. An alternative methodology based on low rank matrices and nuclear norm minimization is also developed for wind field extrapolation in two spatial dimensions. The proposed framework can be employed for monitoring of wind turbine systems utilizing information from a few measured locations as well as in the context of performance-based design optimization of structural systems.

Lastly, the problem of with data-driven sparse identification methods of nonlinear dynamics is considered. In particular, utilizing measured responses a Bayesian compressive sampling technique is developed for determining the governing equations of stochastically excited structural systems exhibiting diverse nonlinear behaviors and also endowed with fractional derivative elements. Compared to alternative state-of-the-art schemes that yield deterministic estimates for the identified model, the herein developed methodology exhibits additional sparsity promoting features and is capable of quantifying the uncertainty associated with the model estimates. This provides a quantifiable degree of confidence when employing the proposed framework as a predictive tool.

Keywords: random vibration, singular parameter matrices, stochastic dynamics, harmonic wavelet, Moore–Penrose inverse, probabilistic model, stochastic field, Compressive-Sampling, nuclear norm minimization, wind field extrapolation, energy harvesting.

Acknowledgments

I would like to express my sincere gratitude to my supervisor and thesis committee chair, Professor Dr.-Ing. Michael Beer, for his insightful mentoring and motivational support throughout my PhD studies. I am especially grateful to him for fostering my scientific endeavors and for providing an excellent working environment. I would also like to place on record my deepest gratitude to Professor Ioannis A. Kougioumtzoglou for his invaluable academic advice and visionary instruction over the years. I am deeply indebted to him for being a continuing source of inspiration and original thinking.

I would like to extend my special thanks to Professor Dr.-Ing. habil. Christian Heipke, Professor Dr.-Ing. habil. Monika Sester and Professor Antonina Pirrotta for kindly agreeing to serve as members of my dissertation defense committee.

I wish to gratefully acknowledge the funding provided by the European Union's Horizon 2020 research and innovation programme under the Marie Skłodowska-Curie grant agreement No 764547. Without this financial support this thesis would not have been possible.

I would also like to express my deepest appreciation to Dr. Vasileios Fragkoulis for helping me navigate through the ups and downs involved in getting a PhD and for his rigorous attitude throughout our collaborations.

Finally, I am truly thankful to my family and friends for their love and genuine encouragement all these years. In particular, I would like to say a heartfelt thank you to my sister, Sofia, who reminds me that home is in fact not that far away and to my brother, Panayotis, who is my life's anchor.

I dedicate this thesis to my parents, Dimitris and Mariza,

for their endless love and support

Table of contents

List of Figures

Chapter 1

Introduction

1.1 Motivation

Structural dynamics is concerned with the prediction and analysis of the vibration response of mechanical and structural systems subjected to dynamic loading. The primary quantities of interest are, typically, system displacements, accelerations and strains, which are a result of the applied excitation and the induced internal forces of the system. Assessing whether these responses reach and/or cross predetermined safety margins is a critical task of response analysis. Among others, this enables evaluation of the reliability of the structure, prediction of its expected lifetime and development of cost-effective designs. Until recently, engineers regarded vibration response to be periodic and deterministic. However, during the 1950s, the need to predict complex vibration behavior of aircraft components motivated a probabilistic treatment of vibration problems (Davenport, 1961; Roberts and Spanos, 2003). In particular, irregularity and lack of repeatability of the response under identical conditions was attributed to the random nature of the applied excitation. It subsequently became evident that both the excitation and the response can be modeled as realizations of a stochastic process and are amenable to statistical analysis in the average sense. Further, earlier contributions in the physics of Brownian motion (Einstein, 1905; Fokker, 1913; Ornstein, 1927), probability theory (Kolmogoroff, 1931; Wiener, 1930; Khintchine, 1934) and information theory (Rice, 1944; Bendat and Turin, 1959) provided readily available mathematical tools, and gave rise to the field of Random Vibration; see, for instance, Refs. Crandall (1958); Elishakoff (1999); Lin (1967); Roberts and Spanos (2003).

Similar to classical vibration theory, structural components are represented by mathematical models specified by a set of parameters whereas excitation-response relationships are given in the form of differential equations. The irregularity of the response can be generally attributed to two sources of uncertainty (Ghanem and Spanos, 2003). The first one relates to the randomness of the model parameters as a result of manufacturing tolerances, variability in the material properties and uncertainty in the geometry, etc. Aiming at quantifying this form of uncertainty, the system parameters can be modeled as random variables and/or random fields (Ghanem and Spanos, 2003; Stefanou, 2009) although alternative approaches have been recently reported to this end (Moens and Vandepitte, 2006). The second source of uncertainty is induced to the system by the applied excitation, which is modeled in a probabilistic framework as a stochastic process. The objective of Random Vibration theory is oriented towards characterizing the system response in terms of low-order statistical moments (mean, variance, etc.) and (ideally) via the specification of the probability density function (PDF), depending on the complexity of the problem.

1.2 Nonlinear random vibration

Several numerical and analytical solution frameworks have been developed over the past decades for determining statistical moments of the system response with various degrees of accuracy and computational efficiency (Ibrahim, 2008; Grigoriu, 2013; Kougioumtzoglou and Spanos, 2013b; Crandall and Mark, 2014). Obtaining an analytical solution for the case of linear, deterministically defined systems subject to stationary Gaussian excitation is a straightforward task. Arguably, one of the most widely used techniques is the frequency domain analysis where the stochastic process is characterized in terms of a power spectral density function (PSD). The response PSD is obtained by linear input-output relationships, which can be efficiently computed by employing fast Fourier transform (FFT) algorithms. Further, physically significant information can be directly inferred from the PSD and well established, deterministic methodologies can be directly extended for ad-

dressing stochastic excitation problems.

Notwithstanding their importance, frequency domain methods are not applicable in nonlinear stochastic phenomena which commonly arise in engineering applications. Typical examples include nonlinear random rocking (Lin and Yim, 1996), flow induced forces (Morison et al., 1950) and geometric stiffness nonlinearities (Mignolet et al., 2013). However, the number of pertinent analytical solution frameworks is rather limited and research efforts have been directed towards developing approximate schemes and numerical simulation methods. These include, indicatively, statistical linearization (Roberts and Spanos, 2003; Socha, 2007), stochastic averaging techniques (Roberts and Spanos, 1986), stochastic equivalent non-linearization (Cai and Lin, 1988), perturbation methods (Nayfeh and Mook, 2008), recently developed path integrals approaches (Naess and Johnsen, 1993; Katsidoniotaki et al., 2022; Petromichelakis and Kougioumtzoglou, 2020) and Monte Carlo simulation (MCS) (Rubinstein, 1981). Among these, MCS is the only method that yields response statistics estimates with a prescribed degree of accuracy by means of a number of statistical experiments. However, computational costs become prohibitive for an increasing number of degrees-of-freedom (DOF), expecially for high degrees of nonlinearity. Overall, it can be argued that statistical linearization is among the most versatile methods, providing a straightforward approximation for low order statistics for a broad class of MDOF nonlinear problems. This is achieved by replacing the original nonlinear equations with a set of equivalent linear equations based on diverse minimization criteria (Elishakoff et al., 2009). Thus, a direct implementation of standard input-output frequency domain approaches is admissible.

1.3 Time-frequency response analysis

In addition to nonlinear behavior, signal non-stationarity poses a notable challenge towards quantifying the system response. Environmental excitations, such as ground motions, typically exhibit time-varying frequency content whereas structural response has transient characteristics. In this

regard, conventional Fourier analysis is not well suited for localizing these temporal variations since the frequency distribution of the signal is averaged over the entire time domain. Fourier transform (FT) variants, e.g., the Short-time Fourier transform (STFT), have also found limited application. In this case, the FT is performed on piecewise segments of the signal, a process also called windowing, which yields a fixed resolution in frequency as dictated by Heisenberg's uncertainty principle. Alternative tools such as the Gabor transform provide lower uncertainty bounds by utilizing a Gaussian function as the window function. However, Gabor bases lack orthogonality, completeness and independence properties that are necessary for obtaining signal representations in a straightforward manner (Goswami and Chan, 2011). Compared to the previously mentioned transforms, the Wigner–Ville distribution yields the highest possible time-frequency resolution. This is achieved via a FT of the correlation function, which is expressed in terms of time averages (Cohen, 1995). The applicability of this transform is nonetheless limited as a result of the introduction of arbitrary correlation terms between signal components. Arguably, transforms originating from wavelet theory address the aforementioned limitations and have been extensively employed in various scientific disciplines.

1.3.1 Review of wavelets-based techniques

Recently developed wavelet-based tools permit a multi-resolution analysis, whereby different frequencies are analyzed with different resolution. Wavelets are oscillatory functions, localized in time and frequency. They are generated by dilating and shifting a "mother" function and offer a time-scale signal decomposition where scale is defined as the frequency equivalent. Large scales reveal global features in the signal and small scales are associated with detailed characteristics. Despite earlier developments, wavelet analysis attracted noteworthy attention in the 1980s, initially in geophysics (Morlet et al., 1982) and theoretical physics (Grossmann and Morlet, 1984). Most notably, the work of Mallat (Mallat, 1988) formalized the systematic construction of an orthogonal wavelet basis and the work of Daubechies (Daubechies, 1988) provided conditions for the

formulation of compactly supported orthonormal wavelet bases. Following these breakthroughs, a theoretical framework was established (see Refs. Daubechies (1992); Mallat (1999); Goswami and Chan (2011) for some indicative textbooks), and since then, wavelets have been utilized in diverse fields of science (Addison, 2017). In regard to structural mechanics, wavelets have been used in system identification (Staszewski, 1997; Ghanem and Romeo, 2000; Kijewski and Kareem, 2003; Kougioumtzoglou et al., 2017a), seismic response analysis (Basu and Gupta, 1997, 1998), stochastic processes representation (Spanos and Failla, 2004; Liang et al., 2007; Wang et al., 2022) and for studying wind effects on structures (Kareem and Kijewski, 2002; Kareem and Wu, 2013).

1.3.2 Harmonic wavelets-based response determination

There exist numerous wavelet families tailored to specific applications. Harmonic wavelets developed originally by Newland (Newland, 1993, 1994), are the most potent tool for time-frequency analysis in vibration problems due to several appealing properties. First, they posses a box-like frequency spectrum in non-overlapping frequency bands, which enables accurate estimation of the power spectrum. This resolution can be varied throughout the signal yielding a trade-off between frequency fidelity and computational efficiency. Secondly, wavelets are given in the form of analytical expressions without the need of expensive, recursive computations. Due to their orthogonality properties, they form an orthogonal basis, which allows for perfect reconstruction of the original signal in terms of wavelet coefficients. Thus, harmonic wavelets can be employed in signal expansions and are suitable for developing analytical solution frameworks. It is also worth noting that the wavelet coefficients are derived from the convolution between the signal and the band-limited, time representation of the wavelet. This operation reduces to multiplication in the frequency domain (Newland, 1999) and can be highly accelerated via the FFT.

In the field of engineering mechanics, research towards joint-time frequency response analysis of nonlinear systems was until recently rather limited. This has changed with with the advent of

wavelets the last few years. Specifically, in Tratskas and Spanos (2003) the frequency response function was extended to the wavelet domain for non-stationary response determination of MDOF linear systems, within the context of stochastic process realizations. Further, in Spanos and Kougioumtzoglou (2012) the locally stationary wavelet (LSW) representation of non-stationary processes (Nason et al., 2000) in conjunction with generalized harmonic wavelets was adopted for estimating the underlying evolutionary power spectrum (EPS). Novel excitation-response relationships pertaining to linear oscillators were derived and the response of a number of nonlinear oscillators was determined via a modified statistical linearization scheme. This approach was later coupled in Kougioumtzoglou and Spanos (2013b) with a stochastic averaging framework for deriving the response of a class of hysteretic systems. Moreover, in the work of Kong et al. (2014a), harmonic wavelets were implemented towards the solution of differential equations describing nonlinear single-degree-of-freedom (SDOF) systems whereas Spanos and coworkers (Spanos et al., 2016) introduced a periodized generalized harmonic wavelet (PGHW) version addressing the limitations of the LSW assumption. The aforementioned methods have also been extended in the past years to address MDOF nonlinear systems (see, for instance, Kong and Li 2015) and to account for combined periodic and stochastic excitations (Kong et al., 2022a).

Within the context of MDOF system response determination it is commonly assumed that the structural parameter matrices are non-singular. However, there exist several engineering applications where this assumption does not hold. In this case, deriving the response statistics is not a straightforward task, especially considering non-stationary excitations. Further, the relevant literature in this direction is quite limited. In an effort to address this gap, in this thesis a framework is proposed for extending the application of wavelets as a time-frequency analysis tool to a broader class of problems, i.e., to systems with singular parameter matrices.

1.4 Systems with singular matrices

In general, utilizing the minimum number of (generalized) coordinates when formulating the equations of motion yields symmetric, positive-definite, and thus, non-singular mass, damping and stiffness matrices. This approach has been established on the basis of analytical mechanics (Ginsberg, 2008) and has been the standard approach in numerical methods such as the finite element method (FEM) (Bathe, 2006). However, in several engineering applications singular matrices appear, in particular, as a direct consequence of the physical properties of the system under consideration.

1.4.1 Diverse engineering applications

A representative example of systems with singular parameter matrices pertains to the translational motion of rigid bodies. For instance, a uniform beam that can move axially as a rigid body gives rise to a stiffness matrix whose determinant is zero (Craig and Kurdila, 2006). By definition, this is a singular matrix. Additionally, highly ill-conditioned and/or singular mass parameter matrices are encountered in motion simulation applications (Maciejewski, 1990), in structures with massless joints and in problems where some degrees of freedom have no associated inertia (Balakrishnan, 1996). Apart from practical considerations, singular matrices can also come about as a consequence of the mathematical formulation of the problem. For instance, systems endowed with singular diffusion matrices can arise within the context of Wiener path integrals (Petromichelakis et al., 2020). Similarly, time domain representations of non-white stochastic excitations by series of filters subject to white noise can also lead to the appearance of singular matrices in the governing equations of motion.

More generally, the occurrence of singular matrices is akin to the absence of derivatives of certain degrees of freedom in the system of differential equations. This is prevalent, for example, in a class of systems exhibiting hysteretic behavior. Specifically, hysteretic loops manifest the energy

dissipation mechanism of the structure in response to the applied force, whereby the restoring force depends on the instantaneous value of the deformation as well as its past time history (Ismail et al., 2009). This has been commonly approximated by the Bouc-Wen model (Bouc, 1971), which has received considerable attention the past years due to its versatility in reproducing a variety of hysteretic patterns. The mathematical description of this model utilizes an auxiliary first order differential equation coupled with the second order differential equation of the original oscillator. Clearly, this renders the mass matrix singular.

A similar effect is also encountered in the equations describing energy harvesting applications such as oscillating water columns (Spanos et al., 2018; Scialò et al., 2022) and vibratory energy harvesting devices (Adhikari et al., 2009). The principle of operation of the latter category of energy harvesters is based on the coupling of smart materials (e.g, piezoelectric patches) with structural components (e.g., cantilever beams), which permits the transformation of ambient vibration into electrical current. In general, such devices can be deployed as stand-alone units for powering low energy consumption adjoining electronics and can, potentially, negate the need for conventional batteries. Indicative fields of application include wireless sensors employed in structural health monitoring (SHM) and medical implants (Safaei et al., 2019). From an engineering perspective, a critical task relates to the optimal choice of physical parameters with the aim of maximizing the amount of harvested energy. Unfortunately, the aforementioned electromechanical coupling often leads to singular matrices in the equations of motion (Adhikari et al., 2009), and thus, hinders the implementation of analytical- and MCS-based schemes, which are a prerequisite for optimization. Further, the presence of nonlinear restoring forces (Daqaq et al., 2014) and the stochastic nature of the excitations (Petromichelakis et al., 2018) adds to the level of difficulty of the analysis.

1.4.2 Redundant coordinate modeling schemes

It is worth noting that systems of equations involving rectangular/singular matrices arise when a redundant (non-generalized) coordinate scheme is employed. This strategy is predominantly adopted in the field of multibody system dynamics and is carried out as part of commercial software (Mariti et al., 2011). Although derivation of the equations of motion via generalized coordinates is a straightforward task for a small number of DOFs, it becomes an arduous process with increasing model complexity (e.g., highly coupled systems with large number DOFs).

Specifically, conventional approaches entail casting the multibody system in a tree configuration in which each component is sequentially joint with several others in order to form the system structure (Schutte and Udwadia, 2011). This process can be accelerated by recursive computational schemes (Critchley and Anderson, 2003), however, it assumes a prescribed model structure. Therefore, in cases where a constraint modification is required, a complete remodeling is called for. Alternatively, Lagrange multipliers are employed (Schutte and Udwadia, 2011) for deriving the equations of motion, albeit obtaining them can be labor-intensive, especially when a large number of DOFs with several non-integrable constraints is considered. Further, ensuring that all constraints are functionally independent may prove challenging and requires problem-specific approaches (Udwadia and Phohomsiri, 2006).

Circumventing these limitations, unconventional coordinate modeling frameworks prove advantageous in deriving the system governing equations of motion in a less labor-intensive manner, and by allowing for enhanced modeling flexibility (Udwadia and Phohomsiri, 2006). In this regard, the mechanical system is modeled as a collection of individual sub-systems whose equations of motion can be obtained in a relatively easy manner. A number of additional constraints is also considered in order to ensure structural compatibility. Utilizing such a scheme implies, in general, some degree of dependence between the coordinates and leads to singular matrices in the equations of motion. In the field of deterministic multibody system dynamics, Udwadia and coworkers (Schutte and Ud-

wadia, 2011; Udwadia and Kalaba, 1992; Udwadia and Phohomsiri, 2006; Udwadia and Kalaba, 2001; Udwadia and Wanichanon, 2013) have developed over the years a framework for handling constrained systems with singular matrices.

1.4.3 General solution treatments

In view of the broad range of problems where singular matrices appear, it is deemed appropriate to examine the implications of matrix invertibility, which is of relevance to stochastic dynamics problems. By definition, the determinant of a singular matrix is equal to zero, and thus, its inverse cannot be defined. Consequently, time domain solutions relying on state-space formulations cannot be derived. Similarly, input-output relationships of random vibration are not applicable in the case of rectangular, rank-deficient matrices, which can arise as a result of utilizing redundant coordinates in forming equations of motion. From a mathematical perspective, ill-conditioned matrices are closely related to singular matrices and impose similar restrictions to the applied solution frameworks. Concisely, ill-conditioned matrices are characterized by a large condition number, and thus, systems with ill-conditioned matrices are very sensitive to small perturbations in the input as well as to roundoff errors. Further, computation of their inverse is prone to large numerical errors and introduces instabilities in the solution process. In the limiting case, i.e., as their condition number tends to infinity, ill-conditioned matrices reduce to singular matrices. Thus, it can be argued that problems pertaining to both classes can be addressed within the same category of solution frameworks.

Limitations stemming from singular and/or ill-conditioned matrices are usually mitigated by means of optimization, or the so-called regularization. Such techniques have been instrumental in developing approximate solutions for a wide range of ill-posed inverse problems (Hansen, 1998; Tikhonov and Arsenin, 1977). However, the inexact nature of the solution does not facilitate closed form expressions, while the uniqueness of the solution is case-dependent and, generally, implied via a

family of possible solutions. What is more, for most classes of nonlinear systems, the system of differential or algebraic equations cannot be posed in a matrix equation form, i.e., $\mathbf{Ax} = \mathbf{b}$, and therefore, is not amenable to (even approximate) solutions.

1.4.4 Stochastic response determination strategies

Considering the brad range of practical applications where singular matrices may appear in conjunction with the unsuitability of conventional of established random vibration techniques, the development of pertinent stochastic response analysis methodologies is of great importance and has been, recently, an area of active research. The works of Fragkoulis et. al (Fragkoulis et al., 2016a; Fragkoulis, 2017) constitute the first contributions in this direction. Utilizing elements from the Moore-Penrose (M-P) generalized matrix inverse theory and by augmenting the equations of motion considering a set of additional constraints (Udwadia and Phohomsiri, 2006), time-domain random vibration results have been generalized to treat systems with singular matrices. In Fragkoulis et al. (2016b), the standard statistical linearization method (SLM) was extended to nonlinear systems with singular matrices and in Kougioumtzoglou et al. (2017b), a frequency domain input-output relationship was established for both linear and nonlinear systems. Further, in Ni et al. (2021) pertinent methodologies were expanded to accommodate a combination of stochastic and deterministic loading applied to systems with singular matrices. In Pirrotta et al. (2021), deterministic and random response solutions were derived for linear systems with singular matrices endowed with fractional derivative elements whereas the random eigenvalue problem was considered in Fragkoulis et al. (2022) and expressions for determining the rate of change of eigenvalues for systems with singular matrices were developed.

Although the aforementioned approaches have been construed on the basis of M-P pseudoinverses, two alternative strategies have been probed for treating linear systems with singular matrices. In this regard, the authors in Antoniou et al. (2017a) employed tools from polynomial matrix theory

and the authors in Karageorgos et al. (2021) formalized an approach based on Kronecker canonical forms of matrix pencils. Both contributions aimed at circumventing issues akin to generalized matrix inverse approaches, which are associated with the choice of the optimal solution.

In passing, despite the considerable body of work on the response determination of systems with singular matrices, the analysis has been limited to stationary excitations and to relatively specific forms of constraint equations. In the present thesis, these points are addressed jointly by providing semi-analytical solution schemes for linear and nonlinear structural systems with singular matrices. A mathematical framework is also introduced to accommodate general forms of constraint equations and to account for non-stationary excitations.

1.5 Data-driven probabilistic modeling of stochastic processes

It is worth noting that the applicability of the excitation-response relationships discussed in the previous sections is conditioned on the existence of accurate probabilistic models accounting for the randomness in the excitation process. Along these lines, it can be asserted that the aspects of randomness are twofold (Ghanem and Spanos, 2003). The first pertains to the inherent, irreducible randomness of the phenomenon under consideration. The second stems from the lack of information about the underlying process and the uncertainty associated with the statistical model. For the case of several environmental processes this model is given by the process PSD.

A large body of work has been devoted in deriving PSD-based, semi-empirical expressions for ground motions and wind loads over the past decades (Davenport, 1961; Housner and Jennings, 1964; Priestley, 1965; Harris, 1968; Lin and Yong, 1987; Simiu and Scanlan, 1996). The practical merit of the majority of these descriptions is that they are given by a few, physically interpretable parameters that can be adjusted to match site-specific conditions. More importantly, PSD functions can be employed within the context of the spectral representation method (SRM) (Shinozuka and Jan, 1972; Di Paola and Zingales, 2000; Chen et al., 2013; Benowitz and Deodatis, 2015) for

generating stochastic process realizations. This becomes vital when frequency-domain approaches are not applicable. For instance, in modern long-span bridges innovative design aspects induce nonlinear aerodynamic forces even in normal operating conditions (Kareem, 2008), and thus, only time-domain-based frameworks provide reliable estimation for the response statistics. Clearly, the degree of uncertainty associated with the PSD can be reduced by collecting additional data.

1.5.1 Sources of missing data

The advent of advanced, low cost sensors in conjunction with widespread measurement campaigns poses as a promising technology towards statistical stochastic process estimation. Nevertheless, there are several challenges when data acquisition strategies are considered. First, data is often stored and wirelessly channeled to centralized units for post processing. Transmission of large volumes of uncompressed data from multiple sensors simultaneously may not be feasible as a result of bandwidth limitations. This can potentially lead to records with missing data segments. Similar effects are often encountered as a consequence of communication errors in wireless sensor networks (WSN). Further, there exist applications (e.g., rotating vibration sensing) that require high sampling rates for capturing frequency ranges of interest. Inherent hardware limitations can impose restrictions on the attainable frequency bands and can be associated with excessive costs. Emerging sub-Nyquist sampling paradigms can, in part, alleviate these difficulties. Budget constraints may also limit the number of deployed sensors and can adversely affect reconstruction accuracy, especially, in cases where spatio-temporally varying stochastic fields are considered. As a remedy, optimal sensor placement strategies (Ranieri et al., 2014) can be implemented in order to generate sensor configurations that maximize the amount of obtained information. However, this often requires a priori knowledge of equipment availability whereas specific sensor placement may not always be physically realizable.

Apart from inherent sensor deployment challenges, environmental conditions such as electromag-

netic interference and extreme weather phenomena can also lead to power outages and equipment failure. This necessitates the development of robust data reconstruction methodologies with respect to extreme data values and data corruption (Comerford et al., 2016). What is more, in real-life applications where, for instance, the role of seismic excitations is instrumental in the reliability assessment, only a few stochastic process realizations might be available and deriving a probabilistic model consistent with the observations without imposing convenient assumptions (e.g., Gaussian process) can be a daunting task. In passing, data processing challenges extend beyond the matter of PSD estimation and their role in the performance of engineering structures is rather critical. Indicatively, nacelle-mounted, 3-D laser scanning devices allow for the prediction of the oncoming wind field before it reaches the wind turbine. This emerging technology coupled with Model Predictive Control (MPC) strategies can, potentially, lead to reduced fatigue loads and improved wind turbine efficiency (Santos, 2007). Nevertheless, the amount of available data is restricted to scanning beam patterns and spatio-temporal discretization (Towers and Jones, 2016).

1.5.2 Review of existing methods for wind field data reconstruction

Considering the preceding discussion, the difficulties arising in data-driven methods can be cast as an inverse problem where the task relates to the reconstruction of the stochastic process (or stochastic field) and its relevant statistics from a limited number of observations. The literature for treating diverse environmental processes is extensive and the range of excitations spans over several environmental and temporal scales (Yang et al., 2010; Gallego et al., 2011; Grover and Lall, 2021). In this context, the discussion herein will be focused on fluctuating wind field data reconstruction and extrapolation techniques in one- and two-dimensional spatial domains and time. This is aimed at obtaining a probabilistic characterization of the underlying stochastic field, which can be utilized to derive and/or calibrate wind speed spectral models within the context of the SRM. Further, the analysis is motivated by the fact that wind excitations are the governing design load for slender structures and long span bridges (Benowitz and Deodatis, 2015). Thus, the presented

methodologies can be potentially used for performance-based design optimization of structural systems.

In this regard, a probabilistic wind field characterization methodology from partial observations was proposed in Pourhabib et al. (2016) for the purpose of short-term wind speed forecasting. Utilizing time-series modeling tools and data from a number of informative locations, the authors proposed a spatio-temporal autoregressive model for predicting the wind speed on a wind farm model. Despite its usefulness, this approach does not yield a wind speed distribution with fine temporal or spatial resolution. Alternative approaches have been established on the basis of computational fluid dynamics (CFD) (Sun et al., 2019b; Qin et al., 2018). The rationale relates to employing measurements from a number of optimally placed sensors on predefined boundary locations and performing CFD simulations in order to obtain a refined wind field representation in a real-time fashion. Accounting for computational overheads, efficient numerical adaptations such as the proper orthogonal decomposition (POD) (Sun et al., 2019a) have been introduced. However, the feasibility of integrating real data from the interior simulation domain is still unclear whereas CFD simulations often require considerable simplifications in the flow models (Wang et al., 2019). Undoubtedly, field measurement campaigns for analyzing wind field statistics have significant practical merit.

An alternative strategy in this direction has been provided from the perspective of real-time state estimation in Towers and Jones (2016). In this work, a Kalman filter implementation was proposed for mitigating discrepancies between measured and target wind velocity measurements in light detection and ranging (LiDAR) devices. The mathematical model was formulated via a simplified version of the Navier–Stokes equations and an Unscented Kalman Filter (UKF) was employed. Despite the reported accuracy of the method in estimating unobserved wind quantities, the analysis was restricted to a deterministic framework. Similarly, it has also been shown that it is possible to identify the wind load acting on a structure from a number of measured responses by solving an inverse state-space problem. Further, a Kriging-based methodology was proposed in Lin and

Li 2020 for statistical interpolation of missing wind field data. Addressing the same problem, a number of neural network implementations and configurations were employed recently (e.g., Qu et al. 2020; Ni and Li 2016; Mohandes and Rehman 2018). Notwithstanding their importance, the preceding methodologies are characterized by certain limitations. Specifically, they are applicable only to a few possible incomplete data configurations and, typically, assume a small percentage of missing data. Further, implementations involving black-box approaches such as neural networks offer limited interpretability and require large amounts of, potentially unavailable, data for training.

1.5.3 Compressive sampling for stochastic wind field statistics estimation

Sparse representation concepts and compressive sampling (CS) tools offer a promising framework for stochastic process statistical estimation in the presence of missing data. CS theory establishes conditions for the existence and the uniqueness of low-dimensional signal representations. This newly developed mathematical formalism, coupled with potent optimization algorithms for signal reconstruction, has resulted to a paradigm shift in data acquisition and signal sensing. Quantization strategies were, until recently, limited by the Nyquist–Shannon sampling theorem, which asserts that a time-signal with maximum frequency f can be uniquely determined at a $f/2$ uniform sampling rate. Under this condition, signals are conventionally sampled at the Nyquist rate and then transformed to a sparse basis where most of the coefficients close to zero can be discarded. This allows for "lossless" data compression since the information is retained in the compressed signal and can be used to perfectly reconstruct the signal back to its original form.

CS has enabled sub-Nyquist rate protocols, whereby analog to digital data conversion happens at the compressed state. This is guaranteed as long as the original signal is sparse in an appropriately constructed basis and on the condition that this basis is incoherent with respect to the original domain. Considering that many environmental stochastic processes, such as wind, exhibit sparsity in the frequency domain, CS can be readily applied to the reconstruction of stochastic process

record with missing data as well as for estimation of relevant statistical quantities. In this case, missing observations leading to ill-posed systems of algebraic equations can be cast into an inverse problem in the context of CS (Candès and Wakin, 2008).

Early efforts in the field of engineering mechanics can be found in Comerford et al. (2016) in which stationary and non-stationary PSD reconstruction from incomplete stochastic process records was achieved via an l_1-norm minimization approach. A sparsity-inducing alternative methodology was proposed in Comerford et al. (2014) utilizing an l_1-norm re-weighting procedure which was later applied in Comerford et al. (2017) to assess the reliability of a real structure. Also, an enhanced l_p-norm $(0 < p < 1)$ minimization was presented in Zhang et al. (2018) with the aim of further promoting sparsity for the reconstruction of power spectra pertaining to various two-dimensional stochastic processes. Notably, CS-based strategies have also been employed in various sea state estimation problems. For instance, in Laface et al. (2017) highly under-sampled water wave records were reconstructed by means of $l_{1/2}$-norm minimization whereas in Malara et al. (2018) sea state characteristics were extrapolated in both space and time from a small number of distributed wave-buoys. More details can be found in the recent review paper Kougioumtzoglou et al. (2020), where a systematic review of CS implementations in diverse engineering mechanics applications is presented.

In general, CS-based techniques have been applied to treat wind field data related problems. Indicatively, in Wang et al. (2019) an efficient data compression methodology was established for efficient storage and transmission of wind monitoring data collected by a WSN operating on large-scale structures. This was achieved via a dedicated sparse dictionary that exploited spatial correlations between wind speed signals. Further, in Tascikaraoglu et al. (2016) a structured-sparse recovery algorithm was applied for enhancing the performance of a spatio-temporal wind speed forecasting framework which utilized observations from a large set of meteorological stations. Conversely, the capabilities of CS-based algorithms with respect to wind field missing data problems have not been

fully explored.

Considering the foregoing examples, it can be noted that the implementation scope of the developed frameworks has been limited to data communication schemes and to wind speed prediction over relatively large areas. In an effort to address this gap in the literature, a CS strategy is proposed in this work for reconstruction and extrapolation of wind speed time histories in previously unmeasured locations along one spatial domain. Further, computational overheads associated with multi-dimensional domains are ameliorated via the employment of a nuclear norm minimization scheme. In passing, the nuclear norm is defined as the sum of the singular values of a matrix and generalizes the notion of vector sparsity to account for matrices.

1.6 Data-driven discovery of structural systems dynamics

It is apparent from the discussion in sections 1.1 and 1.5 that in many engineering applications the randomness in the response can be adequately captured by relying on a probabilistic characterization of the input process in conjunction with versatile numerical techniques for determining the response statistics. However, as mentioned in section 1.1 a significant degree of uncertainty arises when the model parameter values cannot be specified to prescribed levels of accuracy. Modeling procedures that account for this randomness lead to stochastic differential equations (Grigoriu, 2013) that describe the evolution of the system dynamics. As a consequence, the complexity of the analysis increases considerably and solutions lend themselves, predominantly, to numerical schemes. These include indicatively MCS methodologies (Shinozuka and Astill, 1972), perturbation methods (Liu et al., 1986), polynomial chaos expansions (Ghanem and Ghosh, 2007) and stochastic order reduction techniques (Farhat et al., 2018); see also Refs. Ghanem and Spanos (2003); Li and Chen (2009) for a broad perspective.

1.6.1 Review of system identification techniques

Undoubtedly, methodologies for identifying the physical properties of structural systems can greatly enhance the efficiency and accuracy of response determination schemes. As a result, they are also critical in engineering applications. For instance, even though structural systems are modeled in practice under linear assumptions, nonlinear behavior is likely to be exhibited in cases of high amplitude excitations, such as wind gusts or earthquakes (Kougioumtzoglou and Spanos, 2013a). Besides the presence of extreme events, deviation between expected and realistic behavior is manifested even in normal operational conditions when complex, high dimensional structures are considered. It becomes clear that identification techniques are instrumental for reliability assesment and damage detection purposes. The field of system identification formally comprises techniques that employ experimental or field measurements along with a set of prior assumptions in order to furnish a model whose behavior is consistent with the measured data.

These approaches can be broadly classified into parametric and non-parametric methods. The first class assumes a parametric model structure where a finite set of parameters is updated by minimizing an error metric between observation and prediction. Indicative techniques include (but are not limited to) least squares minimization (Gersch et al., 1976), autoregressive, moving-average (ARMA) models (Pi and Mickleborough, 1989), multiple-input-single-ouput (MISO) (Kougioumtzoglou and Spanos, 2013a; dos Santos et al., 2020) and Bayesian (Azam et al., 2015) approaches. The second class of methods is geared towards identifying a linear mapping between the input and the output. Subspace identification (Peeters and De Roeck, 1999) and blind source separation (Yang and Nagarajaiah, 2013) are some representative methods.

The explosive growth of available data accompanied by emerging data science techniques has stimulated research in novel data-driven approaches for identifying dynamical system behavior (Schmidt and Lipson, 2009; Brunton et al., 2016; Raissi et al., 2019). From the perspective of structural identification, pertinent implementations relate to neural networks (Lai et al., 2021) and

sparse regression (Lai and Nagarajaiah, 2019). These frameworks are motivated, primarily, by the fact that in many problems a purely physics-based modeling of the governing dynamics by resorting to first-principles may be unattainable. Along these lines, neural networks can identify nonlinear input-output maps in view of the universal approximation theorem. However, despite their versatility in capturing arbitrarily nonlinear dynamics (as mentioned in section 1.5.1) they are not always interpretable from a physical point of view and their extrapolation capabilities are conditioned on training data. Further, brute-force implementations of neural networks can lead to exceedingly large parameterizations and data overfitting.

1.6.2 Compressive sampling for equation discovery of diverse systems

It can be argued that, for data-driven modeling to be efficacious, the identified model should exhibit sparsity in the sense that the fewest possible terms are considered for the description of the system dynamics. This enhances the interpretability of the model, and provides balance between model complexity and accuracy. The rationale for such data-driven discovery of governing equations and identification of parsimonious system dynamics relates to the fact that the dynamics of most physical systems can be described accurately by considering only very few relevant terms in the appropriate expansion basis; thus rendering the governing equations sparse in a high dimensional nonlinear function space. In this regard, approaches for sparse identification of nonlinear dynamics based on compressive sampling concepts and tools have been proposed recently (Champion et al., 2019; Brunton and Kutz, 2022). In the majority of these methods, the resulting non-square system of linear algebraic equations for the expansion basis coefficients is typically solved by an l_1-norm minimization treatment (e.g., Champion et al. 2019; Cortiella et al. 2021). Note, however, that alternative advanced compressive sampling tools can be employed that exploit additional information in the data and enhance solution sparsity. These approaches can improve solution robutsness to high degreess of missing data. Further, they have the potential of quantifying the uncertainty associated with the model estimates; thus, providing a measurable confidence degree when em-

ployed as a prediction tool. Solution alortihms that exhibit such features are l_p-norm $(0 < p < 1)$ minimization formulations and iterative re-weighting solution schemes, Bayesian approaches, as well as structured sparsity and dictionary learning strategies (Kougioumtzoglou et al., 2020).

In general, sparse regression techniques do not impose a strict model structure to the underlying differential equations of motion and rely on the cardinality of a set of nonlinear candidate functions. Thus, appropriate selection of functions that correspond to diverse structural behavior adversely effect the identification performance. For instance, it has been progressively recognized over the past decades from the engineering community that several materials exhibit a combination of viscous and elastic behavior (Gemant, 1936; Di Paola et al., 2011), which can be adequately captured by resorting to fractional calculus. Clearly, this leads to fractional differential equations governing the dynamics of such systems. Indicative applications pertain to seismic isolation devices such as viscoelastic dampers (Shen and Soong, 1995) and tuned mass damper with fractional derivative damping (Rüdinger, 2006) as well as to the characterization of mechanical behavior of asphalt (Lagos-Varas et al., 2019).

Towards addressing the preceding challenges, a data-driven uncertainty quantification framework is proposed in this thesis for determining the equations of motion of stochastically excited structural systems exhibiting nonlinear behavior and following fractional derivative modeling.

1.7 Contributions

In this thesis, an effort is made to address a number of challenges in the field of Random Vibration. Following the outline of the previous sections the main aspects can be summarized into three key areas. The first pertains to system complexity under consideration which is a result of nonlinear behavior, elements following fractional derivative modeling, high dimensionality and singular parameter matrices in the governing equations of motion. The second relates to the uncertainty associated with the structure of the underlying equations of motion and with the set of relevant

parameters. The third is connected with the excitation process and the corresponding probabilistic model, which typically features non-stationarity and is characterized by high degree of uncertainty as a result of missing data. In view of the above, the following methodologies are proposed.

1.7.1 Stochastic response determination of systems with singular matrices

First, a new response determination treatment is developed for linear and nonlinear systems subject to non-stationary ground excitation. To this end, the excitation process is expanded on the basis of the LSW assumption in conjunction with generalized harmonic wavelets. In addition, utilizing elements from matrix pseudoinverse theory a novel frequency response function is derived. This result can be viewed as the generalization of celebrated input-output relationships of Random Vibration theory in order to account for systems with singular parameter matrices and non-stationary excitations. It is noted that this approach is tailored to systems whose equations of motion are derived via a redundant coordinate modeling scheme. Next, the framework is extended to the case of nonlinear systems. This is achieved by coupling the proposed approach with the SLM. Moreover, an approximate closed-form solution is provided for systems with singular parameter matrices and polynomial nonlinearities. These results have been published in Pasparakis et al. (2021).

The versatility of the proposed framework is subsequently enhanced by circumventing the assumption of "local stationarity" of the excitation (and the response) process. Specifically, a periodized version of GHWs along with a set of interaction coefficients is employed for improving the accuracy of the method especially for systems with a short lived impulse response function. This expands upon previous work on PGHW-based input-output results in order to account for systems with singular parameter matrices. The method is rendered readily applicable to diverse engineering applications by an a appropriate modification which enables the incorporation of general forms of constraint equations in the modeling scheme. The flexibility of the methodology is demonstrated by determining the response PSD of diverse engineering applications such as an energy harvester with

coupled electromechanical equations and an oscillator subject to non-white excitations modeled via auxiliary filter equations. These findings have been published in Pasparakis et al. (2022b).

1.7.2 Wind field data statistical estimation and extrapolation

Furthermore, a data-driven optimization technique is established for the probabilistic characterization of wind field stochastic processes in the presence of incomplete measurements. Specifically, sparse representations by means of a Fourier expansion are exploited for recontructing highly under-sampled wind speed records in the time domain. Next, a suitable expansion basis is constructed utilizing measurements from a number of neighboring locations. A CS minimization algorithm is subsequently proposed for extrapolating wind speed records to various points in a single spatial domain. The practical merit of the proposed approach relates to the fact that the expansion basis is consistent with the frequency-wavenumber spectral representation of the signal. This is particularly advantageous since it incorporates the spatial information of the signal into the minimization algorithm. Hence, the coherence of the wind field between measured and extrapolated locations is preserved.

A novel framework is also introduced for extrapolating wind speed records in two spatial dimensions. In this case, the spatial correlation of the wind speed signals is exploited by resorting to a matrix reshape nuclear norm minimization procedure. This improves notably the computational efficiency of the scheme compared to alternative CS-based approaches. In this regard, the method is rendered applicable to real-time wind speed estimation problems, e.g., for monitoring of wind turbine systems. The extrapolation capability is demonstrated by comparing the estimated statistical quantities with corresponding analytical expressions. It is found that the technique yields significant levels of accuracy even in the presence of a high degree of missing data. These results have been published in Pasparakis et al. (2022a).

1.7.3 Data-driven uncertainty quantification and identification of dynamical systems

Moreover, a data-driven uncertainty quantification methodology is developed for discovering the equations of motion of nonlinear dynamical systems. This is done by relying on measured response data which are cast into a state-variable formulation. This leads to a non-square system of algebraic equations to be solved within the context of sparse regression. In this regard, a Bayesian compressive sampling (BCS) minimization algorithm is employed for deriving a parsimonious model and for quantifying the uncertainty of the estimated coefficient vector. The contribution of this implementation is twofold. First, it exhibits significant sparsity-promoting features. Secondly, it is suitable for identifying diverse engineering systems via an informed construction of the expansion basis. The reliability of the technique is presented by discovering the equations of motion of an electromechanical energy harvester endowed with fractional derivative elements.

1.8 Mathematical preliminaries

In this section the mathematical tools employed throughout the present thesis are briefly reviewed. The ensuing presentation is not intended as an in depth review of the available methodologies, the majority of which has been thoroughly covered in a number of textbooks and academic publications. The scope is rather oriented towards improving readability and for serving as reference for some of the main concepts.

1.8.1 Simulation on non-stationary stochastic processes

In the present thesis, the validity of the proposed techniques is assesed by comparison with MCS data. In this regard, the SRM (Liang et al., 2007) is employed for generating sample realizations

$f(t)$ of a non-stationary stochastic processes $f_0(t)$ in the form

$$f(t) = \sqrt{2} \sum_{j=0}^{N-1} \sqrt{2 S_{f_0 f_0}(t, \omega_j)\, \Delta\omega} \cos(\omega_j t + \varphi_j), \tag{1.1}$$

where t and ω denote time and frequency, respectively. The frequency domain is discretized by $\omega_j = j\Delta\omega, \Delta\omega = \omega_u/N$ and ω_u denotes the upper cut-off frequency. $S_{f_0 f_0}$ is the (two-sided) evolutionary PSD and φ_j are independent uniformly distributed random phase angles between 0 and 2π. The upper cut-off frequency is chosen on the basis that the energy of the signal is contained in this interval by a significant factor α (e.g. 95%) by

$$2 \int_0^{\omega_u} S(\omega) \mathrm{d}\omega \geq \alpha \operatorname{Var}(f), \tag{1.2}$$

where $\operatorname{Var}(f)$ denotes the variance of the process. The simulated process is periodic with $T = 2\pi/\Delta\omega$ and the discretization frequency complies with the Nyquist sampling rate condition which is given by $\Delta t \leq 2\pi/\omega_u$ in order to avoid signal aliasing. Further, it has been shown that for a large number of N the simulated realizations are asymptotically Gaussian.

1.8.2 Generalized matrix inverse theory

Many engineering applications require finding a solution to a linear algebraic system of equations in the form

$$\mathbf{A}\mathbf{x} = \mathbf{b}, \tag{1.3}$$

where $\mathbf{A}$ is either a rectangular $m \times n$ or a square $n \times n$ matrix, $\mathbf{x}$ is an n-dimensional vector and $\mathbf{b}$ is an m-dimensional vector. Clearly, in the case where $\mathbf{A}$ is a square, non-singular matrix the

solution to Eq. (2.1) can be uniquely determined by

$$\mathbf{x} = \mathbf{A}^{-1}\mathbf{b}, \tag{1.4}$$

where $\mathbf{A}^{-1}$ denotes the inverse matrix of $\mathbf{A}$. Following the rationale presented in section 1.4, there exist many cases where $\mathbf{A}$ is rectangular or square but singular. Solutions to this class of problems can be provided by utilizing tools from the generalized matrix inverse theory. In this regard, there exist a number of generalized inverses for any $m \times n$ matrix $\mathbf{A}$. Theorem 1 facilitates the ensuing analysis (Fragkoulis, 2017; Ben-Israel and Greville, 2003).

Theorem 1. *Let* $\mathbf{A} \in \mathbf{C}^{m\times n}$, $\mathbf{B} \in \mathbf{C}^{p\times i}$ *and* $\mathbf{D} \in \mathbf{C}^{m\times q}$. *Then the matrix equation*

$$\mathbf{AXB} = \mathbf{D} \tag{1.5}$$

is consistent if, and only if for some $\mathbf{A}^{(1)}, \mathbf{B}^{(1)}$ *that satisfy the first Penrose equation (Ben-Israel and Greville, 2003)*

$$\mathbf{A}\mathbf{A}^{(1)}\mathbf{A} = \mathbf{A} \tag{1.6}$$

$$\mathbf{B}\mathbf{B}^{(1)}\mathbf{B} = \mathbf{B} \tag{1.7}$$

it holds that

$$\mathbf{A}\mathbf{A}^{(1)}\mathbf{D}\mathbf{B}^{(1)}\mathbf{B} = \mathbf{D}, \tag{1.8}$$

in which case the general solution is

$$\mathbf{X} = \mathbf{A}^{(1)}\mathbf{D}\mathbf{B}^{(1)} + \mathbf{Y} - \mathbf{A}^{(1)}\mathbf{A}\mathbf{Y}\mathbf{B}\mathbf{B}^{(1)} \tag{1.9}$$

for arbitrary $\mathbf{Y} \in \mathbf{C}^{n\times p}$.

For a system of algebraic equations in the form of Eq. (1.3), Theorem 1 is equivalent to the form given by the following corollary

Corollary 1. *Let* $\mathbf{A} \in \mathbf{C}^{m\times n}$ *and b be an* m*-dimensional vector. Then, Eq. (2.1) is consistent if, and only if for some* $\mathbf{A}^{(1)}$

$$\mathbf{A}\mathbf{A}^{(1)}\mathbf{b} = \mathbf{b}, \tag{1.10}$$

in which case the general solution of Eq. (1.3) is

$$\mathbf{x} = \mathbf{A}^{(1)}\mathbf{b} + \left(\mathbf{I} - \mathbf{A}^{(1)}\mathbf{A}\right)\mathbf{y}, \tag{1.11}$$

where $\mathbf{y}$ is an arbitrary n-dimensional vector. If matrix $\mathbf{A}$ satisfies an auxiliary set of conditions (Penrose equations), matrix $\mathbf{A}^{(1)}$ is generalized to the the Moore-Penrose inverse of $\mathbf{A}$. This generalization offers significant methodological merit since it enables the determination of a unique solution for Eq. (2.1). Further details about the conditions of existence of the Moore-Penrose matrix and implementation aspects within the context of random vibration problems are included in the corresponding chapters of this thesis.

1.8.3 Fractional derivatives modeling

A persistent challenge in stochastic dynamics relates to the response determination and reliability assesment of dynamical systems endowed with fractional derivative elements. Specifically, fractional calculus has been extensively employed in several branches of science over the past decades. With regard to engineering problems, its use has been stimulated by necessities pertaining to the modeling of complex material behavior, which has been dictated by advances in theoretical and applied mechanics (e.g., Di Paola et al. (2013); Tarasov (2017)). This has led to the development of several uncertainty quantification frameworks (e.g, Di Matteo et al. (2014); Fragkoulis et al.

(2019); Pirrotta et al. (2021); Kougioumtzoglou et al. (2022)) in the field stochastic dynamics.

From a mathematical perspective, fractional derivatives can be viewed as the generalization of classical integer order derivatives to arbitrary order (Podlubny, 1999). Although integer order derivatives are uniquely determined, there exist several alternative representations for derivatives of fractional order. The most commonly encountered formulations are presented in the remaining part of this section, in which a denotes the order of differentiation, $D^a_{0,t}(\cdot)$ is the fractional operator, β, t are the limits of fractional differentiation and Γ is the Gamma function.

The first one is the Riemann-Liouville representation, given by

$$ {}_{RL}D^a_{0,t}x(t) = \frac{1}{\Gamma(m-a)}\frac{d^m}{dt^m}\int_0^t (t-\tau)^{m-a-1}x(\tau)d\tau, \quad m-1 \leq a < m \in Z^+, \tag{1.12} $$

where Z^+ is the set of real positive numbers. Adopting this expression, the fractional derivative is given by integrating $(m-a)$ times and then by differenting m times the function $x(t)$. An alternative definition is given by Caputo's representation (Caputo, 1967) in the form

$$ {}_{c}D^a_{0,t}x(t) = D^{-(m-a)}_{0,t}\frac{d^m}{dt^m}x(t) = \frac{1}{\Gamma(m-a)}\int_0^t (t-\tau)^{m-a-1}x^{(m)}(\tau)d\tau, \tag{1.13} $$

where $x^{(m)}$ represents the m order derivative of the function $x(t)$. Clearly, this requires the existence of the m order derivative, which typically holds in engineering applications. Further, in Caputo's representation the initial conditions can be expressed by integer order derivatives, which is convenient from a physical point of view. Finally, a third representation based on the Grunwald-Letnikov definition follows the expression

$$ {}_{GL}D^a_{0,t}\mathbf{x}(t) = \sum_{k=0}^{m-1}\frac{x^{(k)}(0)t^{-a+k}}{\Gamma(-a+k+1)} + \frac{1}{\Gamma(m-a)}\int_0^t (t-\tau)^{m-a-1}\mathbf{x}^{(m)}(\tau)d\tau, \tag{1.14} $$

$m-1 \leq a < m \in Z^+$.

Typically, solutions to differential equations containing fractional derivative elements are provided by means of numerical schemes. In the ensuing analysis the linear $L1$-algorithm (Koh and Kelly, 1990) is adopted. The algorithm relies on the Riemann-Liouville representation (1.12) for the modeling of fractional derivative elements.

1.9 Organization of the thesis

This thesis consists of six chapters followed by the list of cited literature. With the exception of chapter 1 and chapter 6, the remaining chapters comprise four independent research articles that address pertinent problems in probabilistic engineering mechanics and Random Vibration theory.

Chapter 1 has an introductory role and outlines the motivation and key areas of focus of the current thesis. Moreover, the contributions, some mathematical prerequisites and the structure of the thesis are also briefly presented.

Chapter 2 presents a novel analytical framework for non-stationary stochastic response determination of multi-degree-of-freedom (MDOF) linear and nonlinear structural systems with singular matrices. This is accomplished utilizing a harmonic-wavelet-based technique and tools from generalized matrix inverse theory.

Chapter 3 focuses on enhancing the veracity of the scheme introduced in Chapter 2 by using a periodized generalized harmonic wavelet approach and by accounting for diverse engineering systems.

Chapter 4 treats the problem of incomplete wind time-histories reconstruction and extrapolation in one and two spatial dimensions, as well as for related stochastic field statistics estimation. This is achieved by invoking concepts and algorithms of sparse representation theory.

In Chapter 5 a data-driven methodology is proposed for inferring the governing equations of motion of stochastically excited systems by employing measured response data and BCS tools.

Chapter 6 provides some concluding remarks and future research directions of this thesis. A list of cited references and publications follows.

Chapter 2

Research article 1: Harmonic wavelets based response evolutionary power spectrum determination of linear and nonlinear structural systems with singular matrices

Harmonic wavelets based response evolutionary power spectrum determination of linear and nonlinear structural systems with singular matrices

George D. Pasparakis[a], V. C. Fragkoulis[a,*], M. Beer[a,b,c]

[a]*Institute for Risk and Reliability, Leibniz Universität Hannover, Callinstr. 34, 30167 Hannover, Germany*

[b]*Institute for Risk and Uncertainty and School of Engineering, University of Liverpool, Liverpool L69 7ZF, UK*

[c]*International Joint Research Center for Engineering Reliability and Stochastic Mechanics, Tongji University, Shanghai, China*

Abstract: A new approximate analytical technique is proposed for determining the response evolutionary power spectrum (EPS) of stochastically excited structural multi-degree-of-freedom (MDOF) linear and nonlinear systems with singular matrices. Such systems can appear, indicatively, when a redundant coordinates modeling is adopted for forming the equations of motion of complex multibody systems. For this case, it can be argued that this modeling approach facilitates the system's stochastic response analysis, since employment of redundant DOFs is associated with computational cost efficient solution frameworks, and potentially provides with enhanced modeling flexibility. In this context, aiming at the joint time-frequency response analysis of MDOF systems, recently developed wavelet-based solution frameworks, which generalize classic input-output relationships of random vibration, are adopted and further generalized in this paper to account for systems with singular matrices. Specifically, resorting to the theory of generalized inverses of singular matrices, as well as to the theory of harmonic wavelets, a Moore-Penrose generalized matrix inverse excitation-response relationship is derived herein for determining the response EPS of linear MDOF systems. Further, a recently developed harmonic-wavelet-based statistical linearization

*Corresponding author

E-mail addresses: george.pasparakis@irz.uni-hannover.de (G. D. Pasparakis), fragkoulis@irz.uni-hannover.de (V. C. Fragkoulis), beer@irz.uni-hannover.de (M. Beer).

technique is also generalized to account for the case of nonlinear MDOF systems. The validity of the proposed technique is demonstrated by pertinent numerical examples.

Keywords: Stochastic Dynamics; Moore-Penrose Inverse; Harmonic Wavelet; Singular Matrix; Evolutionary Power Spectrum; Time-Frequency Analysis

2.1 Introduction

The nature of environmental excitations, such as earthquakes and wind loadings which evolve in time and are described by evolutionary power spectra (EPS) (Priestley, 1965), plays an instrumental role in the efficient analysis of structural systems. In conjunction with the complexity of the considered system, they constitute two critical aspects towards the development of efficient response analysis solution treatments. Therefore, taking into account the non-stationary characteristics of natural excitations, several frameworks have been proposed for determining the system response, as well as for conducting joint time-frequency response analysis, of linear and nonlinear systems; see, indicatively, Refs. (Roberts and Spanos, 2003; Grigoriu, 2013; Li and Chen, 2009; Kougioumtzoglou et al., 2015; Kougioumtzoglou and Spanos, 2014; Spanos and Failla, 2004; Spanos et al., 2005; Spanos and Kougioumtzoglou, 2012; Fragkoulis et al., 2019; dos Santos et al., 2019).

As far as the joint time-frequency response analysis of engineering systems is concerned, the advent of the potent machinery of wavelets has been proved pivotal. It has substantially enhanced the arsenal of the system response characterization methods, when dynamic systems subjected to non-stationary excitation are considered (Spanos and Failla, 2005; Spanos et al., 2005). Specifically, standard excitation-response relationships of random vibration theory, have been extended and generalized in a wavelet-based framework, whereas wavelet-based versions of classic methodologies and techniques, such as the statistical linearization method (Roberts and Spanos, 2003), have also been developed (Spanos and Kougioumtzoglou, 2012; Kong et al., 2014b). Moreover, wavelet analysis has been used in conjunction with fractional calculus, for deriving the EPS of

oscillators endowed with fractional derivative elements (Kougioumtzoglou and Spanos, 2016).

With regards to the complexity of the dynamic systems, it is commonly accepted that the minimum number of independent coordinates/degrees-of-freedom (DOF) is used in forming the system governing equations of motion (Roberts and Spanos, 2003). However, it can be argued that for the case of multibody systems, a redundant coordinates approach potentially facilitates the modeling procedure, while also results in enhanced flexibility and reduced overall computational cost (Udwadia and Kalaba, 1992; Udwadia and Phohomsiri, 2006; de Falco et al., 2005; Critchley and Anderson, 2003; Featherstone, 1984; Schutte and Udwadia, 2011; Pappalardo and Guida, 2018a,b). Further, it also leads to systems with singular matrices, rendering all standard stochastic response analysis frameworks inapplicable. Note, in passing, that singular matrices do not solely appear due to adopting a redundant DOFs modeling. They are also met in diverse engineering systems and applications, such as systems with "massless" joints (Antoniou et al., 2017b; Pirrotta et al., 2019), and in vibratory energy harvesting applications, where they appear due to the coupling between the governing equations of the mechanical and the electrical system (Adhikari et al., 2009).

In this paper, taking into account the aforementioned aspects, a generalized inverse matrix harmonic-wavelet-based treatment is proposed for conducting joint time-frequency response analysis of linear and nonlinear MDOF systems with singular matrices, which are subjected to non-stationary excitation. Specifically, focusing on the determination of the system response EPS, and resorting to the theory of the Moore-Penrose (M-P) generalized matrix inverses, standard harmonic-wavelet-based techniques (Spanos and Kougioumtzoglou, 2012; Kong et al., 2014b) are generalized herein.

In this context, adopting a redundant coordinates modeling of the equations of motion, and also employing the locally stationary wavelet (LSW) representation of a stochastic process (Spanos and Kougioumtzoglou, 2012), an M-P localized in time and frequency domains, harmonic-wavelet-based frequency response function (MP HW-FRF) is derived. This can be construed as a generalization of a recently developed HW-FRF (Kong et al., 2014b), to account for systems with

singular matrices. Further, the MP HW-FRF is used for determining the system response EPS, by constructing an input-output relationship which connects the excitation and response EPS. Next, a recently developed harmonic-wavelet-based statistical linearization methodology (Kong et al., 2014b) is also generalized. In this regard, an equivalent linear system corresponding to the original nonlinear system is defined, and a set of time and frequency dependent expressions for the equivalent linear elements is derived. This is attained by resorting to an iterative solution numerical scheme. The scheme is applied on the coupled set of equations defined by the set of the equivalent elements expressions, and the M-P input-output relationship of the equivalent linear system. Further, although the employment of the M-P inverse framework implies a family of equivalent linear elements, uniquely defined elements are determined by setting equal to zero the arbitrary term of the M-P based family. Finally, the nonlinear system response EPS is estimated by considering the corresponding response EPS of the equivalent linear system. The efficiency of the proposed M-P inverse framework is demonstrated by pertinent examples of linear and nonlinear MDOF systems. The obtained results are compared with results derived by the standard solution treatment of Ref. (Kong et al., 2014b) and are in complete agreement.

2.2 Mathematical preliminaries

2.2.1 Aspects of Moore-Penrose matrix inverse theory

The study of generalized matrix inverses has initiated and flourished mainly as a result of attempting to solve systems of algebraic equations of the form

$$\mathbf{A}\mathbf{x} = \mathbf{b}, \tag{2.1}$$

where $\mathbf{A}$ is either rectangular $m_0 \times n_0$, or square but singular $n_0 \times n_0$ matrix, and $\mathbf{x}$, $\mathbf{b}$ are n_0 vectors. Eq. (2.1) appears in many theoretical problems in mathematics as well as many applied problems.

Clearly, the nature of matrix $\mathbf{A}$ renders its solution impossible. In this regard, the necessity of defining any form of "partial inverse" for rectangular or square but singular matrices gave birth to the theory of generalized matrix inverses (Ben-Israel and Greville, 2003). The Moore-Penrose (M-P) generalized matrix inverse holds an exceptional place among these theoretical results.

Definition 1. *For any matrix* $\mathbf{A} \in \mathbb{C}^{m_0} \times n_0$*, there is a unique matrix* $\mathbf{A}^+ \in \mathbb{C}^{n_0} \times m_0$ *such that*

$$\mathbf{A}\mathbf{A}^+\mathbf{A} = \mathbf{A},\ \mathbf{A}^+\mathbf{A}\mathbf{A}^+ = \mathbf{A}^+, (\mathbf{A}\mathbf{A}^+)^* = \mathbf{A}\mathbf{A}^+,\ (\mathbf{A}^+\mathbf{A})^* = \mathbf{A}^+\mathbf{A}. \tag{2.2}$$

The matrix $\mathbf{A}^+$ defined in Eq. (2.2) is called the M-P inverse of $\mathbf{A}$. If $\mathbf{A} \in \mathbb{R}^{n_0} \times n_0$ is non-singular, then $\mathbf{A}^+$ coincides with $\mathbf{A}^{-1}$. Using the M-P inverse, a closed form solution to the algebraic system of Eq. (2.1) is attained, which highlights its importance for several applications. In this regard, for any matrix $\mathbf{A} \in \mathbb{R}^{m_0 \times n_0}$, Eq. (2.1) implies

$$\mathbf{x} = \mathbf{A}^+\mathbf{b} + (\mathbf{I}_n - \mathbf{A}^+\mathbf{A})\mathbf{y}, \tag{2.3}$$

where $\mathbf{y}$ denotes an arbitrary n_0 vector and $\mathbf{I}_{n_0}$ represents the identity $n_0 \times n_0$ matrix.

By resorting to the M-P matrix inverse theory, classic solution treatments of random vibration have been recently generalized for determining the stationary stochastic response of linear and nonlinear systems with singular matrices (Fragkoulis et al., 2016a,b; Kougioumtzoglou et al., 2017b); see also Refs. Antoniou et al. (2017b); Fragkoulis et al. (2015); Pantelous and Pirrotta (2017); Pirrotta et al. (2019) for additional applications. However, it can be argued that the application of state-of-the-art M-P solution frameworks is considerably limited, since relevant approaches completely ignore the non-stationary characteristics of the system excitation. A more detailed presentation of the M-P inverse theory can be found in Refs. Ben-Israel and Greville (2003) and Campbell and Meyer (2009).

2.2.2 Harmonic wavelets theory elements

Generalized harmonic wavelets

In this section, a concise presentation of the basic elements of wavelets analysis is pårovided for completeness. In this regard, the wavelet transform $[W_\psi f](j,k)$ of a function $f(t)$ is defined as

$$[W_\psi f](j,k) = \frac{1}{\mid j \mid^{1/2}} \int_{-\infty}^{\infty} f(t)\psi^* \left(\frac{t-k}{j}\right) \mathrm{d}t, \tag{2.4}$$

where $\psi(t)$ is the mother wavelet, i.e., the generating function for all basis functions, $[W_\psi f](j,k)$ is the wavelet coefficient at frequency and time scale j and k, respectively, and "*" denotes the complex conjugate operator. Eq. (2.4) is used for conducting joint time-frequency analysis of the function $f(t)$. Further, choosing a different mother wavelet function $\psi(t)$ results in the definition of different families of wavelets. Among them, the so-called generalized harmonic wavelets (GHW) constitute the most often considered family of wavelets in engineering applications (Newland, 1993, 1994). Utilizing the set of parameters (m,n) and k for defining the bandwidth at all scale levels, the members of the GHW family in frequency domain are given by

$$\Psi^G_{(m,n),k}(\omega) = \begin{cases} \frac{1}{(n-m)\Delta\omega} \exp\left(-i\omega\frac{kT_0}{n-m}\right), & m\Delta\omega \le \omega < n\Delta\omega \\ 0, & otherwise \end{cases} \tag{2.5}$$

where $m,n,k \in \mathbb{Z}^+$, T_0 denotes the total time duration and $\Delta\omega = 2\pi/T_0$. The importance of the GHW of Eq. (2.5) stems from the fact that a decoupling of the time-frequency resolution from the values of the central frequency

$$\omega_{c,(m,n),k} = \frac{(n+m)}{2}\Delta\omega, \tag{2.6}$$

which is defined in the intervals $[m\Delta\omega, n\Delta\omega]$ and $\left[\frac{kT_0}{n-m}, \frac{(k+1)T_0}{n-m}\right]$, is attained.

Further, the continuous generalized harmonic wavelet transform (GHWT) of a function $f(t)$ is

defined as the projection of $f(t)$ on the orthogonal basis given by the family of GHWs of Eq. (2.5) (Newland, 1994), that is

$$W^{G}_{(m,n),k}[f] = \frac{n-m}{kT_0}\int_{-\infty}^{\infty} f(t)\overline{\psi^{G}_{(m,n),k}(t)}dt. \tag{2.7}$$

A detailed presentation of the topic is found in Refs. Spanos and Failla (2004, 2005); Spanos et al. (2005).

Locally stationary wavelet representation of non-stationary stochastic processes

In terms of engineering applications, the versatile locally stationary wavelet (LSW) representation of stochastic processes, firstly introduced in Ref. Nason et al. (2000), facilitates the ensuing analysis by allowing for a representation of a given non-stationary process as the summation of sub-processes defined at different scales and translation levels. Specifically, adopting a GHW expansion of the system response and excitation, the LSW forms a set of orthogonal basis functions on any given finite interval. Therefore, it results in the definition of a wavelet spectrum at a particular scale and location providing, in essence, with the joint time-frequency content of the system's non-stationary excitation and the corresponding response.

In this regard, considering the family of GHWs of Eq. (2.7), the generalized harmonic-wavelet-based representation of an n_0 vector process $\mathbf{x}(t)$ takes the form

$$\mathbf{x}(t) = \sum_{(m,n)}\sum_{k}\mathbf{x}_{(m,n),k}(t), \tag{2.8}$$

where the localized process $\mathbf{x}_{(m,n),k}(t)$ at scale (m,n) and translation k, is given by

$$\mathbf{x}_{(m,n),k}(t) = \mathbf{a}_{(m,n),k}\cos\left[\omega_{c,(m,n),k}\left(t-\frac{kT_0}{n-m}\right)\right] + \mathbf{b}_{(m,n),k}\sin\left[\omega_{c,(m,n),k}\left(t-\frac{kT_0}{n-m}\right)\right]. \tag{2.9}$$

In Eq. (2.9), $\omega_{c,(m,n),k}$ denotes the central frequency of Eq. (2.6). Further, $\mathbf{a}_{(m,n),k}$ and $\mathbf{b}_{(m,n),k}$ are statistically independent, zero-mean vector processes, whose variance is related to the EPS matrix $\mathbf{S}^{\mathbf{xx}}_{(m,n),k}$ via the expression (Spanos and Kougioumtzoglou, 2012)

$$\mathbb{E}\left[\mathbf{a}_{(m,n),k}\mathbf{a}^{\mathrm{T}}_{(m,n),k}\right] = \mathbb{E}\left[\mathbf{b}_{(m,n),k}\mathbf{b}^{\mathrm{T}}_{(m,n),k}\right] = 2(n-m)\Delta\omega\mathbf{S}^{\mathbf{xx}}_{(m,n),k}. \tag{2.10}$$

Finally, resorting to the orthogonality properties of monochromatic functions, i.e.,

$$\int_{\frac{kT_0}{n-m}}^{\frac{(k+1)T_0}{n-m}} \cos\left[\omega_{c,(m,n),k}\left(t-\frac{kT_0}{n-m}\right)\right]\cos\left[\omega_{c,(i,j),l}\left(t-\frac{lT_0}{j-i}\right)\right]dt = \begin{cases} \frac{T_0}{2(n-m)} & ,\text{if } (m,n)=(i,j), k=l \\ 0 & ,\text{otherwise} \end{cases} \tag{2.11}$$

and

$$\int_{\frac{kT_0}{n-m}}^{\frac{(k+1)T_0}{n-m}} \sin\left[\omega_{c,(m,n),k}\left(t-\frac{kT_0}{n-m}\right)\right]\sin\left[\omega_{c,(i,j),l}\left(t-\frac{lT_0}{j-i}\right)\right]dt = \begin{cases} \frac{T_0}{2(n-m)} & ,\text{if } (m,n)=(i,j), k=l \\ 0 & ,\text{otherwise} \end{cases} \tag{2.12}$$

and utilizing Eqs. (2.9) and (2.10), the important for the ensuing analysis relationships

$$\mathbb{E}\left[\mathbf{x}_{(m,n),k}(t)\right] = \mathbb{E}\left[\dot{\mathbf{x}}_{(m,n),k}(t)\right] = \mathbb{E}\left[\ddot{\mathbf{x}}_{(m,n),k}(t)\right] = \mathbf{0}, \tag{2.13}$$

$$\mathbb{E}\left[\mathbf{x}_{(m,n),k}(t)\dot{\mathbf{x}}^{\mathrm{T}}_{(m,n),k}(t)\right] = \mathbb{E}\left[\dot{\mathbf{x}}_{(m,n),k}(t)\ddot{\mathbf{x}}^{\mathrm{T}}_{(m,n),k}(t)\right] = \mathbf{0}, \tag{2.14}$$

$$\mathbb{E}\left[\mathbf{x}_{(m,n),k}(t)\mathbf{x}^{\mathrm{T}}_{(m,n),k}(t)\right] = 2\mathbf{S}^{\mathbf{xx}}_{(m,n),k}(n-m)\Delta\omega, \tag{2.15}$$

$$\mathbb{E}\left[\dot{\mathbf{x}}^{\mathrm{T}}_{(m,n),k}(t)\dot{\mathbf{x}}^{\mathrm{T}}_{(m,n),k}(t)\right] = 2\omega^{2}_{c,(m,n),k}\mathbf{S}^{\mathbf{xx}}_{(m,n),k}(n-m)\Delta\omega, \tag{2.16}$$

$$\mathbb{E}\left[\mathbf{x}_{(m,n),k}(t)\ddot{\mathbf{x}}^{\mathrm{T}}_{(m,n),k}(t)\right] = -2\omega^{2}_{c,(m,n),k}\mathbf{S}^{\mathbf{xx}}_{(m,n),k}(n-m)\Delta\omega, \tag{2.17}$$

and

$$\mathbb{E}\left[\ddot{\mathbf{x}}_{(m,n),k}(t)\ddot{\mathbf{x}}^{\mathrm{T}}_{(m,n),k}(t)\right] = 2\omega^{4}_{c,(m,n),k}\mathbf{S}^{\mathbf{xx}}_{(m,n),k}(n-m)\Delta\omega, \tag{2.18}$$

are derived; see also Refs. Spanos and Kougioumtzoglou (2012); Kougioumtzoglou (2013); Kong et al. (2014b).

Note, in passing, that the advantages of employing the LSW representation of Eqs. (2.8) and (2.9), are the simplicity and straightforward application of the representation model. Taking also into account its efficiency in estimating the response EPS (Spanos and Kougioumtzoglou, 2012; Kong et al., 2014b), it is adopted in the ensuing analysis, where the standard harmonic-wavelet-based framework of Ref. Kong et al. (2014b) is generalized to account for systems with singular matrices. However, it is also noted that a less approximate stochastic process representation than that of Eq. (2.9) has been recently used for joint time-frequency response analysis (Spanos et al., 2016; Kong et al., 2016). This consists in the employment of a periodized generalized harmonic wavelets (PGHWs) based framework, and is identified as a potential future extension of the herein developed M-P generalized matrix inverse theoretical framework.

2.3 Stochastic response of systems with singular matrices subjected to non-stationary excitation

2.3.1 Linear systems with singular matrices

The general form of the equations of motion of a lumped-parameter n_0-DOF linear system is given by

$$\mathbf{M}\ddot{\mathbf{q}} + \mathbf{C}\dot{\mathbf{q}} + \mathbf{K}\mathbf{q} = \mathbf{Q}(t), \tag{2.19}$$

where $\mathbf{q}$ denotes the n_0 vector of the generalized coordinates; and $\mathbf{Q}(t)$ represents the n_0 vector of the non-stationary, zero-mean system excitation, whose evolutionary power spectrum matrix is denoted as $\mathbf{S}^{\mathbf{QQ}}(\omega, t)$. Further, $\mathbf{M}, \mathbf{C}$ and $\mathbf{K}$ denote the $n_0 \times n_0$ mass, damping and stiffness matrices of the system. Next, adopting a redundant coordinates modeling, a new coordinates ℓ vector $\mathbf{x}$ ($\ell > n_0$), is considered. Thus, the mass, damping and stiffness $\ell \times \ell$ matrices are given by $\mathbf{M_x}$, $\mathbf{C_x}$ and $\mathbf{K_x}$, whereas $\mathbf{Q_x}$ denotes the corresponding ℓ vector of the system excitation. Considering additional constraints equations, Eq. (2.19) is recast in the form

$$\bar{\mathbf{M}}_\mathbf{x}\ddot{\mathbf{x}} + \bar{\mathbf{C}}_\mathbf{x}\dot{\mathbf{x}} + \bar{\mathbf{K}}_\mathbf{x}\mathbf{x} = \bar{\mathbf{Q}}_\mathbf{x}(t), \tag{2.20}$$

where $\bar{\mathbf{M}}_\mathbf{x}, \bar{\mathbf{C}}_\mathbf{x}$ and $\bar{\mathbf{K}}_\mathbf{x}$ denote the augmented mass, damping and stiffness $(m_0 + \ell) \times \ell$ matrices, given by

$$\bar{\mathbf{M}}_\mathbf{x} = \begin{bmatrix} (\mathbf{I} - \mathbf{A}^+\mathbf{A})\mathbf{M_x} \\ \mathbf{A} \end{bmatrix}, \tag{2.21}$$

$$\bar{\mathbf{C}}_\mathbf{x} = \begin{bmatrix} (\mathbf{I} - \mathbf{A}^+\mathbf{A})\mathbf{C_x} \\ \mathbf{E} \end{bmatrix} \tag{2.22}$$

and

$$\bar{\mathbf{K}}_{\mathbf{x}} = \begin{bmatrix} (\mathbf{I} - \mathbf{A}^{+}\mathbf{A})\mathbf{K}_{\mathbf{x}} \\ \mathbf{L} \end{bmatrix}, \tag{2.23}$$

respectively; whereas $\bar{\mathbf{Q}}_{\mathbf{x}}$ represents the augmented excitation $(m_0 + \ell)$ vector, given by

$$\bar{\mathbf{Q}}_{\mathbf{x}} = \begin{bmatrix} (\mathbf{I} - \mathbf{A}^{+}\mathbf{A})\mathbf{Q}_{\mathbf{x}} \\ \mathbf{F} \end{bmatrix}. \tag{2.24}$$

Further, the $(m_0 \times \ell)$ matrices $\mathbf{A}, \mathbf{E}$ and $\mathbf{L}$ in Eqs. (2.21-2.24) pertain to the system constraints equation

$$\mathbf{A}(\mathbf{x}, \dot{\mathbf{x}}, t)\ddot{\mathbf{x}} = \mathbf{b}(\mathbf{x}, \dot{\mathbf{x}}, t), \tag{2.25}$$

where

$$\mathbf{b} = \mathbf{F} - \mathbf{E}\dot{\mathbf{x}} - \mathbf{L}\mathbf{x}; \tag{2.26}$$

details on the derivation of Eqs. (2.20-2.26) can be found in Refs. Fragkoulis et al. (2016a,b); Kougioumtzoglou et al. (2017b).

Next, focusing on the joint time-frequency response characterization of the system of Eq. (2.20), it is assumed that the system excitation and corresponding response are modeled via the LSW representation of Eq. (2.8). Thus, the augmented system of Eq. (2.20) becomes

$$\bar{\mathbf{M}}_{\mathbf{x}} \sum_{(m,n)} \sum_{k} \ddot{\mathbf{x}}_{(m,n),k}(t) + \bar{\mathbf{C}}_{\mathbf{x}} \sum_{(m,n)} \sum_{k} \dot{\mathbf{x}}_{(m,n),k}(t) + \bar{\mathbf{K}}_{\mathbf{x}} \sum_{(m,n)} \sum_{k} \mathbf{x}_{(m,n),k}(t) = \sum_{(} m, n) \sum_{k} \bar{\mathbf{Q}}_{\mathbf{x},(m,n),k}(t). \tag{2.27}$$

The localized in time and frequency domains ℓ vector process $\mathbf{x}_{(m,n),k}(t)$ and $(m_0 + \ell)$ vector process $\bar{\mathbf{Q}}_{\mathbf{x},(m,n),k}(t)$ of the double summations in Eq. (2.27), are defined in Eq. (2.9) as combinations

of localized monochromatic functions, i.e.,

$$\mathbf{x}_{(m,n),k}(t) = \bar{\mathbf{a}}_{(m,n),k} \cos\left[\omega_{c,(m,n),k}\left(t - \frac{kT_0}{n-m}\right)\right] + \bar{\mathbf{b}}_{(m,n),k} \sin\left[\omega_{c,(m,n),k}\left(t - \frac{kT_0}{n-m}\right)\right] \quad (2.28)$$

and

$$\bar{\mathbf{Q}}_{\mathbf{x},(m,n),k}(t) = \mathbf{e}_{(m,n),k} \cos\left[\omega_{c,(m,n),k}\left(t - \frac{kT_0}{n-m}\right)\right] + \mathbf{f}_{(m,n),k} \sin\left[\omega_{c,(m,n),k}\left(t - \frac{kT_0}{n-m}\right)\right]. \quad (2.29)$$

The terms $\bar{\mathbf{a}}_{(m,n),k}, \bar{\mathbf{b}}_{(m,n),k}$ and $\mathbf{e}_{(m,n),k}, \mathbf{f}_{(m,n),k}$ in Eqs. (2.28-2.29) correspond to statistically independent zero-mean random $(m_0 + \ell)$ vectors, whose variance is given by Eq. (2.10). Substituting Eqs. (2.28-2.29) in Eq. (2.27), and manipulating, yields

$$\omega^4_{c,(m,n),k}\bar{\mathbf{M}}_{\mathbf{x}}\mathbf{S}^{\mathbf{xx}}_{(m,n),k}\bar{\mathbf{M}}^{\mathrm{T}}_{\mathbf{x}} + \omega^2_{c,(m,n),k}\bar{\mathbf{C}}_{\mathbf{x}}\mathbf{S}^{\mathbf{xx}}_{(m,n),k}\bar{\mathbf{C}}^{\mathrm{T}}_{\mathbf{x}} + \bar{\mathbf{K}}_{\mathbf{x}}\mathbf{S}^{\mathbf{xx}}_{(m,n),k}\bar{\mathbf{K}}^{\mathrm{T}}_{\mathbf{x}} - \omega^2_{c,(m,n),k}\bar{\mathbf{M}}_{\mathbf{x}}\mathbf{S}^{\mathbf{xx}}_{(m,n),k}\bar{\mathbf{K}}^{\mathrm{T}}_{\mathbf{x}} - \omega^2_{c,(m,n),k}\bar{\mathbf{K}}_{\mathbf{x}}\mathbf{S}^{\mathbf{xx}}_{(m,n),k}\bar{\mathbf{M}}^{\mathrm{T}}_{\mathbf{x}} = \mathbf{S}^{\bar{\mathbf{Q}}_x\bar{\mathbf{Q}}_x}_{(m,n),k}, \quad (2.30)$$

where $\mathbf{S}^{\bar{\mathbf{Q}}_x\bar{\mathbf{Q}}_x}_{(m,n),k}$ denotes the excitation EPS $(m_0 + \ell) \times (m_0 + \ell)$ matrix, and $\mathbf{S}^{\mathbf{xx}}_{(m,n),k}$ denotes the corresponding response EPS $\ell \times \ell$ matrix, both defined at different frequency and time bands. Further, manipulating Eq. (2.30), the expression

$$\mathbf{R}_{\mathbf{x}}\mathbf{S}^{\mathbf{xx}}_{(m,n),k}\left[-\omega^2_{c,(m,n),k}\bar{\mathbf{M}}^{\mathrm{T}}_{\mathbf{x}} - i\omega_{c,(m,n),k}\bar{\mathbf{C}}^{\mathrm{T}}_{\mathbf{x}} + \bar{\mathbf{K}}^{\mathrm{T}}_{\mathbf{x}}\right] = \mathbf{S}^{\bar{\mathbf{Q}}_x\bar{\mathbf{Q}}_x}_{(m,n),k}, \quad (2.31)$$

is derived, where the $(m_0 + \ell) \times \ell$ matrix $\mathbf{R}_{\mathbf{x}}$ has the form

$$\mathbf{R}_{\mathbf{x}} = \left[-\omega^2_{c,(m,n),k}\bar{\mathbf{M}}_{\mathbf{x}} + \mathrm{i}\omega_{c,(m,n),k}\bar{\mathbf{C}}_{\mathbf{x}} + \bar{\mathbf{K}}_{\mathbf{x}}\right]. \quad (2.32)$$

In Eq. (2.32), $\bar{\mathbf{M}}_{\mathbf{x}}, \bar{\mathbf{C}}_{\mathbf{x}}$ and $\bar{\mathbf{K}}_{\mathbf{x}}$ denote the $(m_0 + \ell) \times \ell$ augmented mass, damping and stiffness matrices of Eqs. (2.21-2.23), whereas $\omega_{c,(m,n),k}$ represents the central frequency of Eq. (2.6).

Note, in passing, that using the minimum number of generalized coordinates for the formulation of the system governing equations of motion (see Eq. (2.19)), results in non-singular mass, damping and stiffness matrices. This, in turn, facilitates the derivation of a closed form, wavelet-coefficient-based excitation-response relationship. Specifically, for the system of Eq. (2.19) it holds (Kong et al., 2014b)

$$\mathbf{S}^{\mathbf{qq}}_{(m,n),k} = \mathbf{H}[\omega_{c,(m,n),k}]\mathbf{S}^{\mathbf{QQ}}_{(m,n),k}\mathbf{H}[\omega_{c,(m,n),k}]^{\mathrm{T}*}, \tag{2.33}$$

where

$$\mathbf{H}[\omega_{c,(m,n),k}] = \left[-\omega^2_{c,(m,n),k}\mathbf{M} + \mathrm{i}\omega_{c,(m,n),k}\mathbf{C} + \mathbf{K}\right]^{-1} \tag{2.34}$$

is the localized harmonic-wavelet-based, frequency response function (HW-FRF). Clearly, the definition of the HW-FRF relies on the existence of the inverse matrix of Eq. (2.34). Thus, it is readily seen that following a redundant DOFs modeling approach, the singular mass, damping and stiffness matrices of Eqs. (2.21-2.23), hinder the derivation of the corresponding HW-FRF. However, employing elements of M-P generalized matrix inverse theory, a generalized HW-FRF is proposed herein to account for the case of systems with singular matrices.

In this regard, utilizing Eq. (2.3), the solution to Eq. (2.31) takes the form

$$\mathbf{S}^{\mathbf{xx}}_{(m,n),k}\left[-\omega^2_{c,(m,n),k}\bar{\mathbf{M}}^{\mathrm{T}}_{\mathbf{x}} - i\omega_{c,(m,n),k}\bar{\mathbf{C}}^{\mathrm{T}}_{\mathbf{x}} + \bar{\mathbf{K}}^{\mathrm{T}}_{\mathbf{x}}\right] = \mathbf{R}^{+}_{\mathbf{x}}\mathbf{S}^{\bar{\mathbf{Q}}_x\bar{\mathbf{Q}}_x}_{(m,n),k} + (\mathbf{I}_\ell - \mathbf{R}^{+}_{\mathbf{x}}\mathbf{R}_{\mathbf{x}})\mathbf{Y}, \tag{2.35}$$

where $\mathbf{R}^{+}_{\mathbf{x}}$ denotes the $\ell \times (m_0 + \ell)$ M-P inverse of $\mathbf{R}_{\mathbf{x}}$, and $\mathbf{Y}$ is an arbitrary $\ell \times (m_0 + \ell)$ matrix. Clearly, the arbitrary matrix $\mathbf{Y}$ implies a family of solutions for Eq. (2.35), instead of a unique solution. Nevertheless, the rank of matrix $\mathbf{R}_{\mathbf{x}}$ facilitates the selection of a unique solution. Specifically, when $\mathbf{R}_{\mathbf{x}}$ has full column rank, i.e., it has linearly independent columns, its M-P inverse

takes the form (Campbell and Meyer, 2009)

$$\mathbf{R}_{\mathbf{x}}^{+} = (\mathbf{R}_{\mathbf{x}}^{*}\mathbf{R}_{\mathbf{x}})^{-1}\mathbf{R}_{\mathbf{x}}^{*}, \tag{2.36}$$

where $\mathbf{R}_{\mathbf{x}}^{*}$ corresponds to the conjugate matrix of $\mathbf{R}_{\mathbf{x}}$. Thus, taking into account Eq. (2.36), Eq. (2.35) is equivalently written as

$$\mathbf{S}_{(m,n),k}^{\mathbf{xx}}\left[-\omega_{c,(m,n),k}^{2}\bar{\mathbf{M}}_{\mathbf{x}}^{\mathrm{T}} - i\omega_{c,(m,n),k}\bar{\mathbf{C}}_{\mathbf{x}}^{\mathrm{T}} + \bar{\mathbf{K}}_{\mathbf{x}}^{\mathrm{T}}\right] = \mathbf{R}_{\mathbf{x}}^{+}\mathbf{S}_{(m,n),k}^{\bar{\mathbf{Q}}_x\bar{\mathbf{Q}}_x}. \tag{2.37}$$

Further, applying the conjugate and transpose operations on both sides of Eq. (2.32) implies

$$\left[-\omega_{c,(m,n),k}^{2}\bar{\mathbf{M}}_{\mathbf{x}}^{\mathrm{T}} - i\omega_{c,(m,n),k}\bar{\mathbf{C}}_{\mathbf{x}}^{\mathrm{T}} + \bar{\mathbf{K}}_{\mathbf{x}}^{\mathrm{T}}\right] = \mathbf{R}_{\mathbf{x}}^{*\mathrm{T}}. \tag{2.38}$$

Also, noting that for full column rank matrix $\mathbf{R}_{\mathbf{x}}$, its conjugate transpose $\mathbf{R}_{\mathbf{x}}^{*\mathrm{T}}$ has full row rank, i.e., its rows are linearly independent, results in (Campbell and Meyer, 2009)

$$\mathbf{R}_{\mathbf{x}}^{*\mathrm{T}}\left(\mathbf{R}_{\mathbf{x}}^{*\mathrm{T}}\right)^{+} = \mathbf{I}_{m+\ell}. \tag{2.39}$$

Therefore, taking into account Eqs. (2.38) and (2.39), and also denoting by $\boldsymbol{\alpha}_{\mathbf{x}}[\omega_{c,(m,n),k}]$ the M-P inverse of matrix $\mathbf{R}_{\mathbf{x}}$ of Eq. (2.32), i.e.,

$$\boldsymbol{\alpha}_{\mathbf{x}}[\omega_{c,(m,n),k}] = \left[-\omega_{c,(m,n),k}^{2}\bar{\mathbf{M}}_{\mathbf{x}} + \mathrm{i}\omega_{c,(m,n),k}\bar{\mathbf{C}}_{\mathbf{x}} + \bar{\mathbf{K}}_{\mathbf{x}}\right]^{+}, \tag{2.40}$$

Eq. (2.37) becomes

$$\mathbf{S}_{(m,n),k}^{\mathbf{xx}} = \boldsymbol{\alpha}_{\mathbf{x}}[\omega_{c,(m,n),k}]\mathbf{S}_{(m,n),k}^{\bar{\mathbf{Q}}_x\bar{\mathbf{Q}}_x}\left(\boldsymbol{\alpha}_{\mathbf{x}}[\omega_{c,(m,n),k}]\right)^{\mathrm{T}*}. \tag{2.41}$$

Matrix $\boldsymbol{\alpha}_{\mathbf{x}}[\omega_{c,(m,n),k}]$ of Eq. (2.40) represents a generalization of the localized in time and frequency

HW-FRF matrix $\mathbf{H}\left[\omega_{c,(m,n),k}\right]$ (see Eq. (2.34)). In this regard, the herein proposed approach can be construed as a generalization of the results in Ref. Kong et al. (2014b), for deriving the response evolutionary power spectrum (EPS) of linear MDOF systems with singular matrices.

2.3.2 Nonlinear systems with singular matrices

In this section, aiming at the response EPS determination of MDOF chain-like nonlinear structural systems with singular matrices, a recently proposed, harmonic-wavelet-based version of the statistical linearization methodology (Spanos and Kougioumtzoglou, 2012; Kong et al., 2014b) is extended. Statistical linearization constitutes one of the most versatile approximate techniques for nonlinear system response determination and/or characterization (Roberts and Spanos, 2003; Socha, 2007), with a wide variety of applications over the last decades. It has been successfully adapted and/or extended for application in conjunction with fractional calculus (Spanos and Evangelatos, 2010; Spanos and Malara, 2014; Fragkoulis et al., 2019) and wavelet-based solutions frameworks (Spanos and Kougioumtzoglou, 2012), among others. The method is applied in two steps, which are summarized as follows. First, the original nonlinear system is replaced with an equivalent linear one, and then, the error between the two systems is formed and minimized (Roberts and Spanos, 2003). Based on the fact that solution frameworks for treating the equivalent linear system are readily available, the rationale behind the method is that the latter can be used as approximations to the solution of the original nonlinear system.

In this regard, adopting a redundant coordinates modeling (Fragkoulis et al., 2016a,b), the equations of motion for the nonlinear version of the system of Eq. (2.20) takes the form

$$\bar{\mathbf{M}}_{\mathbf{x}}\ddot{\mathbf{x}} + \bar{\mathbf{C}}_{\mathbf{x}}\dot{\mathbf{x}} + \bar{\mathbf{K}}_{\mathbf{x}}\mathbf{x} + \bar{\mathbf{\Phi}}_{\mathbf{x}}(\mathbf{x}, \dot{\mathbf{x}}) = \bar{\mathbf{Q}}_{\mathbf{x}}(t), \tag{2.42}$$

where the augmented mass, damping, stiffness matrices and excitation vector are given by Eqs. (2.21-2.23) and Eq. (2.24), respectively. Further, the augmented nonlinear $(m_0 + \ell)$ vector of the

system, which depends on the response displacement $\mathbf{x}$ and the response velocity $\dot{\mathbf{x}}$, is given by (Fragkoulis et al., 2016b)

$$\bar{\mathbf{\Phi}}_{\mathbf{x}} = \begin{bmatrix} (\mathbf{I} - \mathbf{A}^{+}\mathbf{A})\mathbf{\Phi}_{\mathbf{x}} \\ \mathbf{0} \end{bmatrix}. \tag{2.43}$$

In Eq. (2.43), $\mathbf{\Phi}_{\mathbf{x}}$ denotes the nonlinear ℓ vector of the system governing equations of motion, due to adopting a redundant coordinates modeling (Fragkoulis et al., 2016b).

Next, considering the LSW representation of Eq. (2.8) for the system excitation $\mathbf{x}(t)$, and thus assuming that $\mathbf{x}(t)$ is represented by the sum of its wavelet coefficients, an equivalent to Eq. (2.42) linear MDOF system is defined as

$$\bar{\mathbf{M}}_{\mathbf{x}}\ddot{\mathbf{x}} + \sum_{(m,n)}\sum_{k}\bar{\mathbf{C}}_{eq,(m,n),k}\dot{\mathbf{x}}_{(m,n),k} + \sum_{(m,n)}\sum_{k}\bar{\mathbf{K}}_{eq,(m,n),k}\mathbf{x}_{(m,n),k} = \bar{\mathbf{Q}}_{\mathbf{x}}(t). \tag{2.44}$$

In Eq. (2.44), $\bar{\mathbf{C}}_{eq,(m,n),k}$ and $\bar{\mathbf{K}}_{eq,(m,n),k}$ denote the $(m_0 + \ell) \times \ell$ equivalent linear damping and stiffness matrices, which account for the nonlinearity of the nonlinear system of Eq. (2.42), and are both time and frequency dependent. Continuing with the application of the statistical linearization method, the error function $\boldsymbol{\varepsilon}$ is formed as the difference between the original nonlinear system of Eq. (2.42), and its linear equivalent Eq. (2.44), i.e.,

$$\begin{aligned} \boldsymbol{\varepsilon} = {} & \bar{\mathbf{\Phi}}_{\mathbf{x}}\left(\sum_{(m,n)}\sum_{k}\mathbf{x}_{(m,n),k}, \sum_{(m,n)}\sum_{k}\dot{\mathbf{x}}_{(m,n),k}\right) \\ & + \bar{\mathbf{C}}_{\mathbf{x}}\sum_{(m,n)}\sum_{k}\dot{\mathbf{x}}_{(m,n),k} + \bar{\mathbf{K}}_{\mathbf{x}}\sum_{(m,n)}\sum_{k}\mathbf{x}_{(m,n),k} \\ & - \sum_{(m,n)}\sum_{k}\bar{\mathbf{C}}_{eq,(m,n),k}\dot{\mathbf{x}}_{(m,n),k} - \sum_{(m,n)}\sum_{k}\bar{\mathbf{K}}_{eq,(m,n),k}\mathbf{x}_{(m,n),k}. \end{aligned} \tag{2.45}$$

It is noted that for the formulation of Eq. (2.45), Eq. (2.42) is also expressed in terms of the LSW representation of Eq. (2.8). Then, the error function Eq. (2.45) is minimized by considering the orthogonality properties of the monochromatic functions at a given frequency band and time

location (see Eqs. (2.11-2.12)). Specifically, Eq. (2.45) is first post-multiplied by the transpose of the response displacement vector $\mathbf{x}_{(m,n),k}$. Subsequently, integrating with respect to time and ensemble averaging results in zero average error, i.e.,

$$\mathbb{E}\Bigg[\int_{\frac{kT_0}{n-m}}^{\frac{(k+1)T_0}{n-m}} \bar{\mathbf{\Phi}}_{\mathbf{x}}\left(\sum_{(m,n)}\sum_{k}\mathbf{x}_{(m,n),k}, \sum_{(m,n)}\sum_{k}\dot{\mathbf{x}}_{(m,n),k}\right)\mathbf{x}_{(m,n),k}^{\mathrm{T}}\mathrm{dt} + (\bar{\mathbf{C}}_{\mathbf{x}} - \bar{\mathbf{C}}_{eq,(m,n),k})\int_{\frac{kT_0}{n-m}}^{\frac{(k+1)T_0}{n-m}} \dot{\mathbf{x}}_{(m,n),k}\mathbf{x}_{(m,n),k}^{\mathrm{T}}\mathrm{dt} + (\bar{\mathbf{K}}_{\mathbf{x}} - \bar{\mathbf{K}}_{eq,(m,n),k})\int_{\frac{kT_0}{n-m}}^{\frac{(k+1)T_0}{n-m}} \mathbf{x}_{(m,n),k}\mathbf{x}_{(m,n),k}^{\mathrm{T}}\mathrm{dt}\Bigg] = \mathbf{0}. \tag{2.46}$$

In a similar manner, Eq. (2.45) also yields

$$\mathbb{E}\Bigg[\int_{\frac{kT_0}{n-m}}^{\frac{(k+1)T_0}{n-m}} \bar{\mathbf{\Phi}}_{\mathbf{x}}\left(\sum_{(m,n)}\sum_{k}\dot{\mathbf{x}}_{(m,n),k}, \sum_{(m,n)}\sum_{k}\dot{\mathbf{x}}_{(m,n),k}\right)\dot{\mathbf{x}}_{(m,n),k}^{\mathrm{T}}\mathrm{dt} + (\bar{\mathbf{C}}_{\mathbf{x}} - \bar{\mathbf{C}}_{eq,(m,n),k})\int_{\frac{kT_0}{n-m}}^{\frac{(k+1)T_0}{n-m}} \dot{\mathbf{x}}_{(m,n),k}\dot{\mathbf{x}}_{(m,n),k}^{\mathrm{T}} + (\bar{\mathbf{K}}_{\mathbf{x}} - \bar{\mathbf{K}}_{eq,(m,n),k})\int_{\frac{kT_0}{n-m}}^{\frac{(k+1)T_0}{n-m}} \mathbf{x}_{(m,n),k}\dot{\mathbf{x}}_{(m,n),k}^{\mathrm{T}}\Bigg] = \mathbf{0}. \tag{2.47}$$

Further, Eqs. (2.46) and (2.47) can be equivalently written as

$$\mathbb{E}\Bigg[\int_{\frac{kT_0}{n-m}}^{\frac{(k+1)T_0}{n-m}} \bar{\mathbf{\Phi}}_{\mathbf{x}}\left(\sum_{(m,n)}\sum_{k}\mathbf{x}_{(m,n),k}, \sum_{(m,n)}\sum_{k}\dot{\mathbf{x}}_{(m,n),k}\right)\mathbf{x}_{(m,n),k}^{\mathrm{T}}\mathrm{dt}\Bigg] + 4\pi(\bar{\mathbf{K}}_{\mathbf{x}} - \bar{\mathbf{K}}_{eq,(m_i,n_i),k})\mathbf{S}^{\mathbf{xx}}_{(m_i,n_i),k} = \mathbf{0} \tag{2.48}$$

and

$$\mathbb{E}\left[\int_{\frac{kT_0}{n-m}}^{\frac{(k+1)T_0}{n-m}} \bar{\mathbf{\Phi}}_{\mathbf{x}}\left(\sum_{(m,n)}\sum_{k}\dot{\mathbf{x}}_{(m,n),k},\sum_{(m,n)}\sum_{k}\dot{\mathbf{x}}_{(m,n),k}\right)\dot{\mathbf{x}}^{\mathrm{T}}_{(m,n),k}\mathrm{dt}\right] +4\pi(\bar{\mathbf{C}}_{\mathbf{x}}-\bar{\mathbf{C}}_{eq,(m_i,n_i),k})\mathbf{S}^{\dot{\mathbf{x}}\dot{\mathbf{x}}}_{(m_i,n_i),k}=\mathbf{0}. \tag{2.49}$$

Eqs. (2.48) and (2.49) connect, in essence, the localized in frequency and time intervals $m\Delta\omega \leq \omega < n\Delta\omega$ and $\frac{kT_0}{n-m} \leq t < \frac{(k+1)T_0}{n-m}$, response EPS $\mathbf{S}^{\dot{\mathbf{x}}\dot{\mathbf{x}}}_{(m_i,n_i),k}$ and $\mathbf{S}^{\mathbf{xx}}_{(m_i,n_i),k}$, with the corresponding localized equivalent linear elements $\bar{\mathbf{C}}_{eq,(m,n),k}$ and $\bar{\mathbf{K}}_{eq,(m,n),k}$. Furthermore, taking into account Eqs. (2.13-2.18), $\mathbf{S}^{\dot{\mathbf{x}}\dot{\mathbf{x}}}_{(m_i,n_i),k}$ in Eq. (2.49) can be replaced by $\mathbf{S}^{\mathbf{xx}}_{(m_i,n_i),k}$. In this regard, Eqs. (2.48) and (2.49), together with Eq. (2.41), form a coupled system of nonlinear equations to be solved for determining $\bar{\mathbf{C}}_{eq,(m,n),k}$ and $\bar{\mathbf{K}}_{eq,(m,n),k}$, and the response EPS $\mathbf{S}^{\mathbf{xx}}_{(m_i,n_i),k}$. For the solution of the coupled system of equations, the following iterative scheme can be applied (Spanos and Kougioumtzoglou, 2012; Kong et al., 2014b). First, initial values for the equivalent elements $\bar{\mathbf{C}}_{eq,(m,n),k}$ and $\bar{\mathbf{K}}_{eq,(m,n),k}$ are considered, and solving Eq. (2.41), initial values for $\mathbf{S}^{\mathbf{xx}}_{(m_i,n_i),k}$ are derived. Then, the latter is used in conjunction with Eqs. (2.48-2.49) for updating the values of the equivalent elements $\bar{\mathbf{C}}_{eq,(m,n),k}$ and $\bar{\mathbf{K}}_{eq,(m,n),k}$. The process repeats until convergence.

Next, considering the case of polynomial kind nonlinearities, the described statistical linearization methodology results in closed form solutions for determining the equivalent linear elements. This assumption is considered not only for facilitating the ensuing derivation of the closed form solutions, i.e., for simplicity reasons, but also due to its practical merit, as nonlinearities of this kind are often met in structural engineering applications (Roberts and Spanos, 2003; Kong et al., 2014b, 2016). In this regard, considering a redundant coordinates modeling of the equations of motion

given by Eq. (2.19), the cubic nonlinearity ℓ vector is written in the form

$$\mathbf{\Phi}_{\mathbf{x}} = \begin{bmatrix} \varepsilon_1 k_1 x_1^3 \\ \vdots \\ \varepsilon_\ell k_\ell x_\ell^3 \end{bmatrix} + \begin{bmatrix} \lambda_1 c_1 \dot{x}_1^3 \\ \vdots \\ \lambda_\ell c_\ell \dot{x}_\ell^3 \end{bmatrix}, \tag{2.50}$$

where ε_i and λ_i, for $i = 1, 2, \ldots, \ell$, denote the magnitude of the nonlinearity for the stiffness and damping of the system, respectively.

Further, considering the augmented nonlinear vector $\bar{\mathbf{\Phi}}_{\mathbf{x}}$ of Eq. (2.43) in conjunction with Eqs. (2.48-2.49), closed form expressions are derived for the augmented equivalent $(m_0+\ell)\times\ell$ elements $\bar{\mathbf{C}}_{eq,(m,n),k}$ and $\bar{\mathbf{K}}_{eq,(m,n),k}$. These are expressed in terms of summations of the response EPS over all (m_i, n_i) at a specific k, and for all pairs of (m, n) and k. Specifically, for the determination of the equivalent damping element, taking into account Eqs. (2.43) and (2.50), Eq. (2.49) implies

$$\mathbf{D}_d + (\bar{\mathbf{C}}_{\mathbf{x}} - \bar{\mathbf{C}}_{eq,(m_i,n_i),k})\tilde{\mathbf{S}}^{\dot{\mathbf{x}}\dot{\mathbf{x}}}_{(m_i,n_i),k} = \mathbf{0}, \tag{2.51}$$

where $\mathbf{D}_d$ is an $(m_0 + \ell) \times \ell$ matrix whose entries depend on the damping nonlinearity, as well as on the system constraints defined in Eq. (2.25); and $\tilde{\mathbf{S}}^{\dot{\mathbf{x}}\dot{\mathbf{x}}}_{(m_i,n_i),k}$ denotes the local auto/cross EPS $\ell \times \ell$ matrix of the response velocity process $\dot{\mathbf{x}}_{(m,n),k}$. It is noted that, in contrast to the standard linearization approach of Ref. Kong et al. (2014b) where the corresponding local auto/cross EPS matrix is diagonal, matrix $\tilde{\mathbf{S}}^{\dot{\mathbf{x}}\dot{\mathbf{x}}}_{(m_i,n_i),k}$ of Eq. (2.51) potentially has some non-zero off-diagonal entries. This is due to the redundant DOFs employed in the system modeling. Specifically, the dependence between the redundant DOFs which form the coordinates vector $\mathbf{x}$ implies linear dependence between some of the columns of matrix $\tilde{\mathbf{S}}^{\dot{\mathbf{x}}\dot{\mathbf{x}}}_{(m_i,n_i),k}$. Therefore, $\tilde{\mathbf{S}}^{\dot{\mathbf{x}}\dot{\mathbf{x}}}_{(m_i,n_i),k}$ is singular, and thus, in order to derive a closed form expression for the equivalent damping element, a special treatment is required for solving Eq. (2.51).

In this regard, taking into account Eq. (2.3), Eq. (2.51) implies

$$\begin{aligned}\bar{\mathbf{C}}_{eq,(m_i,n_i),k} &= \mathbf{D}_d \left(\tilde{\mathbf{S}}^{\dot{\mathbf{x}}\dot{\mathbf{x}}}_{(m_i,n_i),k}\right)^{+} + \bar{\mathbf{C}}_{\mathbf{x}} \\ &+ \left\{\left((\mathbf{I}_\ell - \left((\tilde{\mathbf{S}}^{\dot{\mathbf{x}}\dot{\mathbf{x}}}_{(m_i,n_i),k})^{\mathrm{T}}\right)^{+} (\tilde{\mathbf{S}}^{\dot{\mathbf{x}}\dot{\mathbf{x}}}_{(m_i,n_i),k})^{\mathrm{T}}\right)\mathbf{Y}_1\right\}^{\mathrm{T}},\end{aligned} \tag{2.52}$$

where $\mathbf{Y}_1$ is a $(m_0+\ell)\times\ell$ matrix of arbitrary elements. In a similar manner, taking into account Eqs. (2.43) and (2.50), Eq. (2.49) yields

$$\begin{aligned}\bar{\mathbf{K}}_{eq,(m_i,n_i),k} &= \mathbf{D}_s \left(\tilde{\mathbf{S}}^{\mathbf{xx}}_{(m_i,n_i),k}\right)^{+} + \bar{\mathbf{K}}_{\mathbf{x}} \\ &+ \left\{\left((\mathbf{I}_\ell - \left((\tilde{\mathbf{S}}^{\mathbf{xx}}_{(m_i,n_i),k})^{\mathrm{T}}\right)^{+} (\tilde{\mathbf{S}}^{\mathbf{xx}}_{(m_i,n_i),k})^{\mathrm{T}}\right)\mathbf{Y}_2\right\}^{\mathrm{T}}.\end{aligned} \tag{2.53}$$

In this case, $\mathbf{D}_s$ is an $(m_0+\ell)\times\ell$ matrix whose entries depend on the stiffness nonlinearity and the constraints of Eq. (2.25), whereas $\tilde{\mathbf{S}}^{\mathbf{xx}}_{(m_i,n_i),k}$ denotes the local auto/cross EPS $\ell\times\ell$ matrix of the response displacement $\mathbf{x}_{(m,n),k}$; $\mathbf{Y}_2$ is a $(m_0+\ell)\times\ell$ matrix of arbitrary elements.

Clearly, due to the arbitrary matrices $\mathbf{Y}_1$ and $\mathbf{Y}_2$, Eqs. (2.52) and (2.53) form a family of solutions, while $\bar{\mathbf{C}}_{eq,(m,n),k}$ and $\bar{\mathbf{K}}_{eq,(m,n),k}$ correspond to the unique damping and stiffness matrices of the equivalent linear system defined in Eq. (2.44). However, taking into account that the M-P generalized matrix inverse framework employed in the derivation of Eqs. (2.52) and (2.53) corresponds, in essence, to the solution of a quadratic (least squares) optimization problem, it is feasible to select a unique solution for each of the equivalent elements. In this regard, the intuitively simplest solution among the family of solutions, which also coincides with the minimal mean square solution of the quadratic problem above (Campbell and Meyer, 2009), is considered. Thus, setting the arbitrary matrices $\mathbf{Y}_1$ and $\mathbf{Y}_2$ equal to null matrix, Eqs. (2.52) and (2.53) become

$$\bar{\mathbf{C}}_{eq,(m_i,n_i),k} = \mathbf{D}_d \left(\tilde{\mathbf{S}}^{\dot{\mathbf{x}}\dot{\mathbf{x}}}_{(m_i,n_i),k}\right)^{+} + \bar{\mathbf{C}}_{\mathbf{x}} \tag{2.54}$$

and

$$\bar{\mathbf{K}}_{eq,(m_i,n_i),k} = \mathbf{D}_s \left(\tilde{\mathbf{S}}^{\mathbf{xx}}_{(m_i,n_i),k}\right)^{+} + \bar{\mathbf{K}}_{\mathbf{x}}, \tag{2.55}$$

respectively. Clearly, Eqs. (2.54) and (2.55) define a unique solution for the equivalent damping and stiffness elements, respectively. Further, they constitute a generalization of the corresponding results in Ref. Kong et al. (2014b), to account for systems with singular matrices and polynomial kind nonlinearities, subjected to non-stationary excitation.

2.4 Numerical examples

2.4.1 Non-stationary stochastic excitation

The considered in the ensuing numerical examples MDOF systems, are subjected to non-stationary stochastic excitation described by non-separable, evolutionary power spectra of the form

$$S(\omega,t) = S_0\left(\frac{\omega}{5\pi}\right)^2 \exp(-c_0 t)t^2 \exp\left(-\left(\frac{\omega}{5\pi}\right)^2 t\right), \tag{2.56}$$

where $S_0, c_0 \in \mathbb{R}$. Eq. (2.56), firstly introduced in Ref. Spanos and Solomos (1983), is used as an indicative seismic excitation, since it encloses the main "build-up" and "die-off" characteristics of the ground motion, while its dominant frequency decreases with time (Beck and Papadimitriou, 1993; Tubaldi and Kougioumtzoglou, 2015; Fragkoulis et al., 2019). The spectral representation method is employed for deriving compatible to the EPS of Eq. (2.56) realizations (Liang et al. (2007)) and the response EPS is obtained by averaging the mean square magnitude of the corresponding wavelet coefficients (Spanos and Kougioumtzoglou, 2012), i.e.,

$$S(\omega,t_k) = \frac{T_0}{2\pi(n-m)}\mathrm{E}\left[\mid W^G_{(m,n),k} \mid^2\right]. \tag{2.57}$$

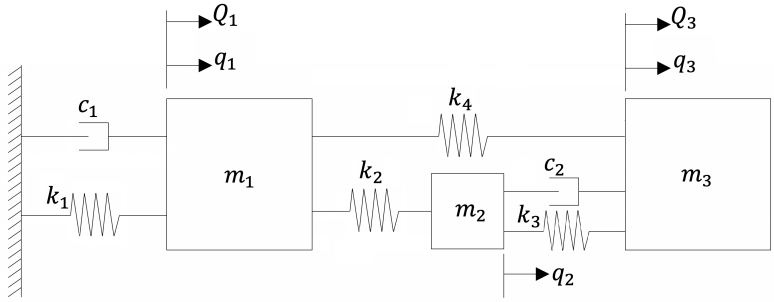

Fig. 2.1: Three degree-of-freedom system subjected to non-stationary stochastic excitation.

The parameter value $n - m = 5$ is used in the ensuing analysis. Moreover, the Mean Instantaneous Frequency (MIF) given by

$$\text{MIF}(t) = \frac{\int_\omega \omega S(t,\omega) d\omega}{\int_\omega S(t,\omega) d\omega} \tag{2.58}$$

is included in the ensuing analysis for capturing the evolution of the "effective instantaneous frequency" for the non-stationary system response (Spanos et al., 2007).

2.4.2 Linear systems with singular matrices

For the assessment of the herein proposed solution framework, the EPS for each DOF of the $3-$DOF linear system depicted in Fig. 2.1, is determined. The system consists of three masses m_1, m_2 and m_3 interconnected with linear springs and dampers. In particular, mass m_1 is connected to the foundation by a linear spring and a linear damper with stiffness and damping coefficients k_1 and c_1, respectively, and to masses m_2 and m_3 by linear springs with stiffness coefficients k_2 and k_4. Further, mass m_2 is connected to mass m_3 by a linear spring of stiffness coefficient k_3 and a linear damper of damping coefficient c_2. The system is subjected to random force $Q_1(t)$ which is applied on mass m_1, and to random force $Q_3(t)$ applied on mass m_3, which are both described by the EPS of Eq. (2.56).

Following, a standard Newtonian approach for the formulation of the system governing equations of motion, and considering the (generalized) coordinates vector $\mathbf{q}^{\mathrm{T}} = \begin{bmatrix} q_1 & q_2 & q_3 \end{bmatrix}$, the mass,

damping and stiffness matrices are given by

$$\mathbf{M_q} = \begin{bmatrix} m_1 & 0 & 0 \\ 0 & m_2 & 0 \\ 0 & 0 & m_3 \end{bmatrix}, \mathbf{C_q} = \begin{bmatrix} c_1 & 0 & 0 \\ 0 & c_2 & -c_2 \\ 0 & -c_2 & c_2 \end{bmatrix} \tag{2.59}$$

and

$$\mathbf{K_q} = \begin{bmatrix} k_1 + k_2 + k_4 & -k_2 & -k_4 \\ -k_2 & k_2 + k_3 & -k_3 \\ -k_4 & -k_3 & k_3 + k_4 \end{bmatrix}, \tag{2.60}$$

respectively. Next, considering a relative displacement modeling, the coordinates vector $\mathbf{y}^{\mathrm{T}} = \begin{bmatrix} y_1 & y_2 & y_3 \end{bmatrix}$ is defined. Vector $\mathbf{y}$ denotes the relative displacement between the adjacent DOFs (Roberts and Spanos, 2003), i.e.,

$$y_1 = q_1,\ y_2 = q_2 - q_1,\ y_3 = q_3 - q_2. \tag{2.61}$$

Thus, the mass, damping and stiffness matrices in the relative coordinates system take the form

$$\mathbf{M} = \begin{bmatrix} m_1 & 0 & 0 \\ m_2 & m_2 & 0 \\ m_3 & m_3 & m_3 \end{bmatrix}, \mathbf{C} = \begin{bmatrix} c_1 & 0 & 0 \\ 0 & 0 & -c_2 \\ 0 & 0 & c_2 \end{bmatrix} \tag{2.62}$$

and

$$\mathbf{K} = \begin{bmatrix} k_1 & -k_2 - k_4 & -k_4 \\ 0 & k_2 & -k_3 \\ 0 & k_4 & k_3 + k_4 \end{bmatrix}, \tag{2.63}$$

respectively. Finally, the excitation vector $\mathbf{Q}(t)$ is given by

$$\mathbf{Q} = \begin{bmatrix} Q_1(t) \\ 0 \\ Q_3(t) \end{bmatrix}, \tag{2.64}$$

where $Q_1(t) = Q_3(t) = Q(t)$. Further, assuming the system and excitation parameter values $m_1 = m_2 = m_3 = 1$, $c_1 = c_2 = 4.3$, $c_3 = 1.4$, $k_1, k_2, k_3 = 256$, $k_4 = 64$ and $S_0 = 10$, $c_0 = 0.15$, and resorting to Eq. (2.33-2.34), the generalized response spectra are estimated. The response EPS for each DOF of the system of Fig. 2.1 is depicted in Figs. 2.2a-2.2c. Also, the MIF of Eq. (2.58) is included for each DOF.

Next, the herein proposed methodology for deriving the EPS of the system response is applied to the system of Fig. 2.1. In this regard, adopting a redundant coordinates modeling of the equations of motion, the $3-$DOF system is decomposed into its component subsystems, as shown in Fig. 2.3. This is attained by considering the coordinates vector

$$\mathbf{x} = \begin{bmatrix} \bar{x}_1 \\ x_2 \\ \bar{x}_3 \\ x_4 \\ \bar{x}_5 \end{bmatrix}, \tag{2.65}$$

where $\bar{x}_1, \bar{x}_3$ and $\bar{x}_5$ denote the displacements of masses m_1, m_2 and m_3, respectively; and x_2, x_4 correspond to the redundant DOFs which, in essence, account for the constraints connecting the partial subsystems (see Fig. 2.3). It holds

$$x_1 + d = x_2 \tag{2.66}$$

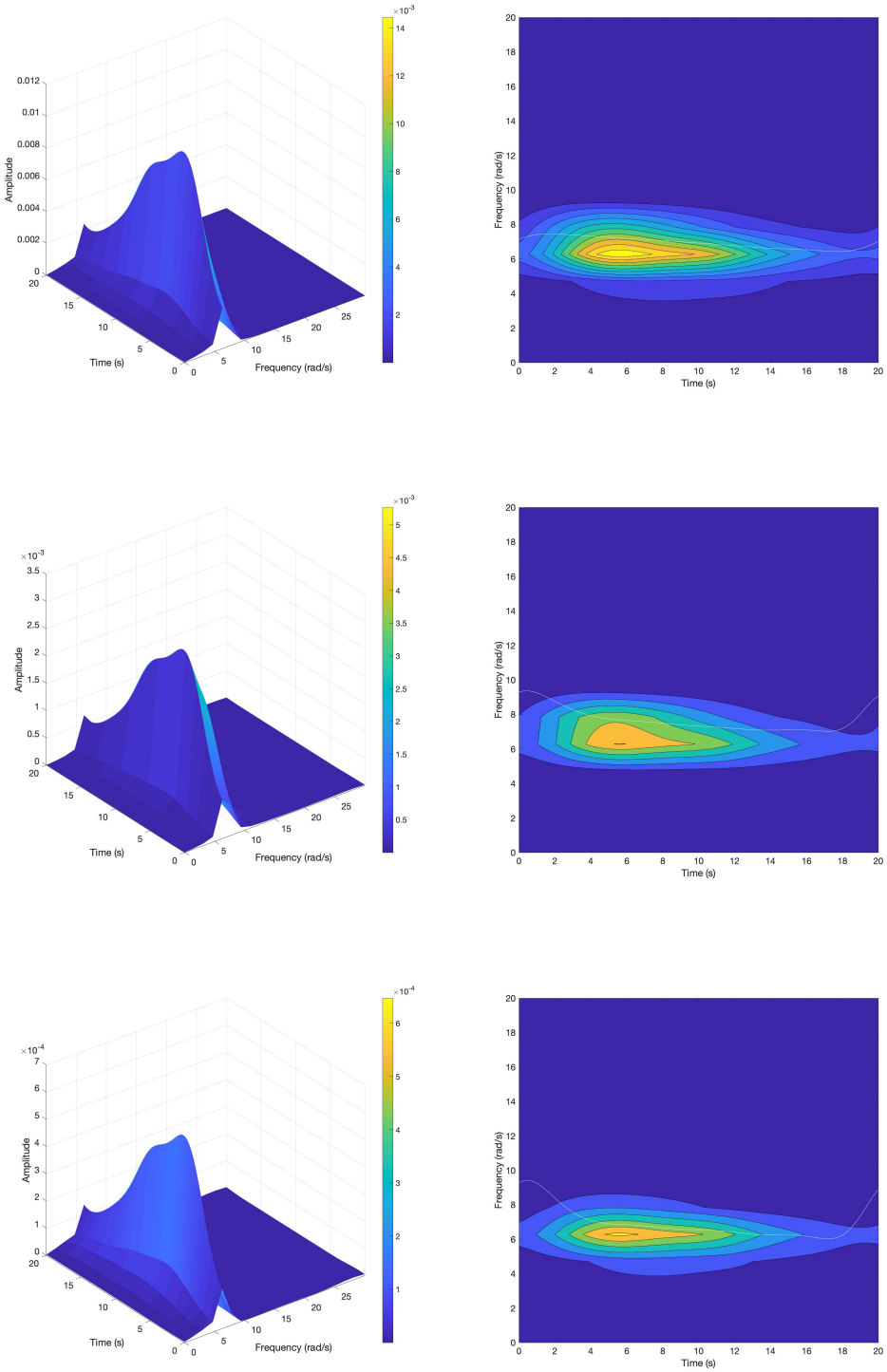

Fig. 2.2: Response EPS of the linear system of Fig. 2.1, subject to non-stationary excitation ($S_0 = 10, c_0 = 0.15$). (a) 1st DOF y_1 of the system. (b) 2nd DOF y_2 of the system. (c) 3rd DOF y_3 of the system.

and

$$x_2 + x_3 + d = x_4, \tag{2.67}$$

where d is the physical length of each mass $m_i, i = 1, 2, 3$. Taking into account the geometry of the system in Fig. 2.3, as well as Eqs. (2.66-2.67), the expressions

$$\bar{x}_1 + l_{1,0} + d = x_2 \tag{2.68}$$

and

$$x_2 + \bar{x}_3 + l_{3,0} + d = x_4, \tag{2.69}$$

where l_i is the unstretched length of the spring for the mass m_i ($i = 1, 2, 3$), form a set of equations which connect the system constraints with the redundant coordinates. Specifically, differentiating twice with respect to time Eqs. (2.68)-(2.69), the 2×5 matrix $\mathbf{A}$ of Eq. (2.25) and the $2-$vector $\mathbf{b}$ of Eq. (2.26) take the form

$$\mathbf{A} = \begin{bmatrix} 1 & -1 & 0 & 0 & 0 \\ 0 & 1 & 1 & -1 & 0 \end{bmatrix} \tag{2.70}$$

and

$$\mathbf{b} = \begin{bmatrix} 0 \\ 0 \end{bmatrix}, \tag{2.71}$$

respectively.

In this regard, the equations of motion are formed, and the augmented mass, damping and stiffness

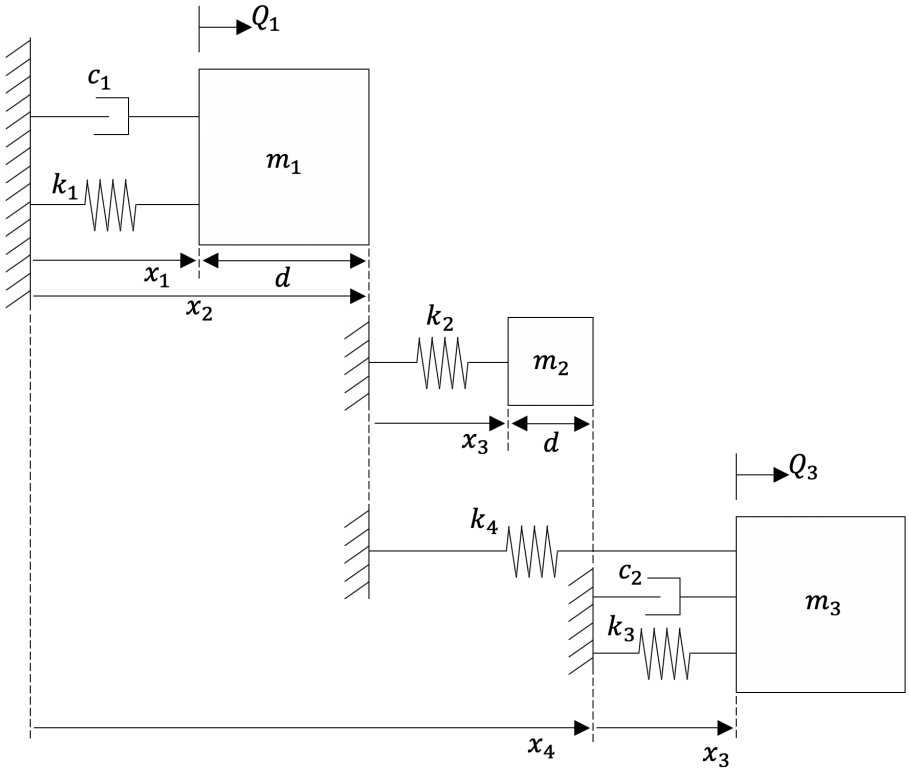

Fig. 2.3: Modeling the three degree-of-freedom system of Fig. 2.1 by using redundant coordinates.

7×5 matrices of Eqs. (2.21-2.23) become

$$\bar{\mathbf{M}}_{\mathbf{x}} = \begin{bmatrix} 0.4 & 0.2 & 0.2 & 0.2 & 0.2 \\ 0.4 & 0.2 & 0.2 & 0.2 & 0.2 \\ -0.2 & 0.4 & 0.4 & 0.4 & 0.4 \\ 0.2 & 0.6 & 0.6 & 0.6 & 0.6 \\ 0 & 0 & 0 & 1 & 1 \\ 1 & -1 & 0 & 0 & 0 \\ 0 & 1 & 1 & -1 & 0 \end{bmatrix}, \bar{\mathbf{C}}_{\mathbf{x}} = \begin{bmatrix} 1.72 & 0 & 0 & 0 & 0 \\ 1.72 & 0 & 0 & 0 & 0 \\ -0.86 & 0 & 0 & 0 & 0 \\ 0.86 & 0 & 0 & 0 & 0 \\ 0 & 0 & 0 & 0 & 4.30 \\ 0 & 0 & 0 & 0 & 0 \\ 0 & 0 & 0 & 0 & 0 \end{bmatrix} \tag{2.72}$$

and

$$\bar{\mathbf{K}}_{\mathbf{x}} = \begin{bmatrix} 102.4 & 12.8 & -51.2 & -12.8 & -12.8 \\ 102.4 & 12.8 & -51.2 & -12.8 & -12.8 \\ -51.2 & -38.4 & 153.6 & 38.4 & 38.4 \\ 51.2 & -25.6 & 102.4 & 25.6 & 25.6 \\ 0 & -64 & 0 & 64 & 320 \\ 0 & 0 & 0 & 0 & 0 \\ 0 & 0 & 0 & 0 & 0 \end{bmatrix}, \tag{2.73}$$

respectively; whereas the augmented excitation vector of Eq. (2.24) takes the form

$$\bar{\mathbf{Q}}_{\mathbf{x}} = \begin{bmatrix} 0.6Q(t) \\ 0.6Q(t) \\ 0.2Q(t) \\ 0.8Q(t) \\ Q(t) \\ 0 \\ 0 \end{bmatrix}. \tag{2.74}$$

Next, the 7×5 matrix $\mathbf{R}_{\mathbf{x}}$ is formed, for which $\text{rank}(\mathbf{R}_{\mathbf{x}}) = 5$. Therefore, utilizing the input-output expression of Eq. (2.41), and taking into account the M-P HW-FRF of Eq. (2.40), the response EPS for $\bar{x}_1$, $\bar{x}_3$ and $\bar{x}_5$ of the equivalent linear system, is obtained in an analytical manner. The corresponding results, along with the MIF of Eq. (2.58), are plotted in Figs. 2.4a, 2.4b and 2.4c. Comparing Fig. 2.4a with Fig. 2.2a, Fig. 2.4b with Fig. 2.2b, and Fig. 2.4c with Fig. 2.2c, it is seen that the results obtained by applying the herein proposed M-P inverse framework are in agreement with those obtained by following the standard formulation. This is also deduced by Fig. 2.5, where the response EPS for each DOF of the two systems (Fig. 2.1 and Fig. 2.3) is determined for both formulations, and is plotted at different time instants ($t = 5.8s$ and $t = 12s$). In this regard, it can

be argued that the herein proposed approach constitutes a generalized matrix inverses extension of the harmonic-wavelet-based technique of Ref. Kong et al. (2014b).

2.4.3 Nonlinear systems with singular matrices

The $2-$DOF chain-like structural nonlinear system of rigid masses m_1 and m_2 that is shown in Fig. 2.6 is considered for demonstrating the efficiency of the linearization scheme. Mass m_1 is connected to the foundation by a nonlinear spring of linear-plus-cubic type, and a nonlinear damper of the same nonlinearity type. Further, mass m_1 is connected to mass m_2 by corresponding linear spring and damper with stiffness and damping coefficients k_2 and c_2, respectively. The nonlinearity magnitude of the nonlinear spring is denoted by ε_1, whereas λ_1 denotes the nonlinearity magnitude of the nonlinear damper. The system is subjected to non-stationary stochastic excitations $\mathbf{Q}_1(t)$ and $\mathbf{Q}_2(t)$, both described by a non-separable EPS of the form given by Eq. (2.56).

Next, the system governing equations of motion are derived. In this regard, the generalized coordinates y_1, y_2 are utilized, and relative displacements are introduced for facilitating the ensuing analysis. Thus, the mass, damping and stiffness matrices for the system of Fig. 2.6 are given by (Roberts and Spanos, 2003)

$$\mathbf{M} = \begin{bmatrix} m_1 & 0 \\ m_2 & m_2 \end{bmatrix}, \ \mathbf{C} = \begin{bmatrix} c_1 & -c_2 \\ 0 & c_2 \end{bmatrix} \tag{2.75}$$

and

$$\mathbf{K} = \begin{bmatrix} k_1 & -k_2 \\ 0 & k_2 \end{bmatrix}, \tag{2.76}$$

respectively. Further, the system nonlinearity is written in the vector form

$$\mathbf{\Phi} = \begin{bmatrix} \varepsilon_1 k_1 y_1^3 + \lambda_1 c_1 \dot{y}_1^3 \\ 0 \end{bmatrix} \tag{2.77}$$

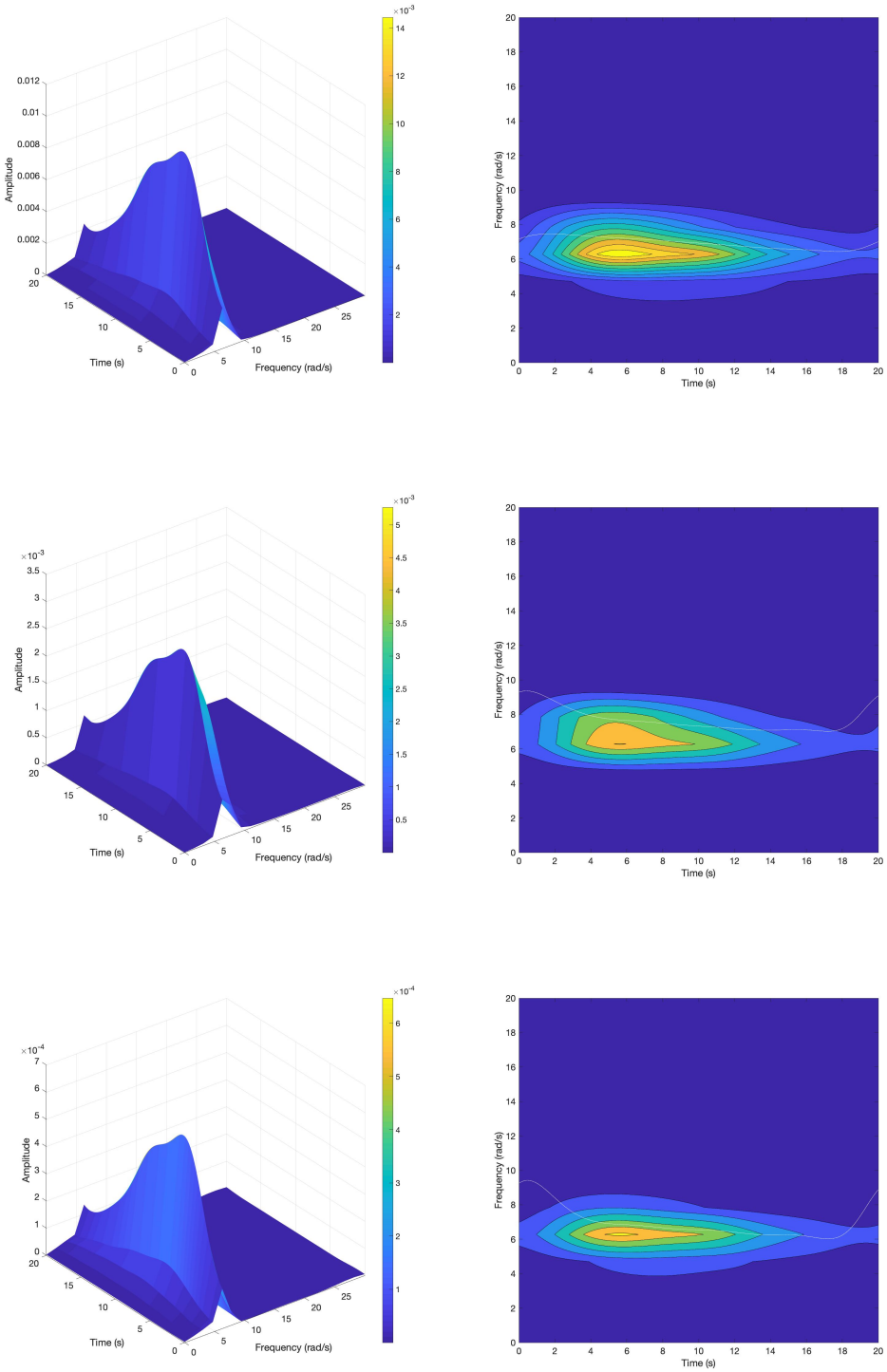

Fig. 2.4: Response EPS of the linear system of Fig. 2.3, subject to non-stationary excitation ($S_0 = 10, c_0 = 0.15$). (a) 1st DOF $\bar{x}_1$ of the system. (b) 3rd DOF $\bar{x}_3$ of the system. (c) 5th DOF $\bar{x}_5$ of the system.

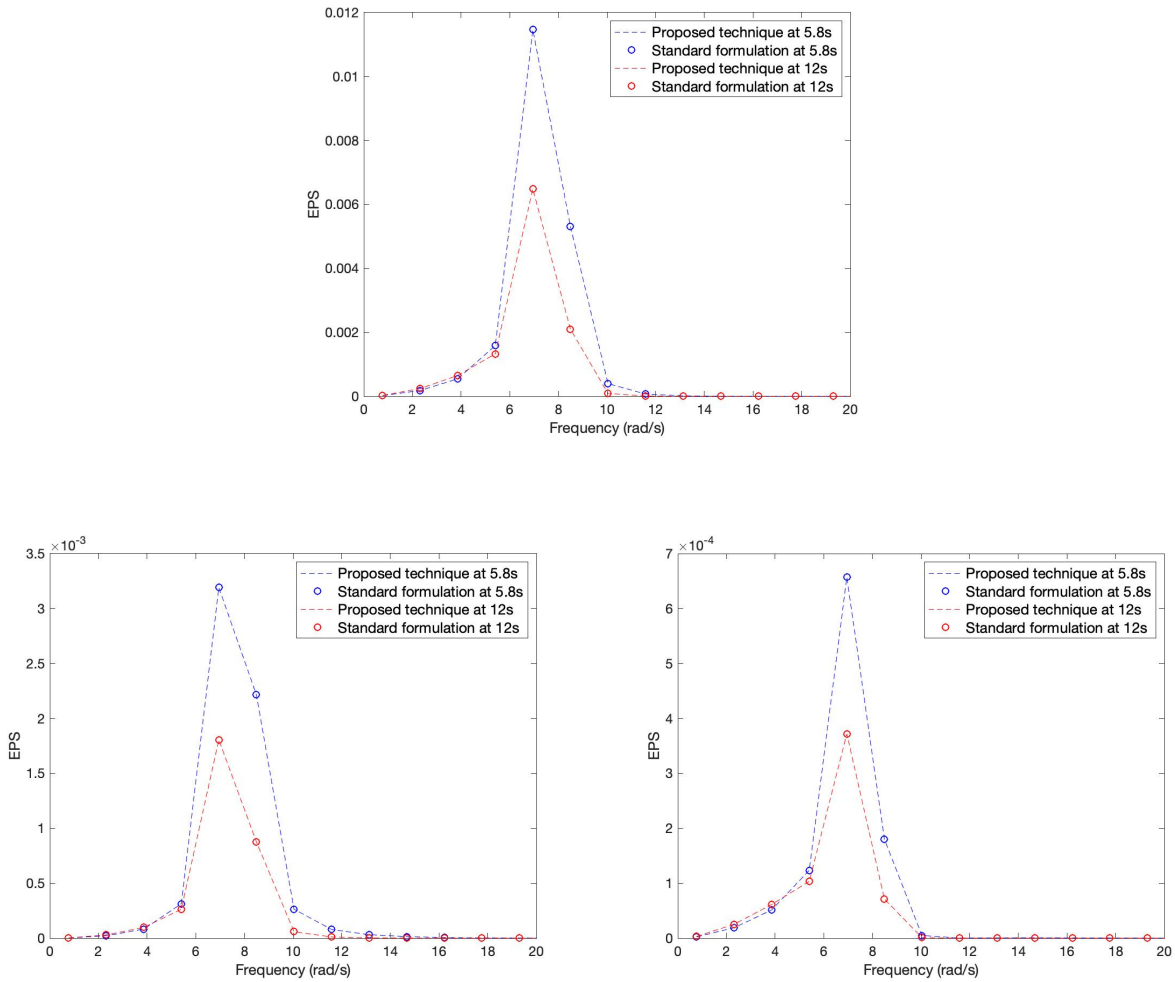

Fig. 2.5: Response EPS of the linear system of Fig. 2.3 at time instants $t = 5.8s$ and $t = 12s$, subject to non-stationary stochastic excitation ($S_0 = 10, c_0 = 0.15$). Comparison between standard formulation and the proposed technique. (a) 1^{st} DOF (y_1 vis-à-vis $\bar{x}_1$); (b) 2^{nd} DOF (y_2 vis-à-vis $\bar{x}_3$); (c) 3^{rd} DOF (y_3 vis-à-vis $\bar{x}_5$).

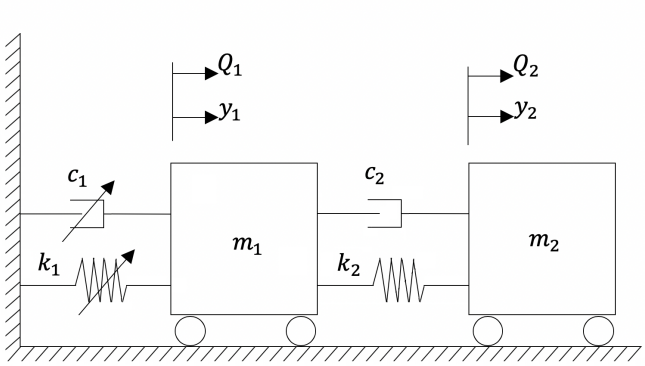

Fig. 2.6: Two degree-of-freedom nonlinear structural system subjected to non-stationary stochastic excitation.

and the system excitation is

$$\mathbf{Q}(t) = \begin{bmatrix} Q_1 \\ Q_2 \end{bmatrix}. \tag{2.78}$$

Then, the standard linearization approach of Ref. Kong et al. (2014b) is followed for determining the response EPS. In this regard, the equivalent linear elements $\mathbf{C}_{eq,(m_i,n_i),k}$ and $\mathbf{K}_{eq,(m_i,n_i),k}$ are given by

$$\mathbf{C}_{eq,(m_i,n_i),k} = 6(n-m)\Delta\omega \begin{bmatrix} \lambda_1 c_1 \sum_j S^{\dot{y}_1\dot{y}_1}_{(m_j,n_j),k} & 0 \\ 0 & 0 \end{bmatrix} + \mathbf{C} \tag{2.79}$$

and

$$\mathbf{K}_{eq,(m_i,n_i),k} = 6(n-m)\Delta\omega \begin{bmatrix} \varepsilon_1 k_1 \sum_j S^{y_1 y_1}_{(m_j,n_j),k} & 0 \\ 0 & 0 \end{bmatrix} + \mathbf{K}, \tag{2.80}$$

respectively. Further, the system parameter values $m_i = 1$, $c_i = 4.3$ and $k_i = 256$ $(i = 1, 2)$, and the nonlinearity magnitude parameters $\varepsilon_1 = 2, \lambda_1 = 0.5$ are considered. It is also assumed for simplicity that $\mathbf{Q}_1(t) = \mathbf{Q}_2(t) = \mathbf{Q}(t)$ and the excitation parameter values are $S_0 = 10$ and $c_0 = 0.15$. Thus, solving the nonlinear set of equations formed by Eqs. (2.79-2.80) and Eqs. (2.33-2.34), leads to determining the evolutionary response power spectrum for the $2-$DOF system of Fig. 2.6. Figs. 2.7a and 2.7b represent the results for the generalized coordinates y_1 and y_2, also including the corresponding MIF.

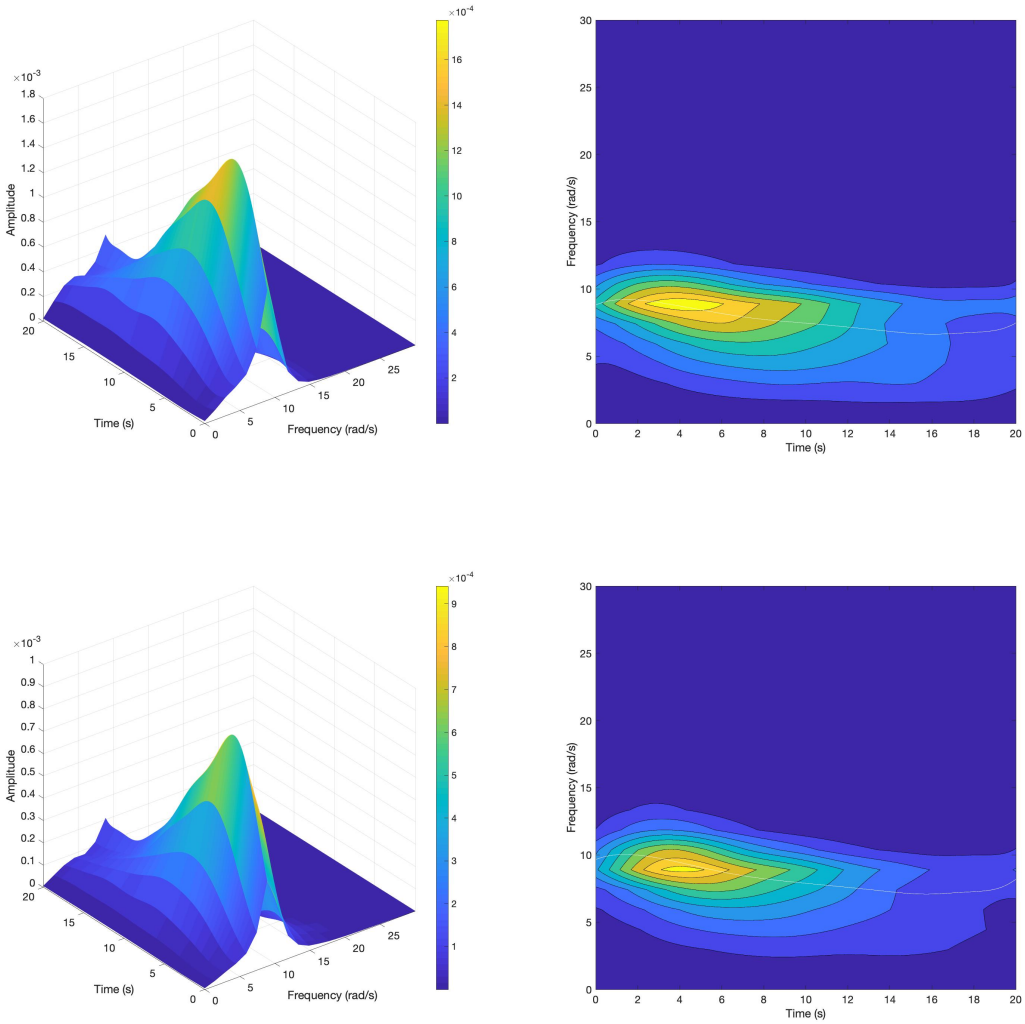

Fig. 2.7: Response EPS of the nonlinear structural system of Fig. 2.6, subject to non-stationary stochastic excitation ($S_0 = 10, c_0 = 0.15$). (a) 1^{st} DOF y_1 ($\varepsilon_1 = 2, \lambda_1 = 0.5$); (b) 2^{nd} DOF y_2.

Next, employing a redundant coordinates modeling for the formulation of the system governing equations of motion, the $2-$DOF system of Fig. 2.6 is decomposed in its partial subsystems, as shown in Fig. 2.8. The independent coordinates $\bar{x}_1, x_2$ and $\bar{x}_3$ describe the equations of motion of the two subsystems, which are also connected to each other by the constraint equation

$$x_2 = \bar{x}_1 + l_0 + d, \tag{2.81}$$

where l_0 is the unstreched length of the spring k_1 and d the physical length of mass m_1. Note, in passing, that the equations of motion for the system of Fig. 2.8 are formed in terms of relative coordinates, and thus, the connection between the independent coordinates $\bar{x}_1, \bar{x}_3$ and the generalized coordinates y_1, y_2 for the two different formulations are given by $\bar{x}_1 = y_1$ and $\bar{x}_3 = y_2$, respectively. Further, twice differentiating the system constraint equations, which are described by Eq. (2.81), matrix $\mathbf{A}$ of Eq. (2.25) becomes

$$\mathbf{A} = \begin{bmatrix} 1 & -1 & 0 \end{bmatrix}, \tag{2.82}$$

whereas taking into account Eq. (2.26), $\mathbf{E} = \mathbf{L} = \mathbf{0}$ and $b = 0$.

Deriving the system governing equations of motion, the augmented mass, damping and stiffness matrices of Eqs. (2.21-2.23) take the form

$$\bar{\mathbf{M}}_{\mathbf{x}} = \begin{bmatrix} 0.5 & 0.5 & 0.5 \\ 0.5 & 0.5 & 0.5 \\ 0 & 1 & 1 \\ 1 & -1 & 0 \end{bmatrix}, \; \bar{\mathbf{C}}_{\mathbf{x}} = \begin{bmatrix} 2.15 & 0 & 0 \\ 2.15 & 0 & 0 \\ 0 & 0 & 4.3 \\ 0 & 0 & 0 \end{bmatrix} \tag{2.83}$$

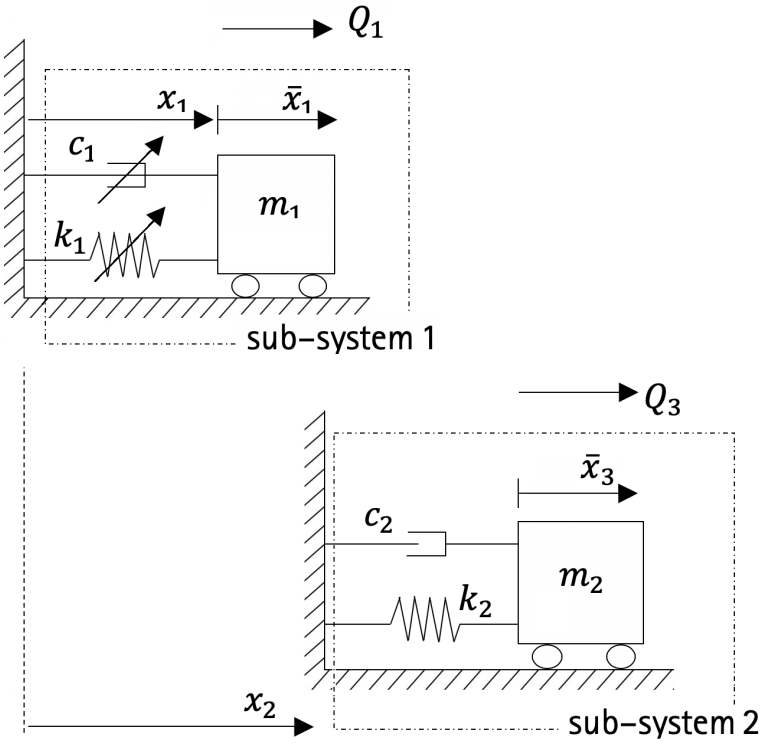

Fig. 2.8: Modeling the two degree-of-freedom system of Fig. 2.6 by using redundant coordinates.

and

$$\bar{\mathbf{K}}_{\mathbf{x}} = \begin{bmatrix} 128 & 0 & 0 \\ 128 & 0 & 0 \\ 0 & 0 & 256 \\ 0 & 0 & 0 \end{bmatrix}, \tag{2.84}$$

respectively. Finally, the augmented system nonlinear vector defined in Eq. (2.43) is given by

$$\bar{\mathbf{\Phi}}_{\mathbf{x}} = \begin{bmatrix} 0.5\varepsilon_1 k_1 \bar{x}_1^3 + 0.5\lambda_1 c_1 \dot{\bar{x}}_1^3 \\ 0.5\varepsilon_1 k_1 \bar{x}_1^3 + 0.5\lambda_1 c_1 \dot{\bar{x}}_1^3 \\ 0 \\ 0 \end{bmatrix}, \tag{2.85}$$

whereas the augmented excitation vector of Eq. (2.24) is given by

$$\bar{\mathbf{Q}}_{\mathbf{x}} = \begin{bmatrix} Q_1 \\ Q_2 \\ Q_2 \\ 0 \end{bmatrix}. \tag{2.86}$$

Taking into account the system nonlinearity of Eq. (2.85), as well as the constraints expression of Eq. (2.81), matrices $\mathbf{D}_d$ and $\tilde{\mathbf{S}}^{\dot{\mathbf{x}}\dot{\mathbf{x}}}_{(m_i,n_i),k}$ in Eq. (2.51) become

$$\mathbf{D}_d = \begin{bmatrix} d_{1,(m,n),k} & d_{1,(m,n),k} & 0 & 0 \\ d_{1,(m,n),k} & d_{1,(m,n),k} & 0 & 0 \\ 0 & 0 & 0 & 0 \\ 0 & 0 & 0 & 0 \end{bmatrix} \tag{2.87}$$

and

$$\tilde{\mathbf{S}}^{\dot{\mathbf{x}}\dot{\mathbf{x}}}_{(m_i,n_i),k} = \begin{bmatrix} s_{1,(m,n),k} & s_{1,(m,n),k} & 0 \\ s_{1,(m,n),k} & s_{1,(m,n),k} & 0 \\ 0 & 0 & s_{3,(m,n),k} \end{bmatrix}, \tag{2.88}$$

respectively, where

$$d_{1,(m,n),k} = \mathbb{E}[(\dot{x}_{1,(m,n),k})^4] + 3 \sum_{(i,j),i\neq m,j\neq n} \mathbb{E}[(\dot{x}_{1,(m,n),k})^2]\mathbb{E}[(\dot{x}_{1,(i,j),k})^2] \tag{2.89}$$

and

$$s_{\rho,(m,n),k} = \mathbb{E}[(\dot{x}_{i,(m,n),k})^2],\ \rho = 1, 3. \tag{2.90}$$

Further, the M-P inverse of matrix $\tilde{\mathbf{S}}^{\dot{\mathbf{x}}\dot{\mathbf{x}}}_{(m_i,n_i),k}$ in Eq. (2.88) is given by Cline (1964)

$$(\tilde{\mathbf{S}}^{\dot{\mathbf{x}}\dot{\mathbf{x}}}_{(m_i,n_i),k})^{+} = \begin{bmatrix} 0.25 s^{-1}_{1,(m,n),k} & 0.25 s^{-1}_{1,(m,n),k} & 0 \\ 0.25 s^{-1}_{1,(m,n),k} & 0.25 s^{-1}_{1,(m,n),k} & 0 \\ 0 & 0 & s^{-1}_{3,(m,n),k} \end{bmatrix}. \tag{2.91}$$

Thus, substituting Eqs. (2.87) and (2.91) into Eq. (2.54), and manipulating, yields

$$\bar{\mathbf{C}}_{eq,(m_i,n_i),k} = 6(n-m)\Delta\omega \begin{bmatrix} \frac{\lambda_1 c_1}{2} \sum_j S^{\dot{\bar{x}}_1 \dot{\bar{x}}_1}_{(m_j,n_j),k} & \frac{\lambda_1 c_1}{2} \sum_j S^{\dot{\bar{x}}_1 \dot{\bar{x}}_1}_{(m_j,n_j),k} & 0 \\ \frac{\lambda_1 c_1}{2} \sum_j S^{\dot{\bar{x}}_1 \dot{\bar{x}}_1}_{(m_j,n_j),k} & \frac{\lambda_1 c_1}{2} \sum_j S^{\dot{\bar{x}}_1 \dot{\bar{x}}_1}_{(m_j,n_j),k} & 0 \\ 0 & 0 & 0 \\ 0 & 0 & 0 \end{bmatrix} + \bar{\mathbf{C}}_{\mathbf{x}}. \tag{2.92}$$

In a similar manner, the augmented equivalent linear stiffness elements are derived in closed form at each frequency band $(n-m)$ and time level k, as functions of the localized response EPS. They are given by

$$\bar{\mathbf{K}}_{eq,(m_i,n_i),k} = 6(n-m)\Delta\omega \begin{bmatrix} \frac{\varepsilon_1 k_1}{2} \sum_j S^{\bar{x}_1 \bar{x}_1}_{(m_j,n_j),k} & \frac{\varepsilon_1 k_1}{2} \sum_j S^{\bar{x}_1 \bar{x}_1}_{(m_j,n_j),k} & 0 \\ \frac{\varepsilon_1 k_1}{2} \sum_j S^{\bar{x}_1 \bar{x}_1}_{(m_j,n_j),k} & \frac{\varepsilon_1 k_1}{2} \sum_j S^{\bar{x}_1 \bar{x}_1}_{(m_j,n_j),k} & 0 \\ 0 & 0 & 0 \\ 0 & 0 & 0 \end{bmatrix} + \bar{\mathbf{K}}_{\mathbf{x}}. \tag{2.93}$$

Noticing that the matrix $\mathbf{R}_{\mathbf{x}}$ of Eq. (2.32) has full rank, and thus, that the M-P HW-FRF of Eq. (2.40) holds, the estimation of the response EPS is attained by resorting to the recursive linearization scheme which is applied to the nonlinear set of Eqs. (2.92-2.93) and Eqs. (2.40-2.41). The linearization process is initialized by considering the linear system response EPS, and continues until convergence. The scheme stops when the maximum values of the percentile difference of the equivalent elements over all frequency bands and time levels become smaller than 10^{-5}. In this

regard, the estimated response EPS for the first DOF $\bar{x}_1$ is depicted in Fig. 2.9a, whereas Fig. 2.9b shows the corresponding EPS for the independent to $\bar{x}_1$, coordinate $\bar{x}_3$. The MIF of Eq. (2.58) is also plotted in the figures for completeness. Comparing Figs. 2.9a and 2.9b with Figs. 2.7a and 2.7b, respectively, it is seen that the corresponding results are in total agreement. This is also highlighted by Fig. 2.10, where the results obtained by applying the standard and alternative approaches are plotted for different time instants ($t = 5s$ and $t = 10s$). Thus, it is concluded that the herein developed M-P harmonic-wavelet-based statistical linearization scheme constitutes a generalization of the results in Ref. Kong et al. (2014b), to account for the case of systems with singular matrices subjected to non-stationary excitation.

2.5 Conclusion

In this paper, a generalized inverse matrix harmonic-wavelet-based technique has been developed for determining the response evolutionary power spectrum (EPS) of stochastically excited multi-degree-of-freedom (MDOF) linear and nonlinear structural systems with singular matrices. The singular matrices appear in the system governing equations of motion due to adopting a redundant coordinates modeling for their formulation. It can be argued, that this approach relates to solutions of reduced computational cost, as well as enhanced modeling flexibility when the problem of forming the equations of motion of complex multibody systems is considered. However, singular matrices also hinder the application of standard solution treatments for estimating the system response EPS. In this regard, resorting to the Moore-Penrose (M-P) matrix inverse theory in conjunction with the generalized harmonic wavelets theory, a solution framework is developed herein for determining the evolutionary response spectra of such systems. Specifically, adopting the locally stationary wavelet representation of a stochastic process, and relying on the theory of the M-P generalized inverse of a singular matrix, an M-P localized in time and frequency, harmonic-wavelet-based frequency response function (M-P HW-FRF) has been constructed. Subsequently, employing the novel M-P HW-FRF, an input-output formula for determining the EPS of the system response has

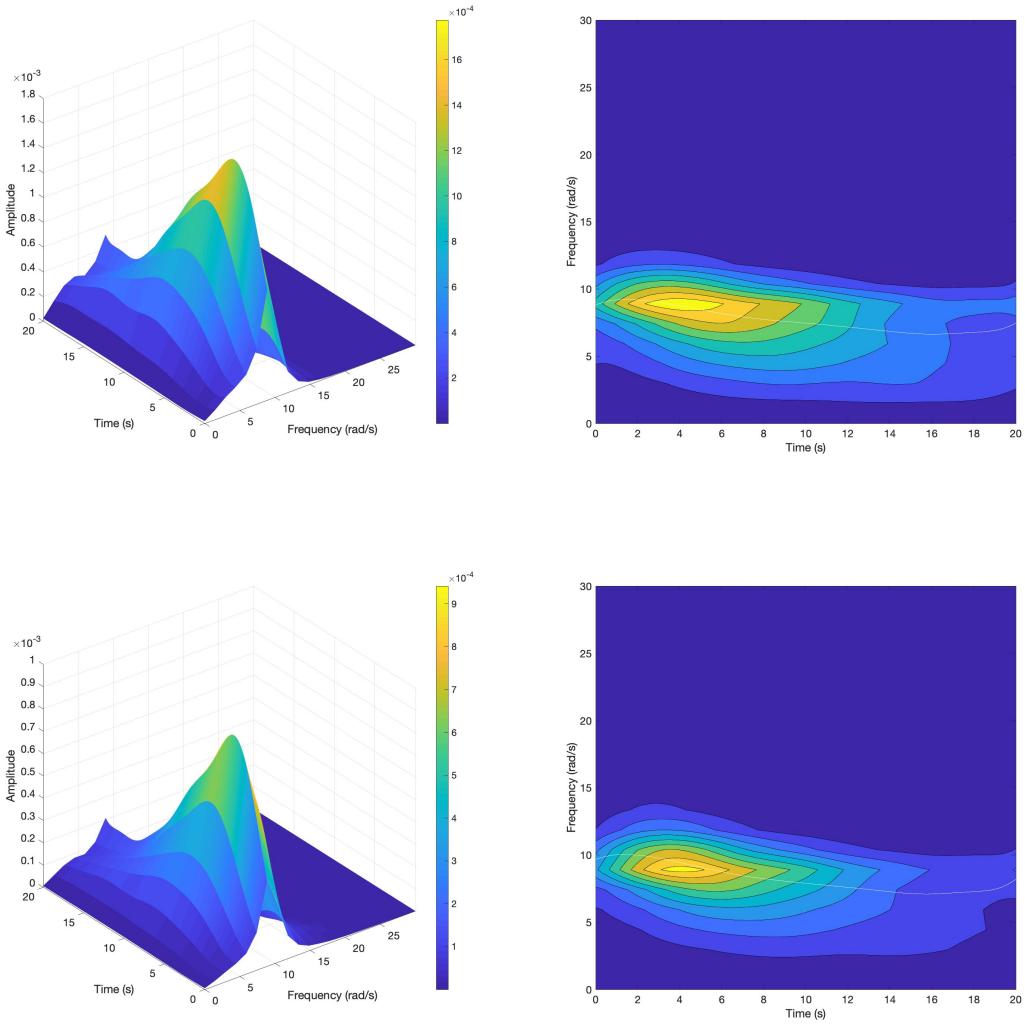

Fig. 2.9: Response EPS of the nonlinear structural system of Fig. 2.8 subject to non-stationary stochastic excitation ($S_0 = 10, c_0 = 0.15$). (a) 1^{st} DOF $\bar{x}_1$ ($\varepsilon_1 = 2, \lambda_1 = 0.5$); (b) 2^{nd} DOF $\bar{x}_3$.

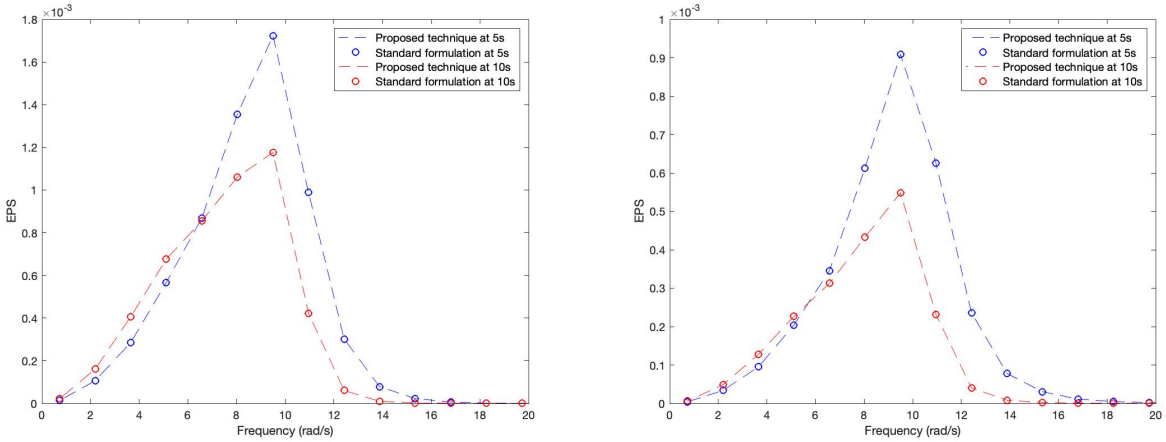

Fig. 2.10: Response EPS of the nonlinear structural system of Figs. 2.6 and 2.8 at time instants $t = 5s$ and $t = 10s$, subject to non-stationary stochastic excitation ($S_0 = 10, c_0 = 0.15$). Comparison between standard formulation and the proposed technique. (a) 1^{st} DOF (y_1 vis-à-vis $\bar{x}_1$); (b) 2^{nd} DOF (y_2 vis-à-vis $\bar{x}_3$).

been derived. This can be construed as a generalization of a recently developed harmonic-wavelet-based input-output formula (Kong et al., 2014b), to account for the case of systems with singular matrices. Further, for the case of nonlinear systems of this kind, a recently derived harmonic-wavelet-based statistical linearization technique (Kong et al., 2014b) has also been generalized. First, an equivalent linear to the original nonlinear system has been defined. Subsequently, closed form solutions have been derived for the time and frequency dependent equivalent linear elements, and the equivalent linear system EPS has been estimated by resorting to the solution of a nonlinear set of equations. A linear and a nonlinear MDOF systems with singular matrices have been considered as numerical examples for assessing the validity of the developed methodology. The applicability of the proposed method to systems subject to a broad category of non-stationary excitations has been highlighted by considering excitations described by evolutionary non-separable spectra.

Acknowledgement

The authors gratefully acknowledge the support and funding from the European Union's Horizon 2020 research and innovation programme under the Marie Skłodowska-Curie grant agreement No 764547.

Conflict of interests

The authors declare that they have no conflict of interest.

Chapter 3

Research article 2: Excitation-response relationships for linear structural systems with singular parameter matrices: A periodized harmonic wavelet perspective

Excitation-response relationships for linear structural systems with singular parameter matrices: A periodized harmonic wavelet perspective

George D. Pasparakis[a], I. A. Kougioumtzoglou [b,*], V. C. Fragkoulis[a], F. Kong[c], M. Beer[a,d,e]

[a]*Institute for Risk and Reliability, Leibniz Universität Hannover, Callinstr. 34, 30167 Hannover, Germany*

[b]*Department of Civil Engineering and Engineering Mechanics, Columbia University, 500 W 120th Street, New York, NY 10027, USA*

[c]*School of Civil Engineering and Architecture, Wuhan University of Technology, China*

[d]*Institute for Risk and Uncertainty and School of Engineering, University of Liverpool, Liverpool L69 7ZF, UK*

[e]*International Joint Research Center for Engineering Reliability and Stochastic Mechanics, Tongji University, Shanghai, China*

Abstract: Novel wavelet-based input-output (excitation-response) relationships are developed referring to stochastically excited linear structural systems with singular parameter matrices. This is done by relying on the family of periodized generalized harmonic wavelets for expanding the excitation and response processes, and by resorting to the concept of Moore-Penrose matrix inverse for solving the resulting overdetermined linear system of algebraic equations to calculate the response wavelet coefficients. In this regard, system response statistics in the joint time-frequency domain, such as the response evolutionary power spectrum matrix, can be determined in a straightforward manner based on the herein derived input-output relationships. The developed technique can be construed as a generalization of earlier efforts in the literature to account for singular parameter matrices in the governing equations of motion. The reliability of the technique is demonstrated by comparing the analytical results with pertinent Monte Carlo simulation data. This is done in conjunction with various diverse numerical examples pertaining to energy harvesters with coupled

*Corresponding author

E-mail addresses: george.pasparakis@irz.uni-hannover.de (G. D. Pasparakis), ikougioum@columbia.edu (I. A. Kougioumtzoglou), kongfan@whut.edu.cn (F. Kong), fragkoulis@irz.uni-hannover.de (V. C. Fragkoulis), beer@irz.uni-hannover.de (M. Beer).

electromechanical equations, oscillators subject to non-white excitations modeled via auxiliary filter equations and structural systems modeled by a set of dependent coordinates.

Keywords: Evolutionary Power Spectrum; Moore-Penrose Matrix Inverse; Joint Time-Frequency Analysis; Random Vibration; Energy Harvesting

3.1 Introduction

Structural systems are often subjected to stochastic excitations exhibiting strong variations both in the time and the frequency domains (Li and Chen, 2009); thus, there is a need for developing efficient joint time-frequency analysis techniques for determining the time-varying frequency content of the system response. In this regard, various standard concepts and tools from random vibration theory have been generalized and extended over the past two decades based on wavelets; see Spanos and Failla (2005); Kougioumtzoglou et al. (2020) for a broad perspective. These wavelet-based techniques have been widely employed for addressing diverse problems including, indicatively, system response analysis and statistics determination (Kareem and Kijewski, 2002; Basu and Gupta, 1997; Psaros et al., 2019a), system identification and damage detection (Kijewski and Kareem, 2003; Spanos et al., 2006; Basu et al., 2008; Kougioumtzoglou et al., 2017a; dos Santos et al., 2020), as well as evolutionary power spectrum (EPS) estimation (Spanos and Failla, 2004; Spanos et al., 2005; Comerford et al., 2016; Zhang et al., 2018).

Further, Spanos and co-workers employed the family of generalized harmonic wavelets (GHWs) for expanding the system excitation and response processes and for deriving an algebraic system of equations to be solved for the response process wavelet coefficients; and thus, for the response process EPS (Spanos and Kougioumtzoglou, 2012; Kougioumtzoglou, 2013). Note that, compared to alternative wavelet families, a significant advantage of GHWs relates to the fact that they possess an additional coefficient that decouples the wavelet resolution in the frequency domain from the central frequency of the wavelet (Newland, 1994). This means that the resolution of the wavelet

analysis can be enhanced in frequency regions of interest. Clearly, this attribute renders GHWs an indispensable tool particularly for structural dynamics applications, where the interest lies typically in resonance phenomena manifesting themselves over relatively small regions in the frequency domain. Further, the technique has been extended to address multi-degree-of-freedom (MDOF) nonlinear systems (Kong et al., 2014b), as well as systems endowed with fractional derivative terms (Kougioumtzoglou and Spanos, 2016).

More recently, Spanos and co-workers developed a novel GHW-based input-output relationship for determining the response EPS of linear systems (Spanos et al., 2016), which circumvented the assumption of "local stationarity" inherent in the early developments in Spanos and Kougioumtzoglou (2012); Kougioumtzoglou (2013); Kong et al. (2014b); Kougioumtzoglou and Spanos (2016) and yielded a higher degree of accuracy in predicting the system response. This was done by relying on a periodized version of GHWs for addressing the non-orthogonality of the GHW basis on a finite time interval, and by deriving interaction coefficients in closed form referring to wavelets at different scales and translation levels. Further, the technique was extended in Kong et al. (2016) to account for nonlinear systems and in Kong et al. (2022b) to address systems with fractional derivative terms.

In this paper, the technique developed in Spanos et al. (2016) is further extended to account for MDOF systems exhibiting singular parameter matrices. This is done in conjunction with the concept of Moore-Penrose (MP) generalized matrix inverse for solving the resulting overdetermined linear system of algebraic equations and for computing the response wavelet coefficients and response EPS matrix. In passing, note that the herein derived input-output relationships can be construed as an enhancement of the respective ones in Pasparakis et al. (2021). In fact, the range of applicability and the accuracy degree of the results in Pasparakis et al. (2021) are limited by the relatively strong assumption of local stationarity, which is removed in this paper. The reliability of the herein developed technique is demonstrated by comparing the analytical results with

pertinent Monte Carlo simulation (MCS) data. This is done in conjunction with various diverse numerical examples exhibiting singular parameter matrices in the governing equations of motion. These include energy harvesters with coupled electromechanical equations, oscillators subject to non-white excitations modeled via auxiliary filter equations, and structural systems modeled by a set of dependent coordinates.

3.2 Mathematical formulation

3.2.1 Preliminaries: Periodized generalized harmonic wavelets

In general, wavelet-based solutions of differential equations governing the response of diverse systems necessitate the determination of coefficients representing the interactions between wavelets (or derivatives/integrals of wavelets) at different scales and translation levels; see, for instance, Beylkin (1992); Chen et al. (1996); Cattani (2005) for some indicative references pertaining to calculation of such interaction coefficients. Specifically, in the field of engineering dynamics, Spanos and co-workers developed recently a periodized version of GHWs to address the non-orthogonality of the GHW basis on a finite interval (Spanos et al., 2016). In this regard, interaction coefficients were derived in closed form and were employed for obtaining an analytical relationship between wavelet coefficients of the system excitation and of the system response. In comparison to alternative earlier efforts towards deriving GHW-based input-output (excitation-response) relationships (e.g., Spanos and Kougioumtzoglou (2012); Kougioumtzoglou (2013)), the approach in Spanos et al. (2016) circumvented the assumption of local stationarity and yielded a higher degree of accuracy in predicting the system response. The basic aspects of the periodized GHWs and the associated interaction coefficients are elucidated in the following for completeness. The interested reader is also directed to Spanos et al. (2016) for a more detailed presentation.

A periodized GHW is defined in the time domain as (Spanos et al., 2016)

$$\psi^{\mathrm{G,per}}_{(m_i,n_i),k}(t) = \frac{1}{n-m}\sum_{q=m_i}^{n_i} e^{\mathrm{i}\Delta\omega q\left(t-\frac{kT_0}{n-m}\right)}\,, \tag{3.1}$$

where (m_i, n_i) denote the scale indices, i is the subscript for the i-th scale, and $k = 0, 1, \ldots, N_t$, with $N_t = (n-m)-1$, denotes the translation index. A uniform constant bandwidth is chosen for all scales under consideration in the ensuing analysis, i.e., $n_i - m_i = n_j - m_j = n - m$, $i, j = 1, 2, \ldots, N_\Omega$, where $N_\Omega = N/2(n-m)$. Further, $T_0 = N\Delta t$ is the time duration of the discretized signal, where N is the total number of sampling points and $\Delta\omega = 2\pi/T_0$.

The periodized GHW of a continuous function $f(t)$ defined in the interval $[0, T_0]$ is given by (Spanos et al., 2016)

$$W^f_{(m_i,n_i),k} = \frac{n-m}{T_0}\int_0^{T_0} f(t)\bar{\psi}^{\mathrm{G,\,per}}_{(m_i,n_i),k}(t)\mathrm{d}t = \frac{n-m}{T_0}\left\langle f(t), \bar{\psi}^{\mathrm{G,per}}_{(m_i,n_i),k}(t)\right\rangle_0^{T_0}, \tag{3.2}$$

where $\langle\cdot\rangle$ represents the inner product over the interval $[0, T_0]$ and the bar over a symbol denotes complex conjugation. Moreover, based on the orthogonality properties of the periodized GHW over a finite time domain, a signal $f(t)$ can be reconstructed as

$$f(t) = \sum_i\sum_k W^f_{(m_i,n_i),k}\psi^{\mathrm{G,per}}_{(m_i,n_i),k}(t) + \sum_i\sum_k \bar{W}^f_{(m_i,n_i),k}\bar{\psi}^{\mathrm{G,per}}_{(m_i,n_i),k}(t). \tag{3.3}$$

If $f(t)$ is a real valued signal, Eq. (3.3) becomes

$$f(t) = 2\mathrm{Re}\left[\sum_i\sum_k W^f_{(m_i,n_i),k}\psi^{\mathrm{G,per}}_{(m_i,n_i),k}\right], \tag{3.4}$$

where $\mathrm{Re}[\cdot]$ denotes the real part of the signal.

Further, the periodized GHW interaction coefficients of the zero-, first- and second-order are given

by

$$C^0_{i,k,j,l} = \left\langle \psi^{\mathrm{G,per}}_{(m_i,n_i),k}(t), \psi^{\mathrm{G,per}}_{(m_j,n_j),l}(t) \right\rangle_0^{T_0} = \begin{cases} \frac{T_0}{n-m}, & i=j, k=l \\ 0, & \text{otherwise} \end{cases}, \tag{3.5}$$

$$\begin{aligned} C^1_{i,k,j,l} &= \left\langle \dot{\psi}^{\mathrm{G,per}}_{(m_i,n_i),k}(t), \psi^{\mathrm{G,per}}_{(m_j,n_j),l}(t) \right\rangle_0^{T_0} \\ &= \begin{cases} \frac{\mathrm{i}\pi(n+m)}{n-m}, & i=j, k=l \\ \frac{2\pi\mathrm{i}}{(n-m)^2} \sum\limits_{q=m_i}^{n_i} q e^{\mathrm{i}2\pi q \frac{l-k}{n-m}}, & i=j, k\neq l \\ 0, & \text{otherwise} \end{cases} \end{aligned} \tag{3.6}$$

and

$$\begin{aligned} C^2_{i,k,j,l} &= \left\langle \ddot{\psi}^{\mathrm{G,per}}_{(m_i,n_i),k}(t), \psi^{\mathrm{G,per}}_{(m_j,n_j),l}(t) \right\rangle_0^{T_0} \\ &= \begin{cases} \frac{-\left(2(n^3-m^3)+3(n^2+m^2)+(n-m)\right)}{3(\pi\Delta\omega)^{-1}(n-m)^2}, & i=j, k=l \\ \frac{-2\pi\Delta\omega}{(n-m)^2} \sum\limits_{q=m_i}^{n_i} q^2 e^{\mathrm{i}2\pi q \frac{l-k}{n-m}}, & i=j, k\neq l \\ 0, & \text{otherwise} \end{cases} \end{aligned} \tag{3.7}$$

respectively.

Clearly, the importance of the closed form expressions in Eqs. (3.5)-(3.7) is paramount for deriving GHW-based input-output (excitation-response) relationships pertaining to second-order (stochastic) differential equations governing the dynamics of diverse engineering systems (Spanos et al., 2016; Xiao et al., 2021; Kong et al., 2022b). In the following section, the stochastic response determination methodology and input-output relationships developed in Spanos et al. (2016) are generalized to account for singular parameter matrices in the system equations of motion.

3.2.2 GHW-based input-output (excitation-response) relationships for linear MDOF systems with singular parameter matrices

In this section, the GHW-based excitation-response relationships derived in Spanos et al. (2016) are generalized to account for MDOF systems exhibiting singular parameter matrices. Specifically, the linear system response EPS matrix is determined by relying on a GHW-based expansion of the response process, by considering the interaction coefficients of Eqs. (3.5)-(3.7), and by employing the MP generalized matrix inverse operation.

In this regard, the governing equations of motion of an n_0-DOF linear time-variant system are given by

$$\mathbf{M}_{\mathbf{x}}(t)\ddot{\mathbf{x}}(t) + \mathbf{C}_{\mathbf{x}}(t)\dot{\mathbf{x}}(t) + \mathbf{K}_{\mathbf{x}}(t)\mathbf{x}(t) = \mathbf{Q}_{\mathbf{x}}(t), \tag{3.8}$$

where $\mathbf{x}$ is the n_0-dimensional response vector; $\mathbf{M}_{\mathbf{x}}(t)$, $\mathbf{C}_{\mathbf{x}}(t)$ and $\mathbf{K}_{\mathbf{x}}(t)$ denote, respectively, the (possibly singular) time-varying mass, damping and stiffness $n_0 \times n_0$ matrices; and $\mathbf{Q}_{\mathbf{x}}(t)$ represents the n_0-dimensional system excitation, which is modeled as a non-stationary zero-mean stochastic process. Next, consider the case that the system is subjected to m_0 linear constraints of the general form (Udwadia and Kalaba, 2007; Fragkoulis et al., 2016a)

$$\mathbf{A}\ddot{\mathbf{x}}(t) + \mathbf{E}\dot{\mathbf{x}}(t) + \mathbf{L}\mathbf{x}(t) = \mathbf{F}(t), \tag{3.9}$$

where $\mathbf{A}, \mathbf{E}$ and $\mathbf{L}$ are $m_0 \times n_0$ coefficient matrices and $\mathbf{F}(t)$ is an m_0-dimensional vector. The combined system of Eqs. (3.8) and (3.9) is cast in the form

$$\tilde{\mathbf{M}}_{\mathbf{x}}(t)\ddot{\mathbf{x}}(t) + \tilde{\mathbf{C}}_{\mathbf{x}}(t)\dot{\mathbf{x}}(t) + \tilde{\mathbf{K}}_{\mathbf{x}}(t)\mathbf{x}(t) = \tilde{\mathbf{Q}}_{\mathbf{x}}(t), \tag{3.10}$$

where $\tilde{\mathbf{M}}_{\mathbf{x}}(t), \tilde{\mathbf{C}}_{\mathbf{x}}(t), \tilde{\mathbf{K}}_{\mathbf{x}}(t)$ and $\tilde{\mathbf{Q}}_{\mathbf{x}}(t)$ denote, respectively, the $(n_0 + m_0) \times n_0$ augmented mass,

damping and stiffness time-varying matrices given by

$$\tilde{\mathbf{M}}_{\mathbf{x}}(t)=\begin{bmatrix}\mathbf{P}\mathbf{M}_{\mathbf{x}}(t)\\ \mathbf{A}\end{bmatrix},\quad \tilde{\mathbf{C}}_{\mathbf{x}}(t)=\begin{bmatrix}\mathbf{P}\mathbf{C}_{\mathbf{x}}(t)\\ \mathbf{E}\end{bmatrix},\quad \tilde{\mathbf{K}}_{\mathbf{x}}(t)=\begin{bmatrix}\mathbf{P}\mathbf{K}_{\mathbf{x}}(t)\\ \mathbf{L}\end{bmatrix} \tag{3.11}$$

and

$$\tilde{\mathbf{Q}}_{\mathbf{x}}(t)=\begin{bmatrix}\mathbf{P}\mathbf{Q}_{\mathbf{x}}(t)\\ \mathbf{F}(t)\end{bmatrix} \tag{3.12}$$

is the augmented excitation (m_0+n_0)-dimensional vector. In Eqs. (3.11) and (3.12), $\mathbf{P}$ is a $(n_0+m_0)\times n_0$ matrix interconnecting the constraints to the equations of motion. In fact, for the special case of utilizing a set of dependent/redundant coordinates, it has been shown (e.g., Schutte and Udwadia (2011); Fragkoulis et al. (2016b); Kougioumtzoglou et al. (2017b); Pirrotta et al. (2021)) that $\mathbf{P}$ takes the form

$$\mathbf{P}=\mathbf{I}-\mathbf{A}^{+}\mathbf{A}, \tag{3.13}$$

where "+" denotes the MP inverse of a matrix. The interested reader is also directed to Antoniou et al. (2017b); Karageorgos et al. (2021) for a broader perspective.

Further, considering the expansion of Eq. (3.4) for the excitation and the response processes, Eq. (3.10) is cast in the form

$$\begin{aligned}&\tilde{\mathbf{M}}_{\mathbf{x}}(t)\sum_i\sum_k\left[\mathbf{W}^{\mathbf{x}}_{(m_i,n_i),k}\ddot{\psi}^{\mathrm{G,per}}_{(m_i,n_i),k}(t)+\bar{\mathbf{W}}^{\mathbf{x}}_{(m_i,n_i),k}\ddot{\bar{\psi}}^{\mathrm{G,per}}_{(m_i,n_i),k}(t)\right]\\ &+\tilde{\mathbf{C}}_{\mathbf{x}}(t)\sum_i\sum_k\left[\mathbf{W}^{\mathbf{x}}_{(m_i,n_i),k}\dot{\psi}^{\mathrm{G,per}}_{(m_i,n_i),k}(t)+\bar{\mathbf{W}}^{\mathbf{x}}_{(m_i,n_i),k}\dot{\bar{\psi}}^{\mathrm{G,per}}_{(m_i,n_i),k}(t)\right]\\ &+\tilde{\mathbf{K}}_{\mathbf{x}}(t)\sum_i\sum_k\left[\mathbf{W}^{\mathbf{x}}_{(m_i,n_i),k}\psi^{\mathrm{G,per}}_{(m_i,n_i),k}(t)+\bar{\mathbf{W}}^{\mathbf{x}}_{(m_i,n_i),k}\bar{\psi}^{\mathrm{G,per}}_{(m_i,n_i),k}(t)\right]=\\ &\sum_i\sum_k\left[\mathbf{W}^{\tilde{\mathbf{Q}}_{\mathbf{x}}}_{(m_i,n_i),k}\psi^{\mathrm{G,per}}_{(m_i,n_i),k}(t)+\bar{\mathbf{W}}^{\tilde{\mathbf{Q}}_{\mathbf{x}}}_{(m_i,n_i),k}\bar{\psi}^{\mathrm{G,per}}_{(m_i,n_i),k}(t)\right].\end{aligned} \tag{3.14}$$

Next, post-multiplying Eq. (3.14) by $\bar{\psi}^{\mathrm{G,per}}_{(m_j,n_j),l}(t)$, integrating over $[0,T_0]$, taking into account the

interaction coefficients in Eq. (3.5)-(3.7), and considering the time-variant matrices $\tilde{\mathbf{M}}_{\mathbf{x}}(t)$, $\tilde{\mathbf{C}}_{\mathbf{x}}(t)$ and $\tilde{\mathbf{K}}_{\mathbf{x}}(t)$ as slowly varying, and thus, approximately constant over the compact support of the GHW (i.e., $\tilde{\mathbf{M}}_{\mathbf{x}}(t) \approx \tilde{\mathbf{M}}_{\mathbf{x},k}$, $\tilde{\mathbf{C}}_{\mathbf{x}}(t) \approx \tilde{\mathbf{C}}_{\mathbf{x},}k$ and $\tilde{\mathbf{K}}_{\mathbf{x}}(t) \approx \tilde{\mathbf{K}}_{\mathbf{x},}k$), yields

$$\sum_i \sum_k \mathbf{B}_{i,k,j,l} \mathbf{W}^{\mathbf{x}}_{(m_i,n_i),k} = \frac{T_0}{n-m} \mathbf{W}^{\tilde{\mathbf{Q}}_{\mathbf{x}}}_{(m_j,n_j),l}, \tag{3.15}$$

where the $(n_0 + m_0) \times n_0$ matrix $\mathbf{B}_{i,k,j,l}$ is given by

$$\mathbf{B}_{i,k,j,l} = C^2_{i,k,j,l} \tilde{\mathbf{M}}_{\mathbf{x},k} + C^1_{i,k,j,l} \tilde{\mathbf{C}}_{\mathbf{x},k} + C^0_{i,k,j,l} \tilde{\mathbf{K}}_{\mathbf{x},k}. \tag{3.16}$$

Furthermore, noticing that the interaction coefficients defined in Eqs. (3.5)-(3.7) are equal to zero for $i \neq j$, and also denoting for simplicity $\mathbf{B}^j_{k,l} = \mathbf{B}_{i,k,j,l}$, Eq. (3.15) is cast, equivalently, in the form

$$\begin{bmatrix} \sum_k \mathbf{B}^j_{k,1} \mathbf{W}^{\mathbf{x}}_{(m_j,n_j),1} \\ \sum_k \mathbf{B}^j_{k,2} \mathbf{W}^{\mathbf{x}}_{(m_j,n_j),2} \\ \vdots \\ \sum_k \mathbf{B}^j_{k,N_t} \mathbf{W}^{\mathbf{x}}_{(m_j,n_j),k} \end{bmatrix} = \frac{T_0}{n-m} \begin{bmatrix} \mathbf{W}^{\tilde{\mathbf{Q}}_{\mathbf{x}}}_{(m_j,n_j),1} \\ \mathbf{W}^{\tilde{\mathbf{Q}}_{\mathbf{x}}}_{(m_j,n_j),2} \\ \vdots \\ \mathbf{W}^{\tilde{\mathbf{Q}}_{\mathbf{x}}}_{(m_j,n_j),N_t} \end{bmatrix}, \tag{3.17}$$

for $l = 1, \ldots, N_t$, with $N_t = n - m$. Alternatively, Eq. (3.17) is written as

$$\mathbf{B}^j \mathbf{W}^j_{\mathbf{x}} = \frac{T_0}{n-m} \mathbf{W}^j_{\bar{\mathbf{Q}}_{\mathbf{x}}}, \tag{3.18}$$

where the $(m_0 + n_0)N_t \times (n_0 N_t)$ matrix $\mathbf{B}^j$ is defined as

$$\mathbf{B}^j = \begin{bmatrix} \mathbf{B}^j_{1,1} & \mathbf{B}^j_{2,1} & \cdots & \mathbf{B}^j_{N_t,1} \\ \mathbf{B}^j_{1,2} & \mathbf{B}^j_{2,2} & \ddots & \mathbf{B}^j_{N_t,2} \\ \vdots & \vdots & \vdots & \vdots \\ \mathbf{B}^j_{1,N_t} & \mathbf{B}^j_{2,N_t} & \cdots & \mathbf{B}^j_{N_t,N_t} \end{bmatrix} \tag{3.19}$$

and the $(n_0 N_t)$- and $(m_0 + n_0)N_t$-dimensional vectors $\mathbf{W}^j_{\mathbf{x}}$ and $\mathbf{W}^j_{\bar{\mathbf{Q}}_{\mathbf{x}}}$ are given by

$$\mathbf{W}^j_{\mathbf{x}} = \begin{bmatrix} \mathbf{W}^{\mathbf{x}}_{(m_j,n_j),1} \\ \mathbf{W}^{\mathbf{x}}_{(m_j,n_j),2} \\ \vdots \\ \mathbf{W}^{\mathbf{x}}_{(m_j,n_j),N_t} \end{bmatrix} \tag{3.20}$$

and

$$\mathbf{W}^j_{\bar{\mathbf{Q}}_{\mathbf{x}}} = \begin{bmatrix} \mathbf{W}^{\tilde{\mathbf{Q}}_{\mathbf{x}}}_{(m_j,n_j),1} \\ \mathbf{W}^{\tilde{\mathbf{Q}}_{\mathbf{x}}}_{(m_j,n_j),2} \\ \vdots \\ \mathbf{W}^{\tilde{\mathbf{Q}}_{\mathbf{x}}}_{(m_j,n_j),N_t} \end{bmatrix}, \tag{3.21}$$

respectively.

Clearly, Eq. (3.18) represents a GHW-based input-output relationship connecting the wavelet coefficients of the excitation and of the response processes. In passing, note that a similar relationship was derived in Spanos et al. (2016) restricted, however, to the special case of matrix $\mathbf{B}^j$ being a square, invertible matrix. Herein, due to the modeling of the system governing equations and the definition of the parameter matrices in Eqs. (3.8)-(3.10), $\mathbf{B}^j$ can become a singular matrix (see also Eq. (3.16)). Thus, a special treatment is required for "inverting" $\mathbf{B}^j$ and solving for the response wavelet coefficient matrix $\mathbf{W}^j_{\mathbf{x}}$ to be used in the calculation of the response EPS matrix. In the fol-

lowing, this is done by resorting to the theory of generalized matrix inverses and to the MP matrix inverse operation; see also Kougioumtzoglou et al. (2017b); Pirrotta et al. (2021); Ni et al. (2021) for some recent indicative papers, and Appendix for more details.

Specifically, considering the MP generalized matrix inverse of $\mathbf{B}^j$, Eq. (3.17) yields (see Appendix)

$$\mathbf{W}_{\mathbf{x}}^{j} = \frac{T_0}{n-m}(\mathbf{B}^j)^{+}\mathbf{W}_{\tilde{\mathbf{Q}}_{\mathbf{x}}}^{j} + (\mathbf{I}_{n_0\times n_0} - (\mathbf{B}^j)^{+}(\mathbf{B}^j))\mathbf{y}_{n_0}, \tag{3.22}$$

where $\mathbf{y}_{n_0}$ is an arbitrary n_0-dimensional vector. It is readily seen that Eq. (3.22) defines a family of solutions for the response wavelet coefficients. Nevertheless, for the special case of matrix $\mathbf{B}^j$ being full rank, i.e., $\text{rank}(\mathbf{B}^j) = n_0 N_t$, its MP matrix inverse is determined, uniquely, in the form (Campbell and Meyer, 2009; Ben-Israel and Greville, 2003)

$$(\mathbf{B}^j)^{+} = \left(\left(\overline{\mathbf{B}^j}\right)^{\mathrm{T}}\mathbf{B}^j\right)^{-1}\left(\overline{\mathbf{B}^j}\right)^{\mathrm{T}}. \tag{3.23}$$

Substituting Eq. (3.23) into the second term of the right hand-side of Eq. (3.22) yields

$$\left(\mathbf{I}_{n_0\times n_0} - (\mathbf{B}^j)^{+}(\mathbf{B}^j)\right)\mathbf{y}_{n_0} = \mathbf{0}, \tag{3.24}$$

and thus, Eq. (3.22) simplifies to

$$\mathbf{W}_{\mathbf{x}}^{j} = \frac{T_0}{n-m}(\mathbf{B}^j)^{+}\mathbf{W}_{\tilde{\mathbf{Q}}_{\mathbf{x}}}^{j}. \tag{3.25}$$

Obviously, Eq. (3.25) can be construed as a generalization of the input-output relationship derived in Spanos et al. (2016) to account for systems with singular parameter matrices in a straightforward manner. Indeed, as shown in the numerical examples in section 3, the herein developed technique can address diverse system modeling yielding singular matrices, including structural systems modeled by a set of dependent coordinates, energy harvesters with coupled electromechanical

equations, and oscillators subject to stochastic excitations modeled via additional auxiliary state equations.

Further, the problem of estimating the system response EPS based on the wavelet coefficients corresponding to an ensemble of realizations is addressed. In this regard, employing Eq. (3.25), multiplying both sides with their Hermitian transposes and taking expectation, yields

$$\mathbb{E}\Big[\mathbf{W}_{\mathbf{x}}^{j}(\mathbf{W}_{\mathbf{x}}^{j})^{\mathrm{T}}\Big] = \Big(\frac{T_0}{n-m}\Big)^2(\mathbf{B}^{j})^{+}\mathbb{E}\Big[\mathbf{W}_{\tilde{\mathbf{Q}}_{\mathbf{x}}}^{j}\Big(\mathbf{W}_{\tilde{\mathbf{Q}}_{\mathbf{x}}}^{j}\Big)^{\mathrm{T}}\Big]\Big((\mathbf{B}^{j})^{+}\Big)^{\mathrm{T}}. \tag{3.26}$$

It is readily seen that based on the formula

$$S_x(\omega_j, t_k) = \frac{T_0}{2\pi(n-m)}\mathbb{E}\Big[\,\big|W_{j,k}^{x}\big|^2\,\Big], \tag{3.27}$$

derived in Spanos et al. (2005); Spanos and Kougioumtzoglou (2012), the diagonal terms in Eq. (3.26) represent response EPS values corresponding to translation levels $k = 1, 2, \ldots, N_t$. Note that additional information (e.g., regarding the phase of the process) is available as well via the off-diagonal elements that provide a measure of the interaction between wavelet coefficients at different time intervals (for a specific scale j). It can be argued that the matrix $\mathbb{E}\Big[\mathbf{W}_{\mathbf{x}}^{j}\Big(\mathbf{W}_{\mathbf{x}}^{j}\Big)^{\mathrm{T}}\Big]$ in Eq. (3.26) can be construed as a form of "auto-correlation" matrix in the wavelet domain; see also Spanos et al. (2016) for a relevant discussion.

3.3 Diverse numerical examples

In this section, various diverse numerical examples are considered for demonstrating the reliability of the herein derived input-output relationship of Eq. (3.26), which can be construed as a generalization of the methodology developed in Spanos et al. (2016) to account for singular matrices. These examples pertain to energy harvesters with coupled electromechanical equations, oscillators subject to non-white excitations modeled via additional filter equations, and structural systems

modeled by a set of dependent coordinates. It is remarked that the results obtained by the analytical technique require approximately 2-3 s of computation time for the considered examples. These are compared with MCS-based estimates (500 realizations) that require approximately 2-3 min of computation time on the same computer, i.e., a MacBook Pro 2018 laptop with a 2.9 GHz 6-Core Intel Core i9 processor and 16 GB RAM.

3.3.1 A class of electromechanical energy harvesting systems

A cantilever beam with piezoelectric patches attached near its clamped ends has been one of the most popular and widely studied electromechanical energy harvesters (e.g., Daqaq et al. (2014); Petromichelakis et al. (2018, 2021)). Following the presentation and detailed discussion in Daqaq et al. (2014), the dynamics of such a system can be approximated by the following general mathematical model of coupled electromechanical equations, expressed in a non-dimensional form as

$$\ddot{q} + 2\zeta\dot{q} + \frac{\mathrm{d}U(q)}{\mathrm{d}q} + \kappa^2 \upsilon = f(t) \tag{3.28}$$

$$\dot{\upsilon} + \alpha\upsilon - \dot{q} = 0 \tag{3.29}$$

where q denotes the response displacement and υ represents the induced voltage in capacitive harvesters or the induced current in inductive ones. Further, ζ is the damping, κ is the coupling coefficient, α is defined as the ratio between the mechanical and electrical time constants of the harvester (see Daqaq et al. (2014)), and $U(q)$ denotes the potential function. Its derivative $\frac{\mathrm{d}U(q)}{\mathrm{d}q}$ represents the restoring force, which is modeled in the ensuing analysis as linear, i.e., $\frac{\mathrm{d}U(q)}{\mathrm{d}q} = q$; see also Petromichelakis et al. (2018, 2021) for alternative nonlinear modeling.

In the following, the excitation $f(t)$ is modeled as a non-stationary stochastic process compatible with the EPS

$$S_f(\omega, t) = d(t)^2 S_0, \tag{3.30}$$

where S_0 denotes the Gaussian white noise constant power spectrum value, and $d(t)$ represents a time-modulating function. Indicatively, Eq. (3.30) can describe approximately the relatively slow variations in time of the intensity of the white noise process, and in this regard, $d(t)$ is given by

$$d(t) = 1 + 0.5\cos(\omega_0 t), \tag{3.31}$$

where $\omega_0 = 0.25\ rad/s$. Further, the parameter values considered herein are $\zeta = 0.1,\ \kappa = 3.25$, $\alpha = 0.8$ and $S_0 = 0.05$.

Although there exist alternative solution treatments in the literature for addressing Eqs. (3.28) and (3.29), and for determining relevant response statistics (e.g., Adhikari et al. (2009); Petromichelakis et al. (2018, 2021)), the herein developed methodology is employed next for determining the response EPS and for demonstrating that singular matrices can be treated in a straightforward and direct manner.

Specifically, similarly to Petromichelakis et al. (2018, 2021) where the stochastic response analysis of Eqs. (3.28) and (3.29) was performed based on a Wiener path integral solution treatment, Eq. (3.28) can be construed as the governing stochastic differential equation constrained by Eq. (3.29); see also Petromichelakis et al. (2020). In this regard, setting $\mathbf{x}^{\mathrm{T}} = \begin{bmatrix} q & v \end{bmatrix}$, and differentiating Eq. (3.29) once with respect to time, the parameter matrices of the constraint Eq. (3.9) become

$$\mathbf{A} = \begin{bmatrix} -1 & 1 \end{bmatrix},\ \mathbf{E} = \begin{bmatrix} 0 & \alpha \end{bmatrix},\ \mathbf{L} = \begin{bmatrix} 0 & 0 \end{bmatrix},\ \mathrm{F} = 0, \tag{3.32}$$

whereas the matrix $\mathbf{P}$ of Eq. (3.13) takes the form

$$\mathbf{P} = \begin{bmatrix} 0.5 & 0.5 \\ 0.5 & 0.5 \end{bmatrix}. \tag{3.33}$$

Further, the parameter matrices in Eq. (3.11) become

$$\tilde{\mathbf{M}}_{\mathbf{x}} = \begin{bmatrix} 0.5 & 0 \\ 0.5 & 0 \\ -1 & 1 \end{bmatrix}, \; \tilde{\mathbf{C}}_{\mathbf{x}} = \begin{bmatrix} -0.40 & 0.5 \\ -0.40 & 0.5 \\ 0 & 0.8 \end{bmatrix}, \; \tilde{\mathbf{K}}_{\mathbf{x}} = \begin{bmatrix} 0.5 & 5.6812 \\ 0.5 & 5.6813 \\ 0 & 0 \end{bmatrix} \tag{3.34}$$

and Eq. (3.12) takes the form

$$\tilde{\mathbf{Q}}_{\mathbf{x}} = \begin{bmatrix} 0.5 \\ 0.5 \\ 0 \end{bmatrix} f(t). \tag{3.35}$$

Therefore, the excitation EPS matrix corresponding to Eq. (3.35) becomes

$$\mathbf{S}^{j}_{\tilde{\mathbf{Q}}_{\mathbf{x}}} = \frac{T_0}{2\pi(n-m)} \begin{bmatrix} \mathbf{S}^{j}_{\tilde{\mathbf{Q}}_{\mathbf{x}},(1,1)} & 0 & \cdots & 0 \\ 0 & \mathbf{S}^{j}_{\tilde{\mathbf{Q}}_{\mathbf{x}},(2,2)} & \cdots & 0 \\ \vdots & \vdots & \ddots & \vdots \\ 0 & 0 & \cdots & \mathbf{S}^{j}_{\tilde{\mathbf{Q}}_{\mathbf{x}},(N_t,N_t)} \end{bmatrix}, \tag{3.36}$$

where

$$\mathbf{S}^{j}_{\tilde{\mathbf{Q}}_{\mathbf{x}},(k,k)} = \begin{bmatrix} 0.25\, d_l^4\, S^{j}_{f,(k,k)} & 0.25\, d_l^4\, S^{j}_{f,(k,k)} & 0 \\ 0.25\, d_l^4\, S^{j}_{f,(k,k)} & 0.25\, d_l^4\, S^{j}_{f,(k,k)} & 0 \\ 0 & 0 & 0 \end{bmatrix}, \tag{3.37}$$

for $0 \leq k \leq N_t$, and is utilized next for defining $\mathbb{E}\left[\mathbf{W}^{j}_{\tilde{\mathbf{Q}}_{\mathbf{x}}} \left(\mathbf{W}^{j}_{\tilde{\mathbf{Q}}_{\mathbf{x}}}\right)^{\mathrm{T}}\right]$ on the right hand-side of Eq. (3.26). Also, utilizing the parameter matrices in Eq. (3.34), the matrix $\mathbf{B}^j$ in Eq. (3.19) is formed for each wavelet band $j = 1, 2, \ldots, 256$ and each time instant to be used in Eq. (3.26). In fact, it is noted that $\mathbf{B}^j$ has full rank, and thus, Eqs. (3.25) and (3.26) can be applied yielding a unique solution for the interaction coefficients of the system response.

In Fig. 3.1a, the response EPS for the voltage v is plotted based on Eqs. (3.26) and (3.27), whereas

in Fig. 3.1b the response EPS for v is estimated based on MCS data. Specifically, first, 500 excitation time histories compatible with the EPS in Eq. (3.30) are generated by the spectral representation method (Liang et al., 2007) with a signal duration $T_0 = 20.46\ s$, and a cut-off frequency equal to $\omega_u = 50\pi\ rad/s$. Second, the coupled system defined by Eqs. (3.28) and (3.29) is solved by resorting to a standard 4^{th} order Runge-Kutta numerical integration scheme, and the response voltage EPS is estimated by utilizing Eq. (3.27) and using a constant frequency band $n - m = 4$. In Fig. 3.2, comparisons are provided between the MCS-based results and the estimates based on the herein developed methodology for two indicative time instants, i.e., $t = 4\ s$ and $t = 10\ s$. It is readily seen that the herein derived input-output relationship of Eq. (3.26), which accounts for singular matrices, exhibits a relatively high degree of accuracy in determining the system response EPS.

3.3.2 Non-white stochastic excitation modeling via auxiliary filter equations

In the field of stochastic engineering dynamics, a non-white excitation process is typically represented in the time domain as the output of a filter subject to white noise (e.g., Roberts and Spanos (2003); Karageorgos et al. (2021); Psaros et al. (2018)). In this regard, the state-variable vector is augmented to account for the additional filter equation associated with the non-white excitation. In many cases, the form of the filter equation leads to a system of governing equations with singular parameter matrices. For example, consider a single-DOF linear oscillator of the form

$$m\ddot{q} + c\dot{q} + kq = h(t), \tag{3.38}$$

where m, c, k are the mass, damping and stiffness parameters of the system and $h(t)$ denotes the excitation, given by

$$h(t) = g(t)y(t). \tag{3.39}$$

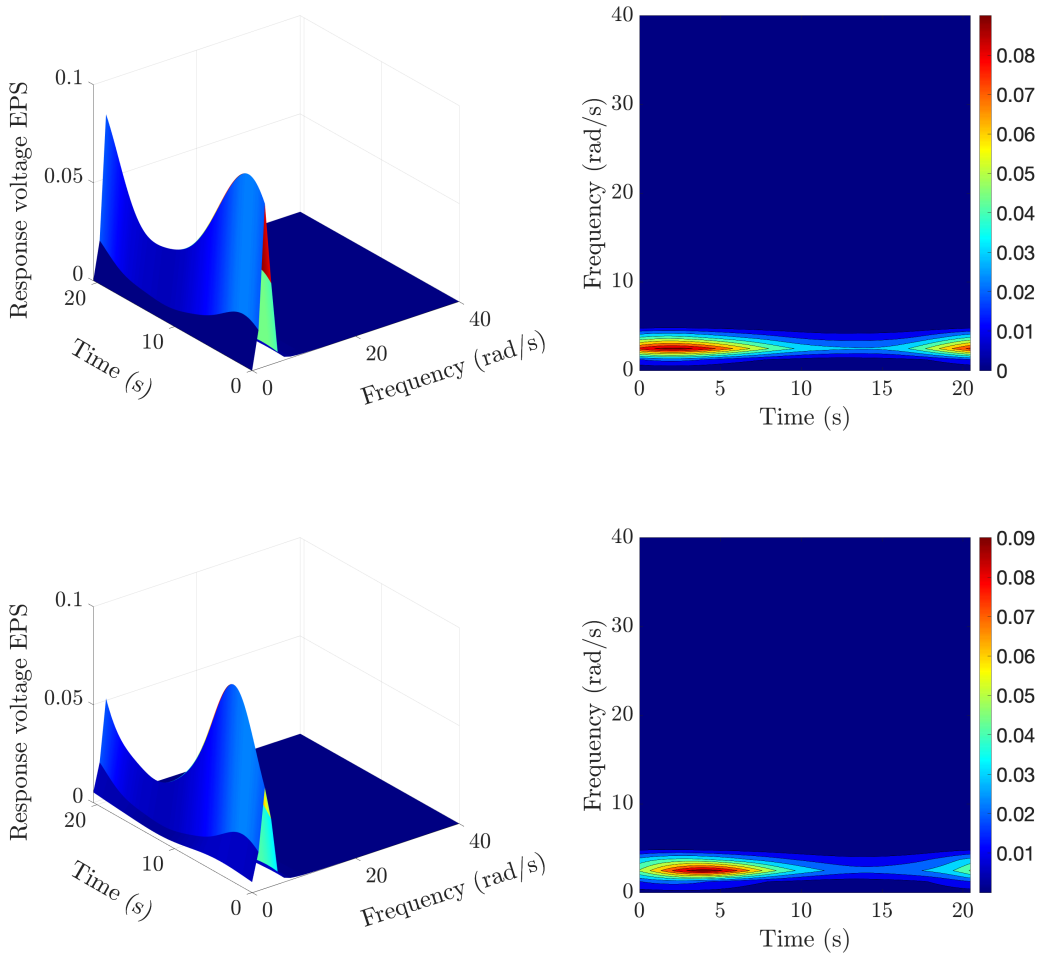

Fig. 3.1: Response voltage EPS estimate pertaining to the energy harvesting system of Eqs. (3.28) and (3.29) subject to time-modulated Gaussian white noise excitation: (a) Analytical closed-form input-output relationship of Eq. (3.26), (b) MCS-based estimate (500 realizations).

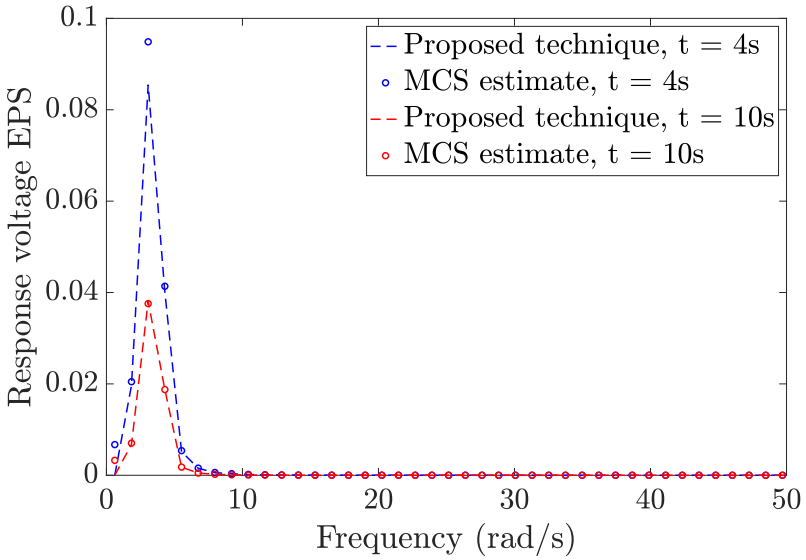

Fig. 3.2: Response voltage EPS estimate pertaining to the energy harvesting system of Eqs. (3.28) and (3.29) subject to time-modulated Gaussian white noise excitation: Comparison for two indicative time-instants between analytical closed-form input-output relationship of Eq. (3.26), and MCS-based estimate (500 realizations).

In Eq. (3.39), $g(t)$ denotes a modulating function of the form (Spanos and Kougioumtzoglou, 2012)

$$g(t) = \lambda(e^{-\alpha t} - e^{-\beta t}), \tag{3.40}$$

where α, β and λ are parameters controlling the shape of the modulating function. Further, the power spectrum of the stochastic process $y(t)$ is given by

$$S_y(\omega) = \frac{S_0}{c_n^2\omega^2 + k_n^2} \tag{3.41}$$

which is expressed in the time domain as the output of the first order linear filter

$$c_n\dot{y} + k_n y = w(t). \tag{3.42}$$

In Eq. (3.42), $w(t)$ is a Gaussian white noise stochastic process with $\mathbb{E}[w(t)w(t+\tau)] = 2\pi S_0 \delta(\tau)$, $\delta(\tau)$ is the Dirac delta function and c_n, k_n are filter parameters.

Next, considering the state vector $\mathbf{x}^{\mathrm{T}} = \begin{bmatrix} q & y & f(t) \end{bmatrix}$, where $f(t) = w(t)$, and taking into account Eqs. (3.38) and (3.42), the governing equations take the form of Eq. (3.8) with

$$\mathbf{M}_{\mathbf{x}} = \begin{bmatrix} m & 0 & 0 \\ 0 & 0 & 0 \\ 0 & 0 & 0 \end{bmatrix}, \; \mathbf{C}_{\mathbf{x}} = \begin{bmatrix} c & 0 & 0 \\ 0 & c_n & 0 \\ 0 & 0 & 0 \end{bmatrix}, \; \mathbf{K}_{\mathbf{x}} = \begin{bmatrix} k & -g(t) & 0 \\ 0 & k_n & -1 \\ 0 & 0 & 1 \end{bmatrix} \tag{3.43}$$

and

$$\mathbf{Q}_{\mathbf{x}}(t) = \begin{bmatrix} 0 \\ 0 \\ w(t) \end{bmatrix}, \tag{3.44}$$

whereas the constraint equation parameter matrices corresponding to Eq. (3.9) become

$$\mathbf{A} = \begin{bmatrix} 0 & c_n & 0 \end{bmatrix}, \; \mathbf{E} = \begin{bmatrix} 0 & k_n & 1 \end{bmatrix}, \; \mathbf{L} = \mathbf{0}, \; \mathrm{F} = 0. \tag{3.45}$$

Therefore, the matrix $\mathbf{P}$ of Eq. (3.13) is given by

$$\mathbf{P} = \begin{bmatrix} c_n & 0 & 0 \\ 0 & 0 & 0 \\ 0 & 0 & c_n \end{bmatrix}. \tag{3.46}$$

Note that the system defined in Eq. (3.43) is time-variant, since the matrix $\tilde{\mathbf{K}}_{\mathbf{x}}(t)$ contains the function $g(t)$. Nevertheless, this poses no difficulty in applying the proposed methodology since it can readily treat time-variant parameter matrices as shown in Eq. (3.8). Further, the matrices of

Eq. (3.10) for the herein considered system take the form

$$\tilde{\mathbf{M}}_{\mathbf{x}}(t) = \begin{bmatrix} m & 0 & 0 \\ 0 & 0 & 0 \\ 0 & 0 & 0 \\ 0 & c_n & 0 \end{bmatrix}, \; \tilde{\mathbf{C}}_{\mathbf{x}}(t) = \begin{bmatrix} c & 0 & 0 \\ 0 & 0 & 0 \\ 0 & 0 & 0 \\ 0 & k_n & 1 \end{bmatrix}, \; \tilde{\mathbf{K}}_{\mathbf{x}}(t) = \begin{bmatrix} k & -g(t) & 0 \\ 0 & 0 & 0 \\ 0 & 0 & 1 \\ 0 & 0 & 0 \end{bmatrix} \tag{3.47}$$

and

$$\tilde{\mathbf{Q}}_{\mathbf{x}}(t) = \begin{bmatrix} 0 \\ 0 \\ 1 \\ 0 \end{bmatrix} w(t). \tag{3.48}$$

Therefore, the excitation EPS matrix corresponding to Eq. (3.48) is written in the form of Eq. (3.36), where

$$\mathbf{S}^{j}_{\tilde{\mathbf{Q}}_{\mathbf{x}},(k,k)} = \begin{bmatrix} 0 & 0 & 0 & 0 \\ 0 & 0 & 0 & 0 \\ 0 & 0 & S^{j}_{w,(k,k)} & 0 \\ 0 & 0 & 0 & 0 \end{bmatrix}, \tag{3.49}$$

for $0 \leq k \leq N_t$, and is utilized next for defining $\mathbb{E}\left[\mathbf{W}^{j}_{\tilde{\mathbf{Q}}_{\mathbf{x}}}\left(\mathbf{W}^{j}_{\tilde{\mathbf{Q}}_{\mathbf{x}}}\right)^{\mathrm{T}}\right]$ on the right hand-side of Eq. (3.26). The parameter values considered herein are $m_1 = 1\ kg/(ms^2)$, $c_1 = 4.3\ Ns/m$, $k_1 = 256\ N/m$, $k_n = 8\ N/m$, $c_n = 1\ Ns/m$ and $S_0 = 1$. The resulting $\mathbf{B}^j$ has full rank, and thus, the simplified expression in Eq. (3.23) is used for computing the MP matrix inverse. This yields a unique solution for the interaction coefficients of the system response, which is determined by Eq. (3.26). The obtained response displacement EPS is shown in Fig. 3.3a, whereas in Fig. 3.3b the response EPS is determined based on MCS data generated by solving numerically Eq. (3.38) via a Runge-Kutta integration scheme in conjunction with the spectral representation methodology (Liang et al., 2007) for generating excitation realizations. Note that the discrepancies observed in

Figs. 3.3a and 3.3b near the ends of the time domain are attributed to "end effects" due to the application of the wavelet transform. The interested reader is directed to Kijewski and Kareem (2002) for more details and possible melioration treatments such as zero-padding. Further, the analytical solution and MCS-based estimate are compared in Fig. 3.4 for two indicative time instants, i.e., $t = 4\ s$ and $t = 7\ s$. Clearly, the results obtained by the herein proposed input-output relationship of Eq. (3.26) for determining the response EPS of systems exhibiting singular matrices are in good agreement with the corresponding MCS estimates.

3.3.3 Structural systems modeled via dependent coordinates

It is common practice in the field of engineering dynamics to utilize the minimum number of coordinates (generalized coordinates) for formulating the system equations of motion (e.g., Roberts and Spanos (2003)). In general, this yields not only non-singular, but also positive definite parameter matrices in the governing equations. Nevertheless, it has been argued recently that the explicit formulation of the equations of motion based on generalized coordinates can be a cumbersome task, and thus, alternative approaches have been proposed based, indicatively, on utilizing a set of dependent/redundant DOFs in conjunction with a number of constraint equations (e.g., Udwadia and Kalaba (2007); Udwadia and Wanichanon (2013); Fragkoulis et al. (2022)). Although this unconventional modeling appears to be advantageous from a computational efficiency perspective (Mariti et al., 2011), it leads to equations of the form of Eq. (3.10) exhibiting singular matrices.

In this section, the herein developed solution methodology based on periodized GHWs is employed for determining the response EPS of a stochastically excited structural system modeled via dependent coordinates. Specifically, the 2-DOF system of Fig. 3.5 is considered, where mass m_1 is connected to the foundation via a spring and a damper with coefficients k_1 and c_1, respectively. Further, it is connected to mass m_2 via a spring and a damper with coefficients k_2 and c_2, respectively. The applied excitation stochastic processes $Q_1(t)$ and $Q_2(t)$ are compatible with an EPS

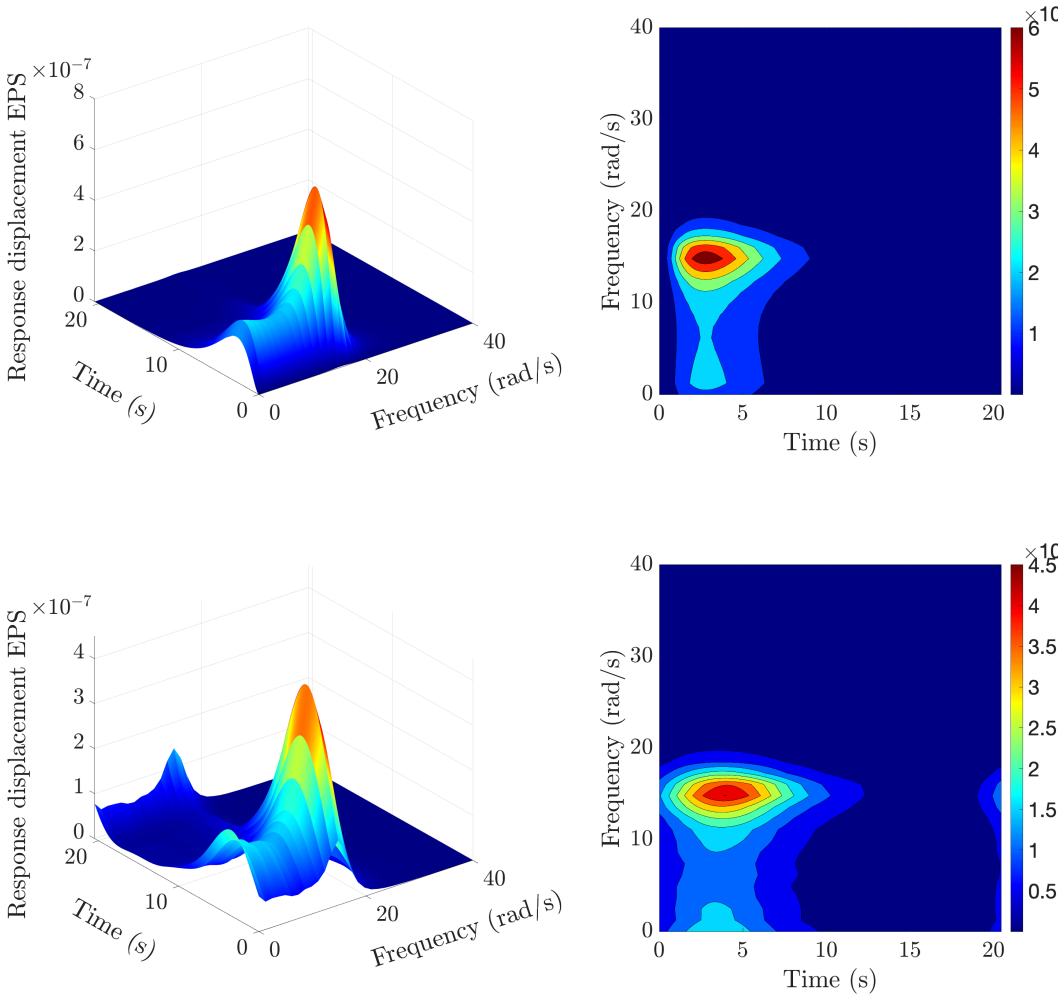

Fig. 3.3: Response displacement EPS pertaining to the oscillator in Eq. (3.38) subject to a time-modulated non-stationary excitation: (a) Analytical closed-form input-output relationship of Eq. (3.26), (b) MCS-based estimate (500 realizations).

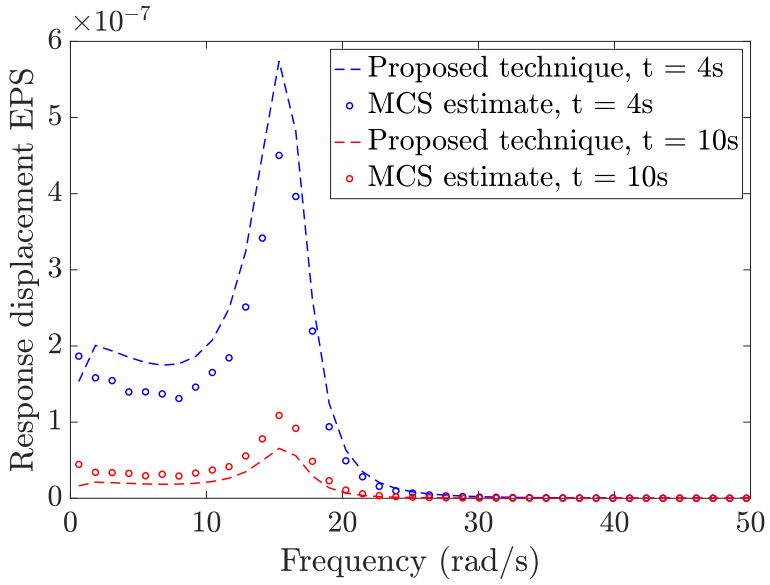

Fig. 3.4: Response displacement EPS pertaining to the oscillator in Eq. (3.38) subject to a time-modulated non-stationary excitation: Comparison for two indicative time instants between analytical closed-form input-output relationship of Eq. (3.26) and MCS-based estimate (500 realizations).

given by

$$S_f(\omega,t) = S_0 \left(\frac{\omega t}{5\pi}\right)^2 \exp(-c_0 t) t^2 \exp\left(-\left(\frac{\omega}{5\pi}\right)^2 t\right). \tag{3.50}$$

It can be argued that the EPS form in Eq. (3.50) comprises some of the main characteristics of earthquake excitations, such as decreasing of the dominant frequency with time (e.g., Spanos and Solomos (1983); Fragkoulis et al. (2019)). The parameter values considered in the ensuing analysis are: $m_i = 1\ kg/(ms^2)$, $c_i = 4.3\ Ns/m$, $k_i = 256\ N/m$, for $i = 1, 2$, and $S_0 = 1\ m^2/s^3$, $c_0 = 0.15$. The system excitation is applied for time $[0, T_0]$, with $T_0 = 20.48\ s$, considering $N_t = 1024$ points and cut-off frequency equal to $10\pi\ rad/s$. Also, a constant bandwidth resolution of $n - m = 4$ is used.

Next, utilizing the generalized coordinates vector $\mathbf{q}^{\mathrm{T}} = \begin{bmatrix} q_1 & q_2 \end{bmatrix}$, the governing equations of mo-

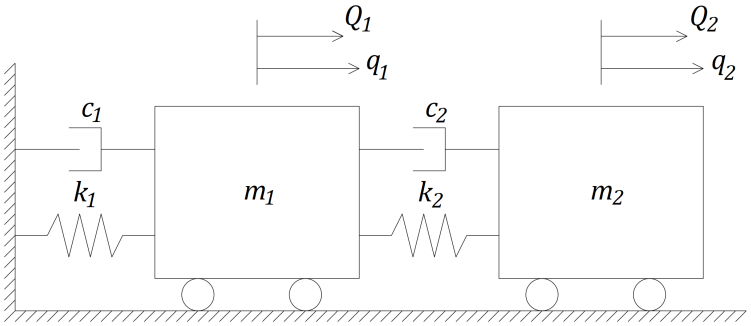

Fig. 3.5: Two-degree-of-freedom linear structural system subjected to non-stationary stochastic excitation.

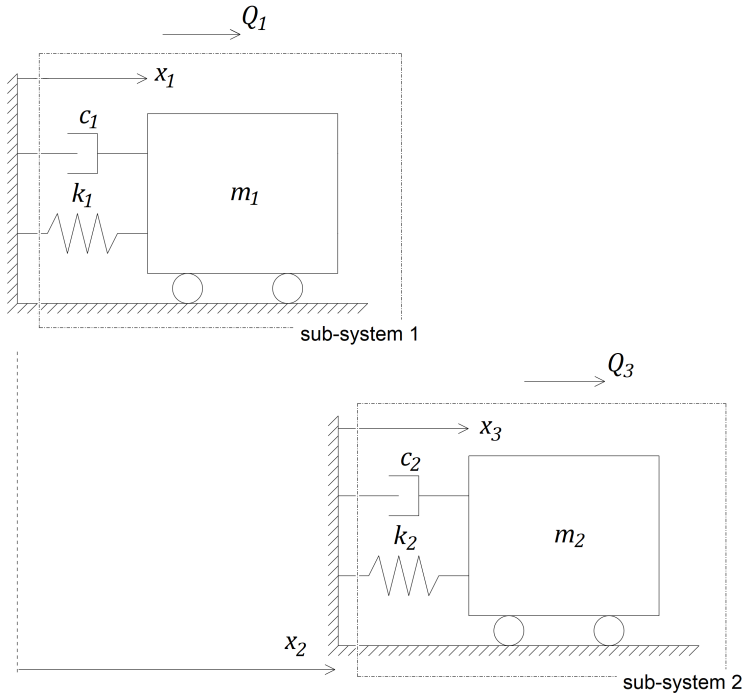

Fig. 3.6: Modeling the system in Fig. 3.5 by using dependent coordinates.

tion become

$$m_1\ddot{q}_1 + (c_1 + c_2)\dot{q}_1 + (k_1 + k_2)q_1 - c_2\dot{q}_2 - k_2q_2 = -m_1Q_1(t), \tag{3.51}$$

$$m_2\ddot{q}_2 - c_2\dot{q}_1 - k_2q_1 + c_2\dot{q}_2 + k_2q_2 = -m_2Q_2(t). \tag{3.52}$$

Further, adopting a dependent coordinates modeling for the derivation of the equations of motion (see Fig. 3.6), the coordinates vector $\mathbf{x}^{\mathrm{T}} = \begin{bmatrix} x_1 & x_2 & x_3 \end{bmatrix}$ is considered in conjunction with the constraint equation

$$x_2 = x_1 + d, \tag{3.53}$$

where d denotes the physical length of mass m_1. In this regard, the parameter matrices corresponding to Eq. (3.8) take the form

$$\mathbf{M_x} = \begin{bmatrix} 1 & 0 & 0 \\ 0 & 1 & 1 \\ 0 & 1 & 1 \end{bmatrix}, \ \mathbf{C_x} = \begin{bmatrix} 4.3 & 0 & 0 \\ 0 & 0 & 0 \\ 0 & 0 & 4.3 \end{bmatrix}, \ \mathbf{K_x} = \begin{bmatrix} 256 & 0 & 0 \\ 0 & 0 & 0 \\ 0 & 0 & 256 \end{bmatrix} \tag{3.54}$$

and

$$\mathbf{Q_x} = \begin{bmatrix} Q_1 \\ Q_3 \\ Q_3 \end{bmatrix}, \tag{3.55}$$

whereas twice differentiating the constraint Eq. (3.53), the matrices in Eq. (3.9) take the form

$$\mathbf{A} = \begin{bmatrix} 1 & -1 & 0 \end{bmatrix}, \ \mathbf{E} = \mathbf{L} = \mathbf{0}_{1\times 3}, \ \mathrm{F} = 0. \tag{3.56}$$

Also, the matrix $\mathbf{P}$ in Eq. (3.13) is given by

$$\mathbf{P} = \begin{bmatrix} 0.5 & 0.5 & 0 \\ 0.5 & 0.5 & 0 \\ 0 & 0 & 1 \end{bmatrix}, \tag{3.57}$$

and thus, the matrices in Eqs. (3.11) and (3.12) become

$$\tilde{\mathbf{M}}_{\mathbf{x}} = \begin{bmatrix} 0.5 & 0.5 & 0.5 \\ 0.5 & 0.5 & 0.5 \\ 0 & 1 & 1 \\ 1 & -1 & 0 \end{bmatrix}, \tilde{\mathbf{C}}_{\mathbf{x}} = \begin{bmatrix} 2.15 & 0 & 0 \\ 2.15 & 0 & 0 \\ 0 & 0 & 4.3 \\ 0 & 0 & 0 \end{bmatrix}, \tilde{\mathbf{K}}_{\mathbf{x}} = \begin{bmatrix} 128 & 0 & 0 \\ 128 & 0 & 0 \\ 0 & 0 & 256 \\ 0 & 0 & 0 \end{bmatrix} \tag{3.58}$$

and

$$\tilde{\mathbf{Q}}_{\mathbf{x}} = \begin{bmatrix} Q_1 \\ Q_3 \\ Q_3 \\ 0 \end{bmatrix}. \tag{3.59}$$

Accordingly, the excitation EPS matrix corresponding to Eq. (3.59) is written as in Eq. (3.36), where

$$\mathbf{S}^{j}_{\tilde{\mathbf{Q}}_{\mathbf{x}},(k,k)} = \begin{bmatrix} S^{j}_{f,(k,k)} & 0 & 0 & 0 \\ 0 & S^{j}_{f,(k,k)} & S^{j}_{f,(k,k)} & 0 \\ 0 & S^{j}_{f,(k,k)} & S^{j}_{f,(k,k)} & 0 \\ & 0 & 0 & 0 \end{bmatrix}, \tag{3.60}$$

for $0 \leq k \leq N_t$, and is utilized next for defining $\mathbb{E}\left[\mathbf{W}^{j}_{\tilde{\mathbf{Q}}_{\mathbf{x}}}\left(\mathbf{W}^{j}_{\tilde{\mathbf{Q}}_{\mathbf{x}}}\right)^{\mathrm{T}}\right]$ on the right hand-side of Eq. (3.26). The matrix $\mathbf{B}^{j}$ in Eq. (3.19) is constructed for each wavelet band $j = 1, 2, \ldots, 128$, and each time instant, and since it has full rank, its MP inverse is given by Eq. (3.23). Next, the response displacement EPS is determined by utilizing Eq. (3.26). The analytical results pertaining

to the 1^{st} and 3^{rd} DOF of the system in Fig. 3.6 are shown in Figs. 3.7a and 3.8a, respectively.

Further, the technique is also applied to the system of Eqs. (3.51-3.52), which is modeled based on generalized (independent) coordinates. Clearly, based on Figs. (3.5-3.6), $q_1 = x_1$ and $q_2 - q_1 = x_3$. In this regard, $\mathbf{B}^j$ in the resulting Eq. (3.18) is a square invertible matrix, and thus, Eq. (3.18) can be readily solved for the response wavelet coefficients $\mathbf{W}_{\mathbf{q}}^j$ to be used for determining the response power spectra via Eqs. (3.26-3.27). In fact, the computed power spectra $S_{q_1}(\omega, t)$ and $S_{q_2-q_1}(\omega, t)$ are plotted in Figs. 3.7b and 3.8b, respectively. As anticipated due to the relationships $q_1 = x_1$ and $q_2 - q_1 = x_3$, note that $S_{x_1}(\omega, t)$ in Fig. 3.7a and $S_{x_3}(\omega, t)$ in Fig. 3.8a are identical to $S_{q_1}(\omega, t)$ and $S_{q_2-q_1}(\omega, t)$, respectively.

Overall, it is seen that the solution obtained by the herein developed technique accounting for dependent coordinates and singular matrices is identical to the solution determined based on an alternative system modeling employing generalized (independent) coordinates and featuring square, invertible, matrices. In other words, the herein proposed solution treatment of a system with singular matrices does not introduce any additional approximations compared to treating an equivalent system with square invertible matrices.

Also, note that, for cases of square invertible matrices, the technique can be construed as an extension of the standard periodized GHW technique in Spanos et al. (2016) to treat MDOF systems. Furthermore, MCS-based EPS estimates (500 realizations) are also included in Figs. 3.7c and 3.8c, whereas response EPS estimates at two indicative time instants are plotted in Fig. 3.9. Comparisons indicate a satisfactory degree of accuracy exhibited by the periodized GHW technique.

3.4 Concluding remarks

In this paper, a technique based on periodized GHWs has been developed for joint time-frequency response analysis of linear systems with singular parameter matrices. This has been done by resorting to concepts and tools related to the MP generalized matrix inverse theory. Specifically,

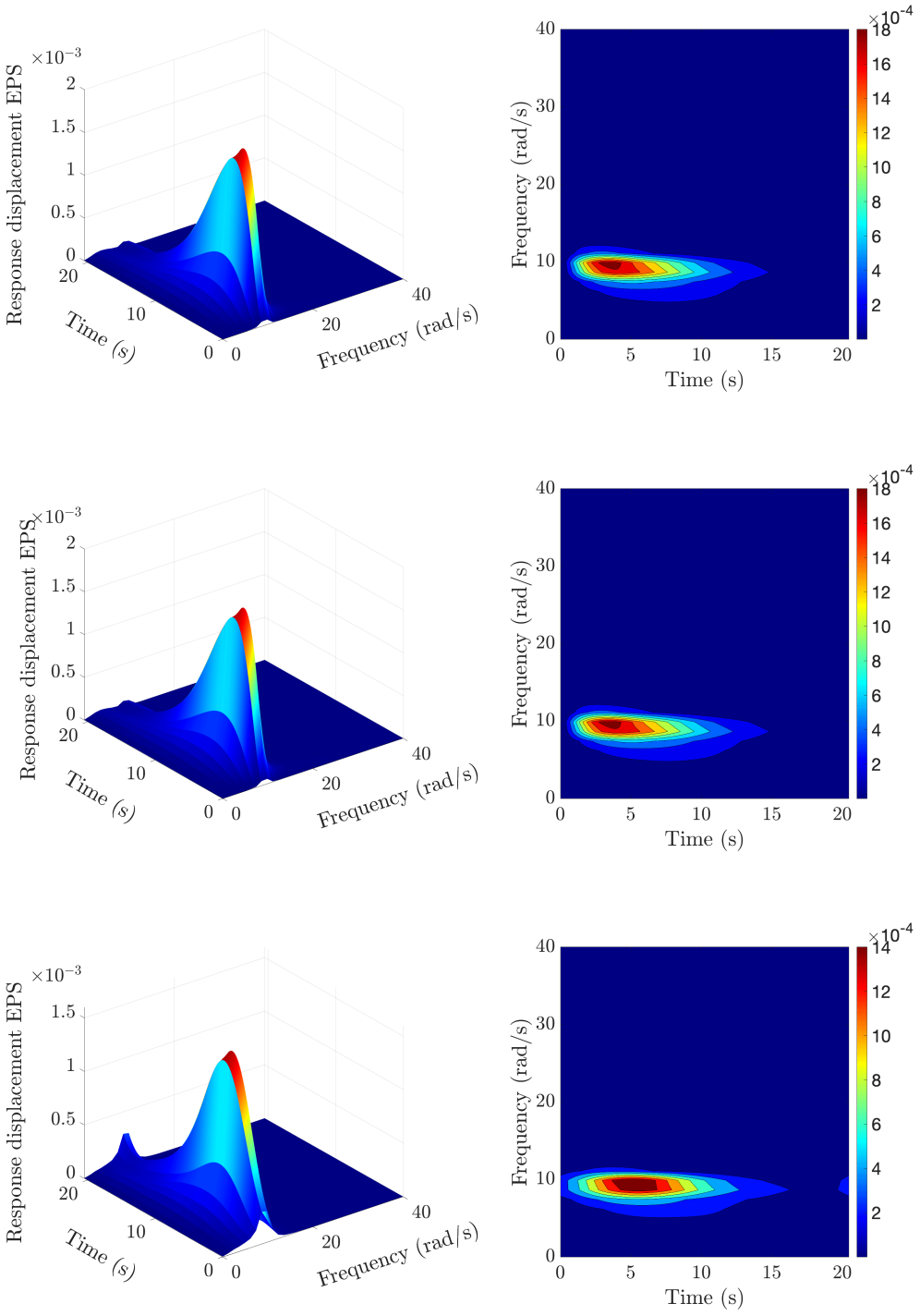

Fig. 3.7: Response EPS of a 2-DOF linear system subject to non-stationary stochastic excitation described by the non-separable EPS in Eq. (3.50): (a) EPS for displacement x_1 based on Eq. (3.26) with a singular $\mathbf{B}^j$ matrix (dependent coordinates), (b) EPS for displacement q_1 based on Eq. (3.26) with a square invertible $\mathbf{B}^j$ matrix (generalized coordinates), (c) MCS-based estimate (500 realizations).

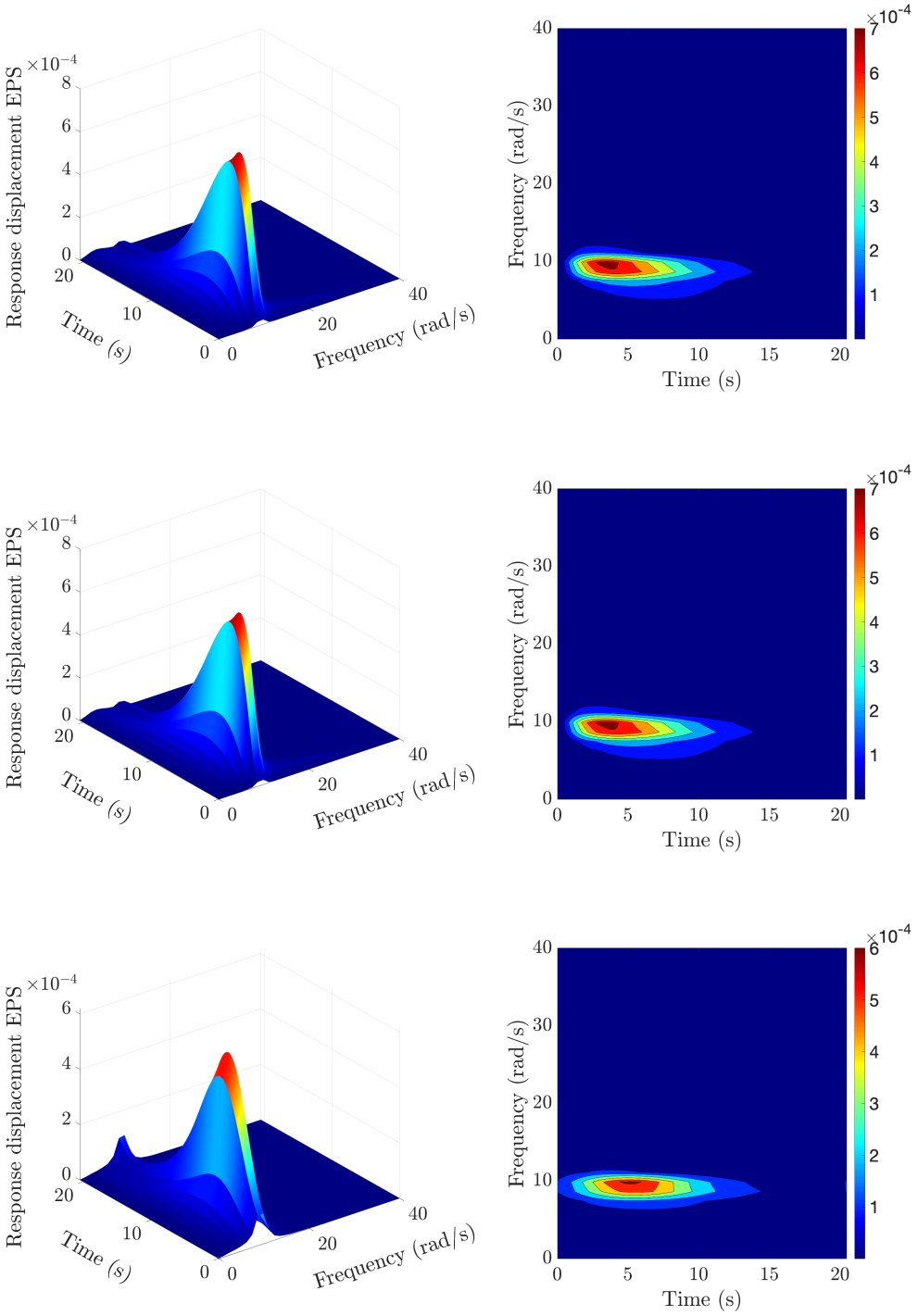

Fig. 3.8: Response EPS of a 2-DOF linear system subject to non-stationary stochastic excitation described by the non-separable EPS in Eq. (3.50): (a) EPS for displacement x_3 based on Eq. (3.26) with a singular $\mathbf{B}^j$ matrix (dependent coordinates), (b) EPS for displacement $q_2 - q_1$ based on Eq. (3.26) with a square invertible $\mathbf{B}^j$ matrix (generalized coordinates), (c) MCS-based estimate (500 realizations).

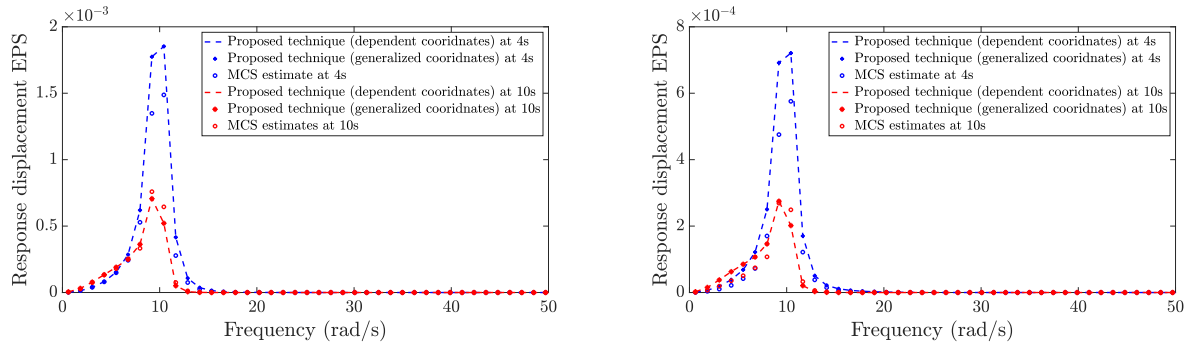

Fig. 3.9: Response EPS of a 2-DOF linear system subject to non-stationary stochastic excitation described by the non-separable EPS in Eq. (3.50) for two indicative time instants: (a) comparisons between analytically determined EPS for x_1, q_1, and MCS estimates (500 realizations), and (b) comparisons between analytically determined EPS for x_2, $q_2 - q_1$, and MCS estimates (500 realizations).

considering GHW-based expansions for the excitation and response processes of the system, novel input-output relationships have been derived in the wavelet domain. These have been used for determining the EPS matrix of the system response.

The developed technique can be construed as a generalization of earlier efforts in the literature to account for singular parameter matrices in the governing equations of motion, while its reliability has been demonstrated by comparing the analytical results with pertinent MCS data. This has been done in conjunction with various diverse numerical examples pertaining to energy harvesters with coupled electromechanical equations, oscillators subject to non-white excitations modeled via auxiliary filter equations, and structural systems modeled by a set of dependent coordinates.

Note in passing that the MP matrix inverse operation involves the solution of an optimization problem based on L_2-norm minimization. In this regard, exploring the potential of alternative optimization schemes based, for instance, on L_p-norm ($0 < p < 1$) minimization is identified as future work (e.g., Kougioumtzoglou et al. (2020); He et al. (2019)).

Acknowledgement

The authors gratefully acknowledge the support from the European Union's Horizon 2020 research and innovation programme under the Marie Skłodowska-Curie grant agreement No 764547, and from the German Research Foundation under Grant No. FR 4442/2-1.

Appendix

Consider a linear system of equations in the form

$$\mathbf{A}\mathbf{x} = \mathbf{b}, \tag{3.61}$$

where $\mathbf{A}$ is either a rectangular $m \times n$, or a square but singular $n \times n$ matrix, and $\mathbf{x}$, $\mathbf{b}$ are n-dimensional vectors. It is readily seen that solving Eq. (3.61) necessitates the generalization of the concept of matrix inverse, which has given birth to the theory of generalized matrix inverses (Ben-Israel and Greville, 2003). In particular, the Moore-Penrose (MP) generalized matrix inverse is utilized throughout the paper.

Definition. For any matrix $\mathbf{A} \in \mathbb{C}^{m\times n}$, there is a unique matrix $\mathbf{A}^+ \in \mathbb{C}^{n\times m}$ such that:

$$\mathbf{A}\mathbf{A}^+\mathbf{A} = \mathbf{A}, \quad \mathbf{A}^+\mathbf{A}\mathbf{A}^+ = \mathbf{A}^+, \quad \overline{\mathbf{A}\mathbf{A}^+} = \mathbf{A}\mathbf{A}^+, \quad \overline{\mathbf{A}^+\mathbf{A}} = \mathbf{A}^+\mathbf{A}. \tag{3.62}$$

The matrix $\mathbf{A}^+$ of the Definition is called the MP inverse of $\mathbf{A}$. If $\mathbf{A}$ is a square, real and non-singular matrix, then $\mathbf{A}^+$ coincides with the inverse of $\mathbf{A}$, i.e., $\mathbf{A}^+ = \mathbf{A}^{-1}$. Using the MP inverse, a closed form solution to the algebraic system of Eq. (3.61) is attained. In this regard, for any matrix $\mathbf{A} \in \mathbb{R}^{m\times n}$, Eq. (3.61) yields

$$\mathbf{x} = \mathbf{A}^+\mathbf{b} + (\mathbf{I}_n - \mathbf{A}^+\mathbf{A})\mathbf{y}, \tag{3.63}$$

where $\mathbf{y}$ denotes an arbitrary n-dimensional vector and $\mathbf{I}_n$ represents the $n \times n$ identity matrix. A more detailed presentation of the topic can be found in Campbell and Meyer (2009) and Ben-Israel and Greville (2003).

Chapter 4

Research article 3: Wind data extrapolation and stochastic field statistics estimation via compressive sampling and low rank matrix recovery methods

Wind data extrapolation and stochastic field statistics estimation via compressive sampling and low rank matrix recovery methods

George D. Pasparakis[a], Ketson R.M. dos Santos[b], I. A. Kougioumtzoglou[c,*], M. Beer[a,d,e]

[a]*Institute for Risk and Reliability, Leibniz Universität Hannover, Callinstr. 34, 30167 Hannover, Germany*

[b]*Earthquake Engineering and Structural Dynamics Laboratory (EESD), École Polytechnique Fédérale de Lausanne (EPFL)*

[c]*Department of Civil Engineering and Engineering Mechanics, Columbia University*

[d]*Institute for Risk and Uncertainty and School of Engineering, University of Liverpool, Liverpool L69 7ZF, UK*

[e]*International Joint Research Center for Engineering Reliability and Stochastic Mechanics, Tongji University, Shanghai, China*

Abstract: A methodology based on compressive sampling is developed for incomplete wind time-histories reconstruction and extrapolation in a single spatial dimension, as well as for related stochastic field statistics estimation. This relies on l_1-norm minimization in conjunction with an adaptive basis re-weighting scheme. Indicatively, the proposed methodology can be employed for monitoring of wind turbine systems, where the objective relates to either reconstructing incomplete time-histories measured at specific points along the height of a turbine tower, or to extrapolating to other locations in the vertical dimension where sensors and measurement records are not available. Further, the methodology can be used potentially for environmental hazard modeling within the context of performance-based design optimization of structural systems.

Unfortunately, a straightforward implementation of the aforementioned approach to account for two spatial dimensions is hindered by significant, even prohibitive in some cases, computational cost. In this regard, to address computational challenges associated with higher-dimensional domains, a methodology based on low rank matrices and nuclear norm minimization is developed next for

*Corresponding author

E-mail addresses: george.pasparakis@irz.uni-hannover.de (G. D. Pasparakis), ketson.santos@epfl.ch (Ketson R.M. dos Santos), ikougioum@columbia.edu (I. A. Kougioumtzoglou), beer@irz.uni-hannover.de (M.Beer).

wind field extrapolation in two spatial dimensions. The efficacy of the proposed methodologies is demonstrated by considering various numerical examples. These refer to reconstruction of wind time-histories with missing data compatible with a joint wavenumber-frequency power spectral density, as well as to extrapolation to various locations in the spatial domain.

Keywords: Wind data; Stochastic field; Sparse representations; Compressive sampling; Low-rank matrix.

4.1 Introduction

Estimating wind field model related statistics relies, typically, on information provided by data acquisition systems such as distributed sensor networks and LIDAR acquisition systems (e.g., (Frehlich et al., 1998), (Harris et al., 2006)). In many real-life cases, however, the measured data are corrupted and incomplete. Also, it is often required to extrapolate relevant wind field information to points of interest, where there are no measurements due to limited equipment availability. Clearly, developing methodologies for accurate reconstruction and extrapolation of wind field data is of paramount importance to the analysis, design and monitoring of engineering systems such as wind turbines; see, for instance, Carassale and Solari (2006). Further, it is worth noting that such methodologies can be used potentially for environmental hazard modeling within the context of performance-based design optimization of structural systems (e.g., Comerford et al. (2017), Mitseas et al. (2016)).

Indicatively, a wavelet-based fluid motion estimator was developed in Dérian et al. (2015) for estimating wind fields based on backscatter data. Further, a dimension reduction approach based on computational fluid dynamics data was applied in Qin et al. (2018) for wind field reconstruction. Also, several machine learning approaches based on various neural network implementations and configurations were employed recently for wind data reconstruction and extrapolation (e.g., Qu et al. (2020); Ni and Li (2016); Mohandes and Rehman (2018)). Moreover, surrogate modeling

based on Kriging was proposed in Lin and Li (2020), whereas Kalman filtering was used in Towers and Jones (2016) for wind field estimation based on a limited number of LIDAR measurements.

Nevertheless, most of the aforementioned approaches are characterized by significant limitations. For example, in many cases the techniques appear efficacious only for relatively small percentages of missing data, whereas results based on black-box approaches such as neural networks are not always interpretable. Alternatively, various methodologies based on compressive sampling (CS) have been developed recently, which appear promising for stochastic process statistics estimation based on realizations with incomplete/missing data (e.g., Comerford et al. (2016); Laface et al. (2017); Zhang et al. (2018)). The interested reader is also directed to the recent review paper by Kougioumtzoglou et al. (Kougioumtzoglou et al., 2020) for a broad perspective on theoretical concepts and diverse applications of sparse representations and CS approaches in engineering mechanics.

In this paper, a methodology based on CS is developed, which relies on l_1-norm minimization in conjunction with an adaptive basis re-weighting scheme, for incomplete wind field time-histories reconstruction and extrapolation in a single spatial (vertical) dimension. Next, to address computational challenges associated with higher-dimensional domains, a methodology based on low rank matrices and nuclear norm minimization is developed for wind field extrapolation in two spatial dimensions. The efficacy of the proposed methodologies is demonstrated by considering various numerical examples. These refer to reconstruction of wind time-histories with missing data compatible with a joint wavenumber-frequency power spectral density (PSD), as well as to extrapolation to various locations in the spatial domain.

4.2 Wind field spectral representation

In various engineering applications, the wind field can be conveniently modeled as a stochastic wave (e.g., Benowitz and Deodatis (2015)). This facilitates the efficient simulation of realizations corresponding to a large number of points in the spatial domain, while circumventing the need for

cross-PSD related calculations; see also Shinozuka and Deodatis (1996). In this section, following closely Chen et al. (2018), the basic elements associated with Monte Carlo simulation (MCS) of a wind field compatible with a joint wavenumber-frequency PSD are reviewed for completeness.

4.2.1 Wind field time-histories simulation in a single spatial dimension

A homogeneous wind field in the vertical dimension is related to a wavenumber-frequency PSD (e.g., Benowitz and Deodatis (2015), Chen et al. (2018)) given by

$$S^{(\mathrm{WF})}(k,\omega) = \frac{1}{2\pi}\int_{-\infty}^{\infty} S^{(\mathrm{F})}(\xi,\omega)e^{-ik\xi}\mathrm{d}\xi \tag{4.1}$$

where ω, ξ, k denote the frequency, spatial distance and wavenumber, respectively. Further,

$$S^{(\mathrm{F})}(\xi,\omega) = S_0(\omega)\rho(\xi,\omega) = S_0(\omega)\exp\left(-\frac{C_z}{2\pi U_{10}}|\omega||\xi|\right) \tag{4.2}$$

where $S_0(\omega)$ is the auto-PSD and $\rho(\xi,\omega)$ represents the coherence function. Combining Eq. (4.1) and Eq. (4.2), $S^{(\mathrm{WF})}(k,\omega)$ takes the form

$$S^{(\mathrm{WF})}(k,\omega) = S_0(\omega)\rho^{(\mathrm{WF})}(k,\omega) = S_0(\omega)\frac{C_z}{2\pi^2 U_{10}}\frac{|\omega|}{\left(\frac{C_z}{2\pi U_{10}}\right)^2\omega^2 + k^2} \tag{4.3}$$

where C_z is an exponential decay coefficient and U_{10} is the mean wind velocity at a height of 10m. Next, Eq. (4.3) can be used in conjunction with the spectral representation method (SRM) (Deodatis and Shinozuka, 1989) for generating wind velocity records in the form

$$\begin{aligned} X(z,t) = &\sum_{i=1}^{N_k}\sum_{j=1}^{N_\omega}\sqrt{4S^{(\mathrm{WF})}\left(k_i,\omega_j\right)\Delta k\Delta\omega} \\ &\times\left[\cos\left(k_i z + \omega_j t + \varphi_{ij}\right) + \cos\left(k_i z - \omega_j t + \tilde{\varphi}_{ij}\right)\right] \end{aligned} \tag{4.4}$$

where φ_{ij} and $\tilde{\varphi}_{ij}$ represent two sets of independent random phase angles uniformly distributed over $[0, 2\pi]$ $k_i = i\Delta k$ with $\Delta k = k_u/N_k$ denotes the discretized wavenumber domain with an upper cut-off wavenumber k_u; and $\omega_j = j\Delta\omega$ with $\Delta\omega = \omega_u/N_\omega$ is the discretized frequency domain with an upper cut-off frequency ω_u. In the ensuing analysis and numerical examples, the Davenport PSD is considered (e.g. Deodatis and Shinozuka (1989), Simiu and Scanlan (1996)); that is,

$$S^{\text{Davenport}}(\omega) = 2.0u_*^2 \frac{\left(\frac{1200}{2\pi U_{10}}\omega\right)^2}{|\omega|\left(1+\left(\frac{1200}{2\pi U_{10}}\omega\right)^2\right)^{4/3}} \tag{4.5}$$

where u_* denotes the shear flow velocity. Further, the parameters values used are $U_{10} = 31.88$ m/s, $u_* = 1.691$ m/s and $C_z = 10$.

4.2.2 Wind field time-histories simulation in two spatial dimensions

In this section, following closely Chen et al. (2018), a generalization of the results outlined in section 4.2.1 is presented to account for a two-dimensional spatial domain. In this regard, the joint wavenumber-frequency PSD of Eq. (4.3) takes the form

$$\begin{aligned} S^{(\text{WF})}(k_y, k_z, \omega) &= S^{\text{Davenport}}(\omega) \cdot \rho^{(\text{WF})}(k_y, k_z, \omega) \\ &= \frac{u_*^2}{\pi C_{1z} C_{1y}\left(\frac{1}{2\pi U_{10}}|\omega|\right)^2} \frac{\left(\frac{1200}{2\pi U_{10}}\omega\right)^2}{|\omega|\left(1+\left(\frac{1200}{2\pi U_{10}}\omega\right)^2\right)^{4/3}} \\ &\times \frac{1}{\left(1+\left[\left(\frac{1}{C_{1y}}k_y\right)^2+\left(\frac{1}{C_{1z}}k_z\right)^2\right]/\left(\frac{1}{2\pi U_{10}}|\omega|\right)^2\right)^{\frac{3}{2}}} \end{aligned} \tag{4.6}$$

where

$$\rho^{(\mathrm{WF})}\left(k_y, k_z, \omega\right) = \frac{1}{2\pi C_{1z} C_{1y}} \frac{1}{\left(\frac{1}{2\pi U_{10}}|\omega|\right)^2} \times \frac{1}{\left(1 + \left[\left(\frac{1}{C_{1y}} k_y\right)^2 + \left(\frac{1}{C_{1z}} k_z\right)^2\right] / \left(\frac{1}{2\pi U_{10}}|\omega|\right)^2\right)^{\frac{3}{2}}} \tag{4.7}$$

In Eqs. (4.6)-(4.7), C_{1z} and C_{1y} are the exponential decay coefficients corresponding to the vertical and horizontal directions, respectively, and k_z and k_y denote the respective wavenumbers. Next, realizations compatible with the PSD of Eq. (4.6) can be generated based on the SRM (e.g., Benowitz and Deodatis (2015), Chen et al. (2018)). In this context, Eq. (4.4) becomes

$$\begin{aligned} X(z,y,t) = \sum_{i=1}^{N_{k_z}} \sum_{j=1}^{N_{k_y}} \sum_{m=1}^{N_\omega} & \sqrt{4 S^{(\mathrm{WF})}\left(k_i^{(z)}, k_j^{(y)}, \omega_m\right) \Delta k_i^{(z)} \Delta k_j^{(y)} \Delta \omega^{(m)}} \\ & \cdot \Big[\cos\left(k_i^{(z)} z + k_j^{(y)} y + \omega_m t + \varphi_{ijm}^{(1)}\right) \\ & + \cos\left(k_i^{(z)} z + k_j^{(y)} y - \omega_m t + \varphi_{ijm}^{(2)}\right) \\ & + \cos\left(k_i^{(z)} z - k_j^{(y)} y + \omega_m t + \varphi_{ijm}^{(3)}\right) \\ & + \cos\left(k_i^{(z)} z - k_j^{(y)} y - \omega_m t + \varphi_{ijm}^{(4)}\right)\Big] \end{aligned} \tag{4.8}$$

$k_j^{(y)} = j\Delta k_y, j = 1, 2, \ldots, N_{k_y}$ and $k_i^{(z)} = i\Delta k_z, i = 1, 2, \ldots, N_{k_z}$ are the discretized wavenumber domains in y and z directions with a number of points N_{k_y} and N_{k_z}, respectively. Further, $\varphi_{ijm}^{(1)}$, $\varphi_{ijm}^{(2)}$, $\varphi_{ijm}^{(3)}$ and $\varphi_{ijm}^{(4)}$ represent four different sets of independent random phase angles uniformly distributed in $[0, 2\pi]$.

Regarding computational implementation aspects, it is readily seen that the Davenport PSD of Eq. (4.5) exhibits a singularity at the origin, which can be addressed, however, based on a frequency shift scheme (e.g., Benowitz and Deodatis (2015), Zerva (1992)). In this regard, it is reasonable to consider an uneven discretization scheme, which is denser near the origin of the wavenumber domains.

4.3 Wind field reconstruction and extrapolation in the joint space-time domain: A compressive sampling treatment

Research efforts during the past fifteen years have focused on identifying and exploiting low-dimensional representations of high-dimensional data, as well as on establishing conditions guaranteeing unique representation in the low-dimensional space (e.g., Candes et al. (2006), Donoho (2006)). These theoretical results, coupled with potent convex optimization numerical algorithms, have triggered the birth of the currently expanding field of CS and have led to numerous impactful contributions in a wide range of application areas (e.g., Eldar and Kutyniok (2012)). The interested reader is also directed to the recent review paper by Kougioumtzoglou et al. (Kougioumtzoglou et al., 2020) and to references therein for a broad perspective on theoretical concepts and diverse applications of sparse representations and CS approaches in engineering mechanics.

In this section, first, a CS approach based on l_1-norm minimization in conjunction with an adaptive basis re-weighting scheme is developed for wind field time-histories reconstruction and extrapolation in a single spatial dimension. Second, to address computational challenges associated with multi-dimensional domains, a CS approach based on nuclear norm minimization is developed for wind field extrapolation in two spatial dimensions.

4.3.1 Reconstruction and extrapolation in a single spatial dimension: l_1-norm minimization in conjunction with an adaptive basis re-weighting scheme

Theoretical aspects

In this section, the CS-based methodology developed in Malara et al. (2018) for extrapolation of random wave field data in the joint space-time domain is adapted and extended to account for wind stochastic field extrapolation. Indicatively, this methodology can be employed for cases of

monitoring wind turbine systems, where the objective is to either reconstruct incomplete time-histories measured at specific points along the height of a turbine tower, or to extrapolate to other locations in the vertical dimension where sensors and measurement records are not available.

Consider an $n_0 \times 1$ column vector $\mathbf{y}_0$ denoting a measured time history, which can be expanded by employing a basis matrix $\mathbf{A}_0$ of dimensions $n_0 \times n_0$ in the form $\mathbf{y}_0 = \mathbf{A}_0\mathbf{x}$, where $\mathbf{x}$ is the corresponding coefficient vector. Clearly, the sparsity degree of the coefficient vector $\mathbf{x}$ (i.e., number of non-zero elements) depends on the choice of the basis matrix $\mathbf{A}$ (e.g, polynomial, Fourier, etc). Resorting to a CS-based solution approach and considering a relatively high degree of sparsity, the coefficient vector $\mathbf{x}$ can be determined with satisfactory accuracy even if the system of equations $\mathbf{y}_0 = \mathbf{A}_0\mathbf{x}$ is underdetermined. Specifically, consider an $(n_0 - n_m) \times 1$ column vector $\mathbf{y}$ representing an under-sampled time history at a specific location along the height of a wind turbine. n_0 denotes the original sample and n_m is the number of randomly missing data. Further, considering a sampling matrix $\mathbf{A}$ of dimensions $(n_0 - n_m) \times n_0$ leads to the underdetermined system of equations $\mathbf{y} = \mathbf{A}\mathbf{x}$, where the objective relates to determining the coefficient vector $\mathbf{x}$ assumed to be sparse. According to CS theory (e.g., Kougioumtzoglou et al. (2020)), the problem can be cast in a convex optimization setting via minimizing the l_1-norm of $\mathbf{x}$; that is,

$$\mathbf{min} \; || \; \mathbf{x} \; ||_{l_1} \text{ subject to } \mathbf{y} = \mathbf{A}\mathbf{x} \tag{4.9}$$

Clearly, the use of the l_1-norm promotes sparsity, whereas Eq. (4.9) can be readily solved by standard gradient optimization algorithms (e.g., Kougioumtzoglou et al. (2020)). Alternatively, the constraint in Eq. (4.9) can be relaxed and replaced by $|| \; \mathbf{y} - \mathbf{A}\mathbf{x} \; ||_{l_2} \leq \varepsilon$ to account for possible presence of noise.

Nevertheless, as also shown in Comerford et al. (2014); Comerford et al. (2017), Zhang et al. (2018), an adaptive basis re-weighting scheme can further promote sparsity and yield solution

• Initialize re-weighting matrix $\mathbf{W}$, $\mathbf{W}_2 = \mathbf{I}_{n_0}$ where $\mathbf{I}$ is the identity matrix
while $\mid \mathbf{W}_2 - \mathbf{W} \mid > threshold$ **do**
$\mathbf{W} = \mathbf{W}_2$
$\mathbf{W}_2 =$zeros(n_0, n_0)
• Generate re-weighting matrix via least squares
for $i = 1$ to m **do** $\triangleright$ $m =$ number of available time-histories
$\mathbf{x} = (\mathbf{AW})^{\mathrm{T}} \left((\mathbf{AW})(\mathbf{AW})^{\mathrm{T}}\right) \mathbf{y}_i$
$\mathbf{x} = [\mathrm{x}_1, \mathrm{x}_2, \mathrm{x}_3, \ldots, \mathrm{x}_{n_0-1}, \mathrm{x}_{n_0}]$
$\mathbf{W}_2 = \mathbf{W}_2 + \mathrm{diag}\Big(\Big[\;||\; \mathrm{x}_2, \mathrm{x}_1 \;||, ||\; \mathrm{x}_2, \mathrm{x}_1 \;||, ||\; \mathrm{x}_3, \mathrm{x}_2 \;||, ||\; \mathrm{x}_3, \mathrm{x}_2 \;||, \ldots,$
$||\; \mathrm{x}_{n_0/2}, \mathrm{x}_{n_0/2-1} \;||, ||\; \mathrm{x}_{n_0/2}, \mathrm{x}_{n_0/2-1} \;|| \;\Big]\Big)$
end for
$\mathbf{W}_2 = \dfrac{\mathbf{W}_2}{\mathrm{Mean}(\mathbf{W}_2)} + \mathrm{bias} \cdot I_{n_0}$
end while
• Use l_1 minimization to compute the coefficient vector $\mathbf{x}$
$\mathbf{x} = \min \mid \mathbf{x} \mid_{l_1}$ subject to $\mathbf{y} = \mathbf{AW}_2\mathbf{x}$

Fig. 4.1: Mechanization of l_1-norm minimization with an adaptive basis.

estimates of enhanced accuracy. In this regard, Eq. (4.9) becomes

$$\mathbf{min} \;||\; \mathbf{x} \;||_{l_1} \text{ subject to } \mathbf{y} = \mathbf{AWx} \tag{4.10}$$

where $\mathbf{W}$ is a re-weighting diagonal matrix. The rationale of the scheme relates to matrix $\mathbf{W}$ being used to appropriately weigh the columns of the basis matrix $\mathbf{A}$. To this aim, the entries of $\mathbf{W}$ correspond to the magnitudes of the components of $\mathbf{x}$. This promotes sparsity as it reduces the contribution of the smaller components of vector $\mathbf{x}$. Concisely, the mechanization of the re-weighting scheme is shown in Fig. (4.1), whereas the interested reader is directed to Comerford et al. (2017), Zhang et al. (2018) for a detailed presentation and discussion.

Clearly, the scheme is best suited to problems where an ensemble of time-histories with incomplete data points is available and the objective relates to determining statistics based on the ensemble average, such as estimating the underlying process PSD. Nevertheless, even in cases where only a single (relatively long) time-history is available, the scheme can be still implemented under the assumptions of stationarity and ergodicity by considering a partition of the record into smaller time

intervals.

Further, it is shown that the above methodology can be readily adapted to be used for extrapolating wind time-histories corresponding to specific points along the vertical dimension based on measured data at neighboring locations. Specifically, consider a number of $N + M$ wind velocity records, each composed of length n data points and corresponding to a vertical height z_i. The objective refers to inferring wind velocity time histories at M distinct points from N measurement locations as depicted in Fig. (4.2). In this regard, the measured records can be represented as a column vector $\mathbf{y}$ of dimension $nN \times 1$ to be used in the formulation of Eq. (4.9), or alternatively, of Eq. (4.10). Next, the sampling matrix $\mathbf{A}$ can be constructed based on the SRM of Eq. (4.4). In particular, matrix $\mathbf{A}$ is formed as the tensor product of trigonometric basis functions (e.g., Psaros et al. (2019b)) spanning the frequency and wavenumber domains. For the frequency domain a basis can be constructed as

$$\mathbf{B}_1 = \Big[\cos(\omega_0 \mathrm{t}) \;\; \sin(\omega_1 \mathrm{t}) \;\; \cdots \;\; \sin(\omega_{\frac{\mathrm{n}}{2}-1} \mathrm{t}) \;\; \cos(\omega_{\frac{\mathrm{n}}{2}} \mathrm{t})\Big] \tag{4.11}$$

with $\omega_\ell = 2\pi\ell/n, \;\; \ell = 0, \cdots, n/2$, whereas for the wavenumber domain the basis becomes

$$\mathbf{B}_2 = \Big[\cos(\mathrm{k}_0 \mathrm{z}) \;\; \sin(\mathrm{k}_1 \mathrm{z}) \;\; \cdots \;\; \sin(\mathrm{k}_{N/2-1} \mathrm{z}) \;\; \cos(\mathrm{k}_{N/2} \mathrm{z})\Big] \tag{4.12}$$

with $k_m = 2\pi m/N, \;\; m = 0, \cdots, N/2$. The tensor product of $\mathbf{B}_1$ and $\mathbf{B}_2$ produces a new basis for the joint wavenumber-frequency domain in the form

$$\mathbf{B} = \mathbf{B}_1 \otimes \mathbf{B}_2 \tag{4.13}$$

The complete matrix $\mathbf{B}$ is of dimensions $n(N+M) \times n(N+M)$. However, considering that time-histories at M locations of interest are not available, $\mathbf{B}$ becomes an $nN \times n(N+M)$ sampling matrix $\mathbf{A}$ to be used in Eq. (4.9) (or, alternatively, in Eq. (4.10)) for extrapolating for the M locations; see

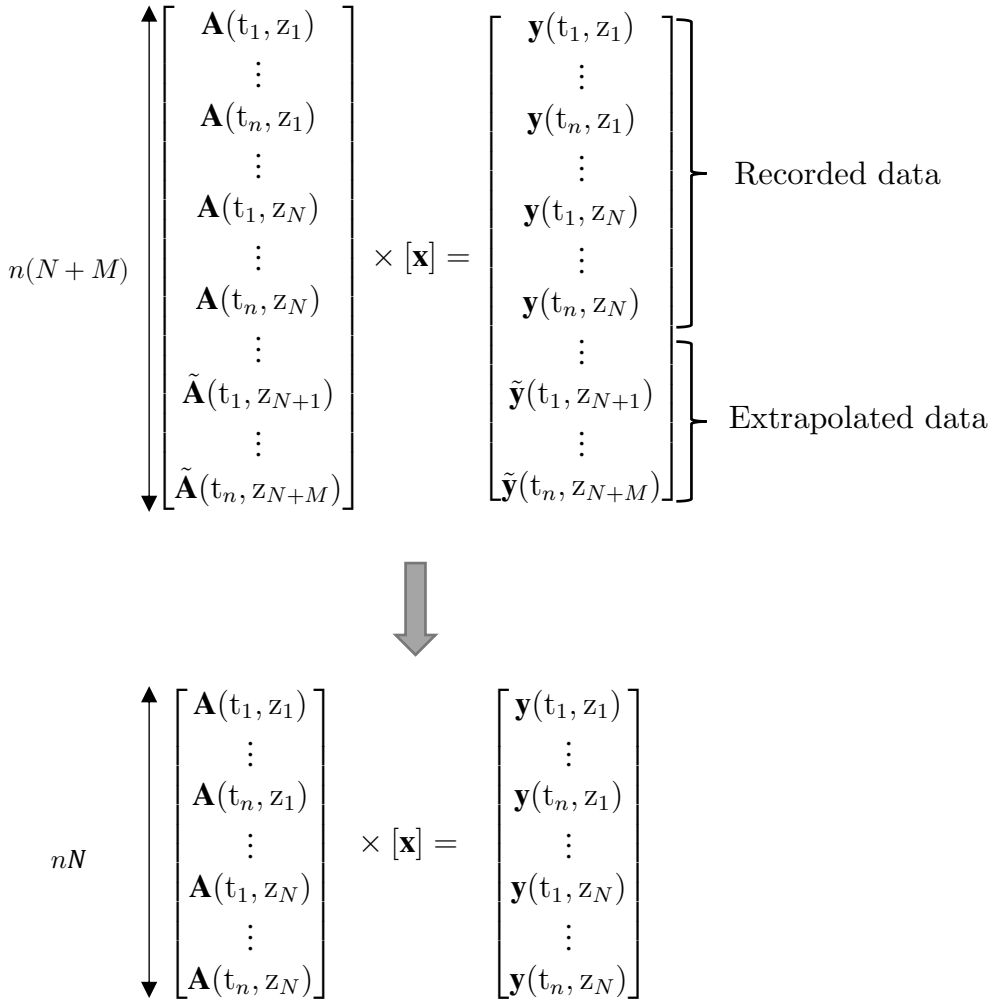

Fig. 4.2: Sampling matrix construction for CS-based extrapolation in a single spatial dimension.

also Fig. (4.2). Obviously, comparing with the dimensions of matrix $\mathbf{A}$ defined in Eq. (4.9) yields $n_0 - n_m = nN$ and $n_0 = n(N + M)$. In passing, it is noted that over-complete dictionaries can be employed as well for constructing matrices $\mathbf{B}_1$ and $\mathbf{B}_2$ to enhance the respective domain resolution (e.g., Chen et al. (2001), Van Den Berg and Friedlander (2009)).

Numerical examples

In this section, the efficacy of the proposed CS-based approach is assessed, first, in conjunction with the problem of reconstructing wind time-histories with missing data, and second, in conjunction with extrapolating to various locations in the one-dimensional spatial domain.

To this aim, 50 time-histories compatible with the PSD of Eq. (4.3) are generated by the SRM of Eq. (4.4). The parameter values used are: time duration T_0 = 255.75 s; upper cut-off frequency $w_u = 8\pi$ rad/s; $dt = 2\pi/w_u = 0.0125$ s; $\Delta\omega = 2\pi/T_0 = 0.0246$ rad/s; upper cut-off wavenumber $k_u = \pi$ rad/m; $\Delta k = 0.002$ rad/m. Next, for each time-history, 40% of missing data are introduced in uniformly random gaps. The records are then reconstructed based on the adaptive basis re-weighting approach by utilizing Eq. (4.10).

Two indicative wind velocity time-histories are shown in Fig. (4.3) corresponding to vertical heights of 50m and 62m, together with their reconstructed counterparts. It is seen that although there are notable discrepancies between the target and the reconstructed records, the main features of the time-histories are estimated satisfactorily in an average sense. This is very encouraging considering that the proposed CS-based approach in this paper focuses on estimating stochastic field statistics (e.g., PSD) defined as averages over an ensemble of realizations. Indeed, in Fig. (4.4) the PSD corresponding to a vertical height of 62m is shown, estimated as the ensemble average of the Fourier transform of the reconstructed time-histories with 40% missing data. Similarly, the cross-correlation and the coherence function referring to the two locations at 50m and 62m are also estimated based on the ensemble average of the reconstructed time-histories and are shown in

Fig. (4.5). Clearly, in all cases, comparisons with the target quantities demonstrate the capability of the CS-based methodology to estimate stochastic field statistics based on an ensemble of realizations with a relatively high degree of accuracy considering the rather large amount of missing data.

Next, the configuration shown in Fig. (4.6) is considered where the objective is to extrapolate for the entire time-history at a height of 62m and determine related statistics by utilizing measured records corresponding to heights of 50, 56, 68 and 74m. In this regard, Fig. (4.7) shows an indicative target time-history at 62m generated via Eq. (4.4) together with its estimated counterpart based on Eq. (4.9). Further, the CS-based estimated PSD at 62m is plotted in Fig. (4.8) and compared with the target PSD, whereas the estimated cross-correlation and the coherence function between the extrapolation point at 62m and two other indicative points are shown in Figs. (4.9) and (4.10), respectively. It is readily seen that the accuracy degree exhibited by the proposed CS-based methodology is, in general, satisfactory. As anticipated, however, and also observed in Fig. (4.10), the accuracy degree of the technique in estimating coherence values decreases for increasing distance between the considered points in the spatial domain.

4.3.2 Reconstruction and extrapolation in two spatial dimensions: Low-rank matrices and nuclear norm minimization

Theoretical aspects

In this section, an alternative CS approach based on nuclear norm minimization is developed to account for wind field extrapolation in two spatial dimensions. The rationale relates to the fact that a straightforward application of the CS approach proposed in section 4.3.1 based on l_1-norm minimization becomes computationally intensive, and even prohibitive in some cases, for an increasing number of dimensions. In particular, adapting the methodology in section 4.3.1 for addressing two spatial dimensions yields a sampling matrix $\mathbf{A}$ in Eq. (4.13) with a prohibitively large number of

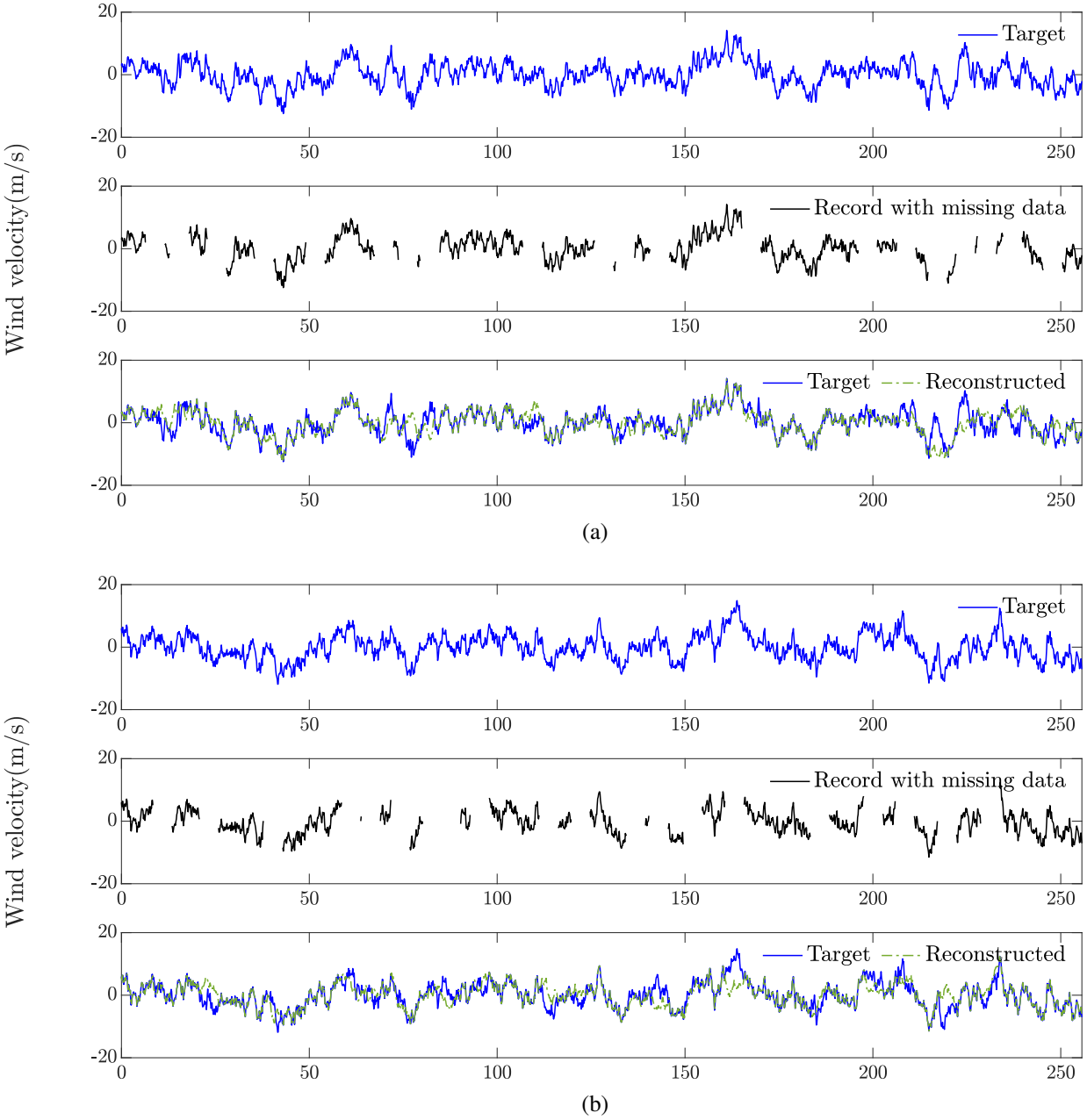

Fig. 4.3: Indicative wind velocity time-histories at a height of (a) 50m and (b) 62m; comparisons between the target and the CS-based reconstructed records considering 40% missing data.

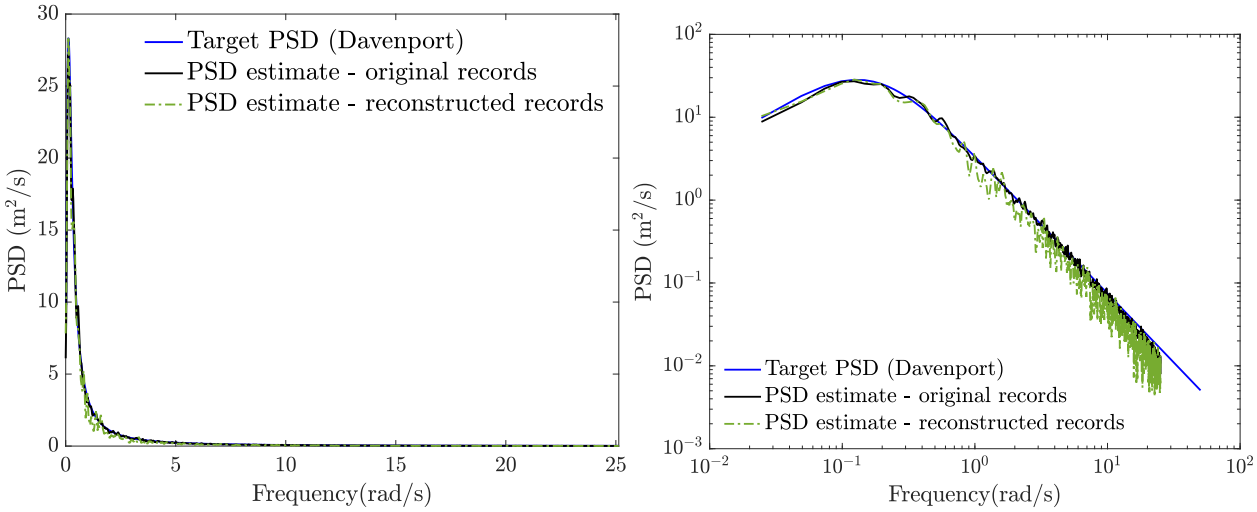

Fig. 4.4: Estimated PSD corresponding to a vertical height of 62m based on the ensemble average of reconstructed time-histories with 40% missing data; (a) linear scale and (b) logarithmic scale.

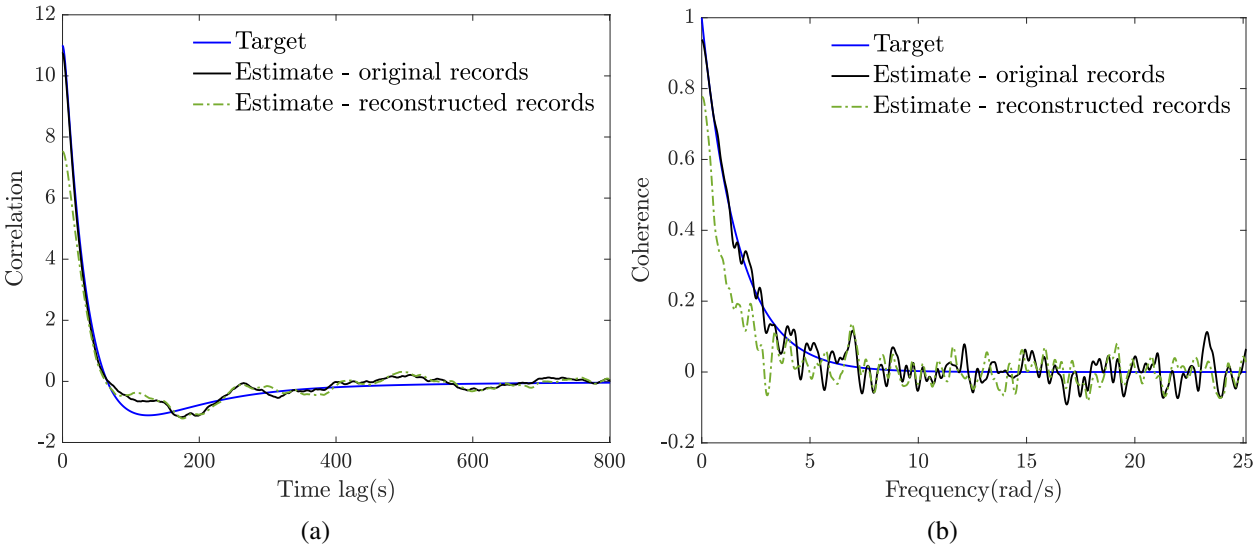

Fig. 4.5: (a) Cross-correlation and (b) coherence function estimated based on the ensemble average of reconstructed time-histories with 40% missing data corresponding to vertical heights of 50 and 62m.

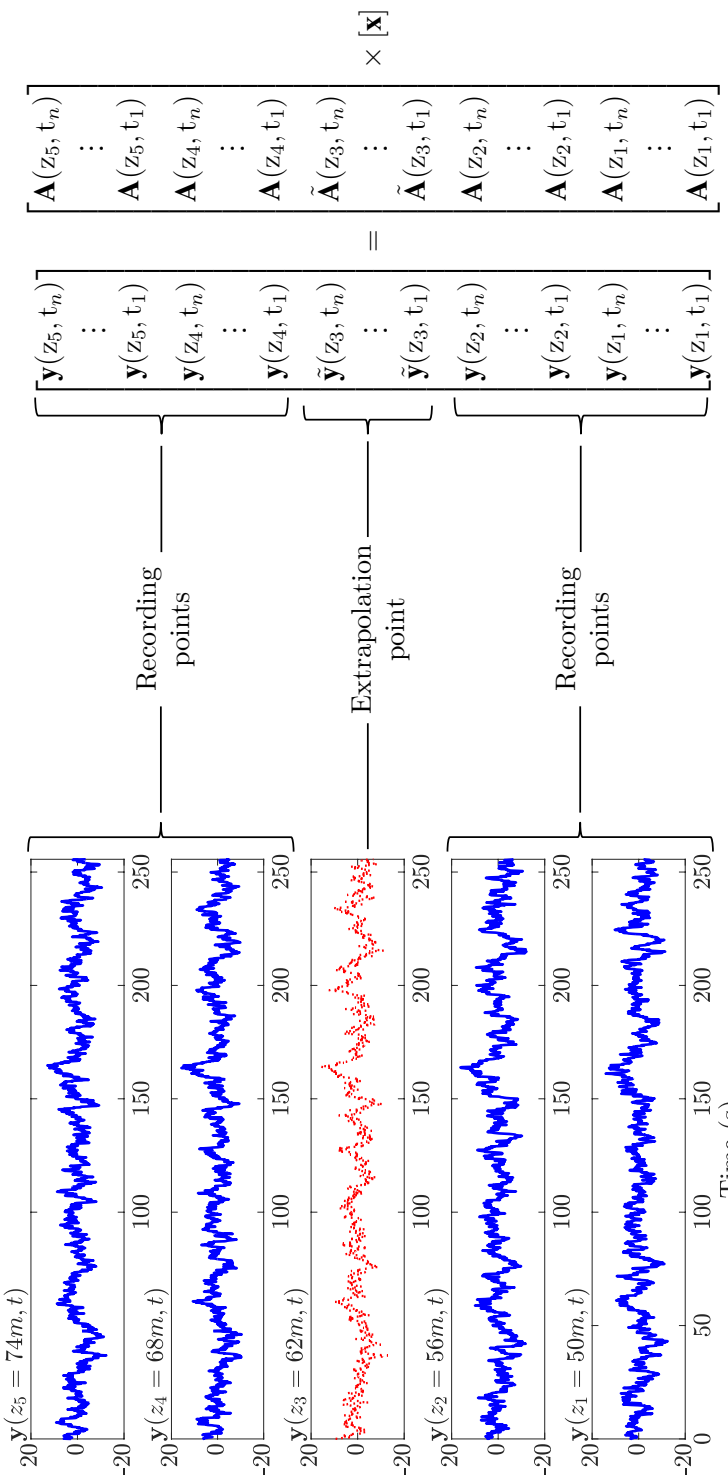

Fig. 4.6: Schematic representation of the extrapolation scheme in a single spatial dimension via compressive sampling.

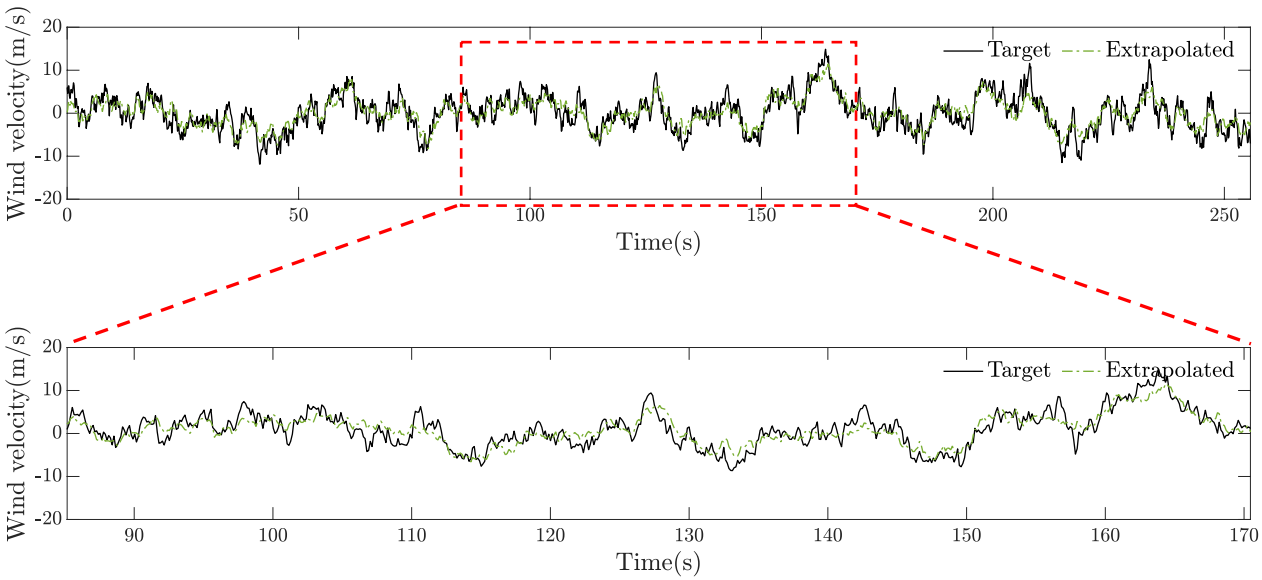

Fig. 4.7: Indicative wind velocity time-history at a height of 62m; comparisons between the target and the extrapolated records.

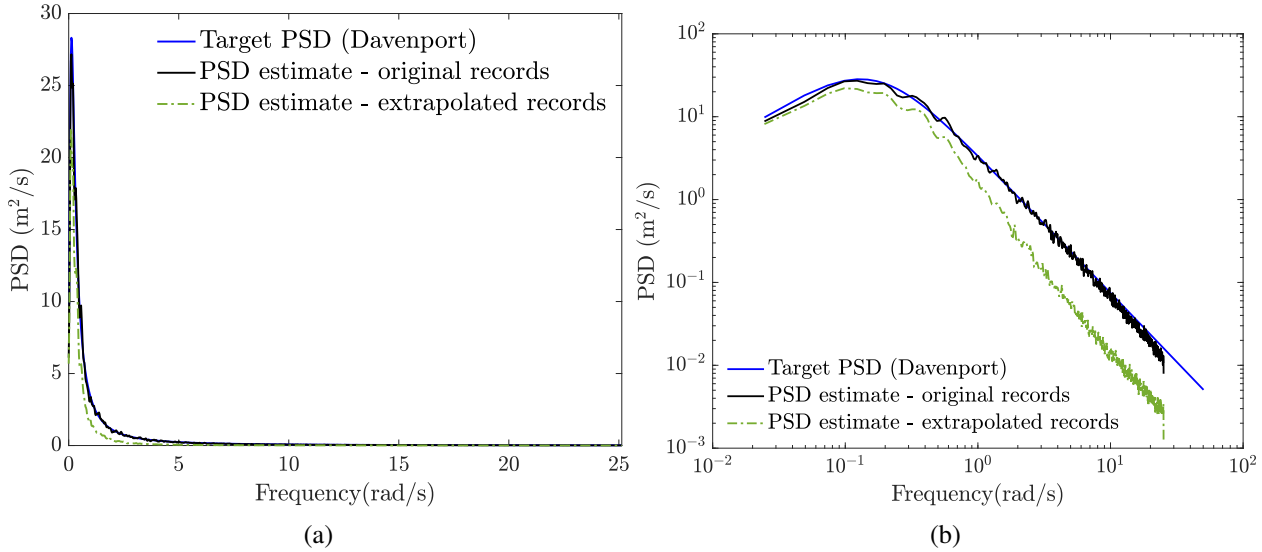

Fig. 4.8: Estimated PSD corresponding to a vertical height of 62m based on the ensemble average of CS-based extrapolated time-histories; (a) linear scale and (b) logarithmic scale.

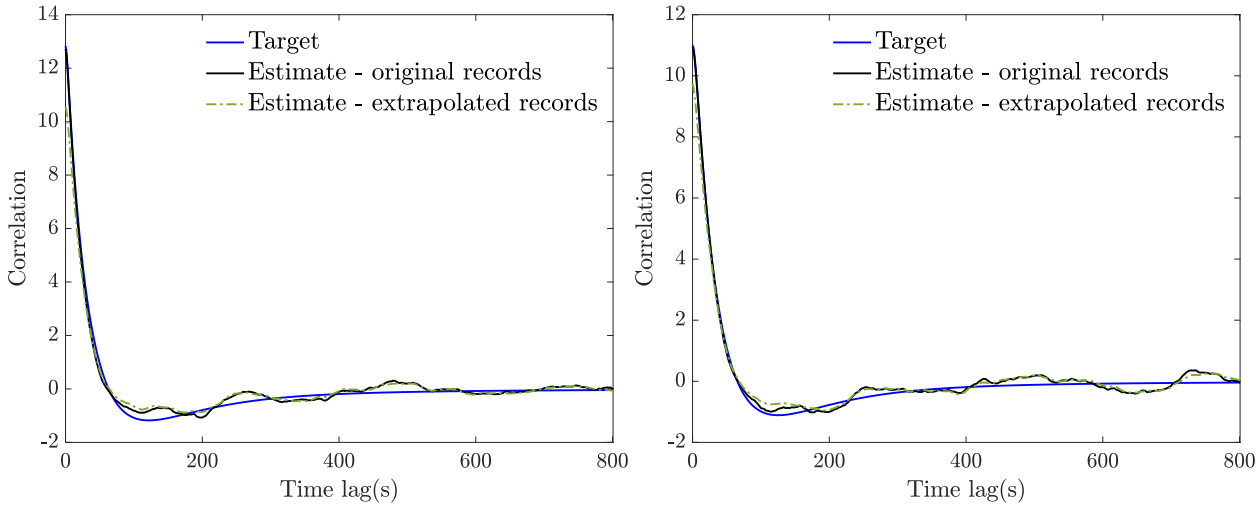

Fig. 4.9: Cross-correlation function estimated by employing CS-based extrapolated time-histories at 62m and original records at (a) 56m and (b) 74m.

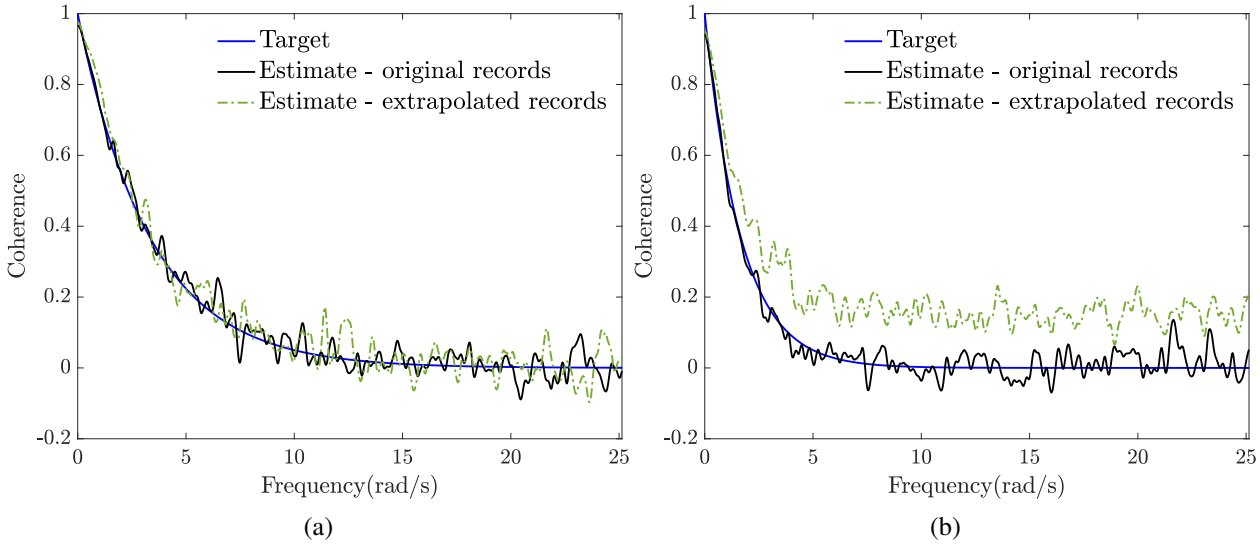

Fig. 4.10: Coherence function estimated by employing CS-based extrapolated time-histories at 62m and original records at (a) 56m and (b) 74m.

elements. Clearly, this renders the subsequent numerical implementation of the methodology at least a rather daunting, if not impossible, task. Thus, there is a need for developing alternative, more computationally efficient, approaches to address more sophisticated and realistic wind field modeling accounting for two spatial dimensions.

In this regard, the concept of a matrix norm is invoked in this section, and specifically, the nuclear norm of a matrix is employed (given as the sum of its singular values), which can be construed as a generalization of the l_1-norm to account for matrices (e.g., Meyer (2000), Friedland and Lim (2018)). In fact, minimizing the nuclear norm of low rank matrices can be viewed as an extension of minimizing the l_1-norm of sparse vectors, and thus, low rank matrices with a relatively large number of missing entries can be reconstructed with high probability (Candès and Recht, 2009). Based on the above argument, the data extrapolation problem in two spatial dimensions can be recast as a "basis-free" matrix completion problem at each time instant by appropriately re-arranging the measured data in matrix form. In passing, it is worth mentioning that nuclear norm minimization in conjunction with low rank matrices has been used recently in various civil engineering applications. Indicatively, by proposing a matrix reshape scheme, a low-rank representation of large-scale structural seismic and typhoon responses was identified in Yang et al. (2015), which proved to be beneficial for efficient data compression. The scheme was coupled in Yang and Nagarajaiah (2016) with a nuclear norm minimization algorithm for recovering of multi-channel structural response time-histories with randomly missing data.

Next, considering a matrix $\mathbf{M} \in \mathbb{R}^{n \times n}$ of rank $r << n$, with only $l < n^2$ of its entries observed, the problem of reconstructing the complete matrix can be formally expressed as

$$\begin{aligned} &\text{minimize} \quad \|\mathbf{Y}\|_* \\ &\text{subject to} \quad Y_{k,l} = M_{k,l}, \quad (k,l) \in \Omega, \end{aligned} \tag{4.14}$$

where $\|\cdot\|_*$ denotes the nuclear norm and Ω is the index set of observed entries. In general, a smaller value of rank r dictates fewer required observed matrix entries for successful matrix

completion. More specific relationships between n, r, and l can be found, indicatively, in Candès and Recht (2009); see also Kougioumtzoglou et al. (2020) for a broader perspective. Eq. (4.14) represents a convex optimization problem, and a variety of algorithms have been developed for its solution; see, for instance, Cai et al. (2010), Lin et al. (2010) as well as Kougioumtzoglou et al. (2020) and references therein. In the ensuing analysis, the Augmented Lagrangian Method (ALM) is employed (Lin et al., 2010) for recasting Eq. (4.14) into an unconstrained optimization problem and for determining the missing matrix entries; see also Hestenes (1969); Rockafellar (1973); Powell (1978). An indicative mechanization of ALM is shown in Fig. (4.11), whereas the interested reader is directed to Lin et al. (2010) for more details.

Numerical examples

In this section, the efficacy of the proposed CS methodology based on low-rank matrices and nuclear norm minimization is assessed in conjunction with extrapolating to various locations in the two-dimensional spatial domain.

Specifically, the extrapolation configuration considered in this section is shown in Fig. (4.12), where 50 two-dimensional wind velocity realizations compatible with the PSD of Eq. (4.6) are generated based on the SRM of Eq. (4.8). Next, time-histories at 12 out of the 36 grid points are considered missing. It is readily seen that, at a given time instant, extrapolating for the aforementioned 12 locations in the two-dimensional domain can be formulated as a matrix completion problem in the form of Eq. (4.14), where $\mathbf{Y}$ represents a matrix with 36 elements. Note that the low-rank assumption, required for a successful implementation of the nuclear norm minimization solution approach, can be adequately justified by considering the dependence (by construction based on Eqs. (4.6)-(4.7)) between time-histories corresponding to different locations in the two-dimensional spatial domain. In this regard, applying the ALM shown in Fig. (4.11), the time-histories corresponding to the 12 grid points are determined. An indicative extrapolated record associated with location P_2 in Fig. (4.12) is shown in Fig. (4.13). Next, the PSD estimated based on the ensemble average of

Input: observation set Ω, sampled entries $\mathcal{P}_\Omega(\boldsymbol{M_j})$ **Output:** A_k, E_k
$Y_0 = 0; E_0 = 0;$
while not converged **do**
// solve: $\mathbf{A}_{k+1} = \arg\min_{\boldsymbol{A}} L\left(\boldsymbol{A}, \boldsymbol{E}_k, \boldsymbol{Y}_k, \mu_k\right)$
$[\boldsymbol{U}, \boldsymbol{S}, \boldsymbol{V}] = \text{svd}\left(\boldsymbol{D} - \boldsymbol{E}_k + \mu_k^{-1}\boldsymbol{Y}_k\right)$
$A_{k+1} = \boldsymbol{U}\mathcal{S}_{\mu_k^{-1}}[\boldsymbol{S}]V^T$ ▷ $\mathcal{S}$: soft thresholding (shrinkage) operator
// solve: $\boldsymbol{E}_{k+1} = \arg\min_{\pi_\Omega(\boldsymbol{E})=0} L\left(\boldsymbol{A}_{k+1}, \boldsymbol{E}, \boldsymbol{Y}_k, \mu_k\right)$
$\boldsymbol{E}_{k+1} = \pi_{\bar{\Omega}}\left(\boldsymbol{M}_j - \boldsymbol{A}_{k+1} + \mu_k^{-1}\boldsymbol{Y}_k\right)$
$\boldsymbol{Y}_{k+1} = \boldsymbol{Y}_k + \mu_k\left(\boldsymbol{M}_j - \boldsymbol{A}_{k+1} - \boldsymbol{E}_{k+1}\right); \mu_{k+1} = \rho\mu_k$
$k \quad k+1$
end while

Fig. 4.11: Augmented Lagrange Multipliers (ALM) Method based on Lin et al. (2010).

.

the extrapolated time-histories corresponding to location P_2 is shown in Fig. (4.14), whereas the estimated cross-correlation and the coherence function between points P_1 and P_3 are presented in Fig. (4.15). Clearly, the proposed methodology exhibits a high degree of accuracy in estimating related statistics. To further assess its performance, the more challenging configuration shown in Fig. (4.16) is considered, where only 18 out of the 36 grid points are measurement locations. Indicatively, Fig. (4.17) shows the estimated PSD at location P_1 as shown in Fig. (4.16). The estimated cross-correlation and coherence functions between points P_1 and P_2 and between points P_1 and P_3 are shown in Figs. (4.18) and Figs. (4.19), respectively. The accuracy degree exhibited remains satisfactory, although it tends to deteriorate as the distance between the locations increases.

4.4 Concluding remarks

In this paper, first, a CS approach based on l_1-norm minimization in conjunction with an adaptive basis re-weighting scheme has been developed for wind field time-histories reconstruction and extrapolation in a single spatial dimension. Second, to address computational challenges associated with higher-dimensional domains, a CS approach based on nuclear norm minimization has been developed for wind field extrapolation in two spatial dimensions. Various numerical examples

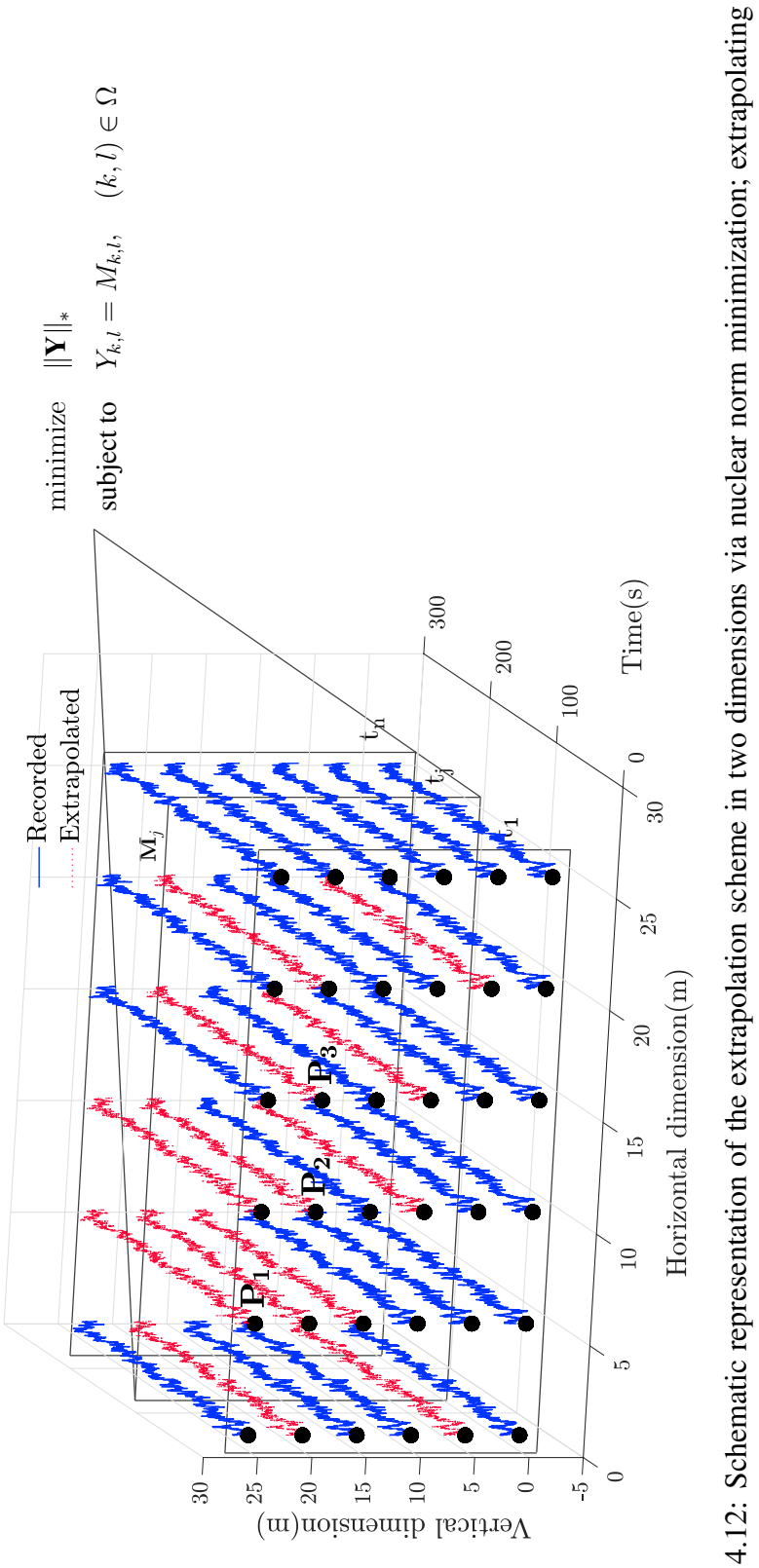

Fig. 4.12: Schematic representation of the extrapolation scheme in two dimensions via nuclear norm minimization; extrapolating to 12 grid points based on 24 measurement locations.

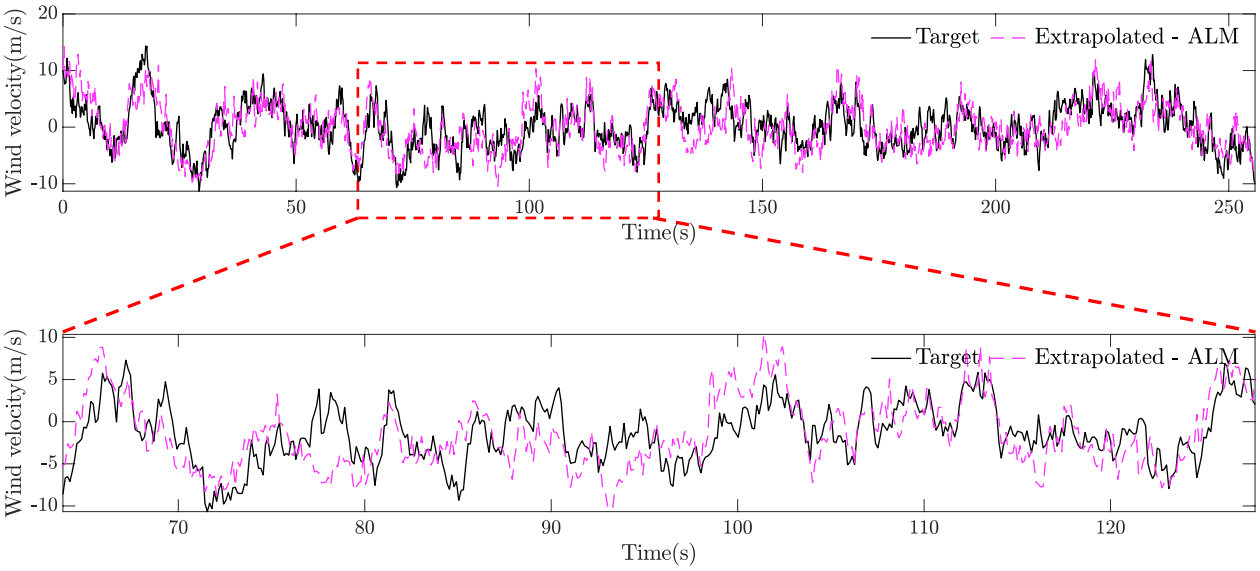

Fig. 4.13: Extrapolated time history at point P_2 of Fig. (4.12).

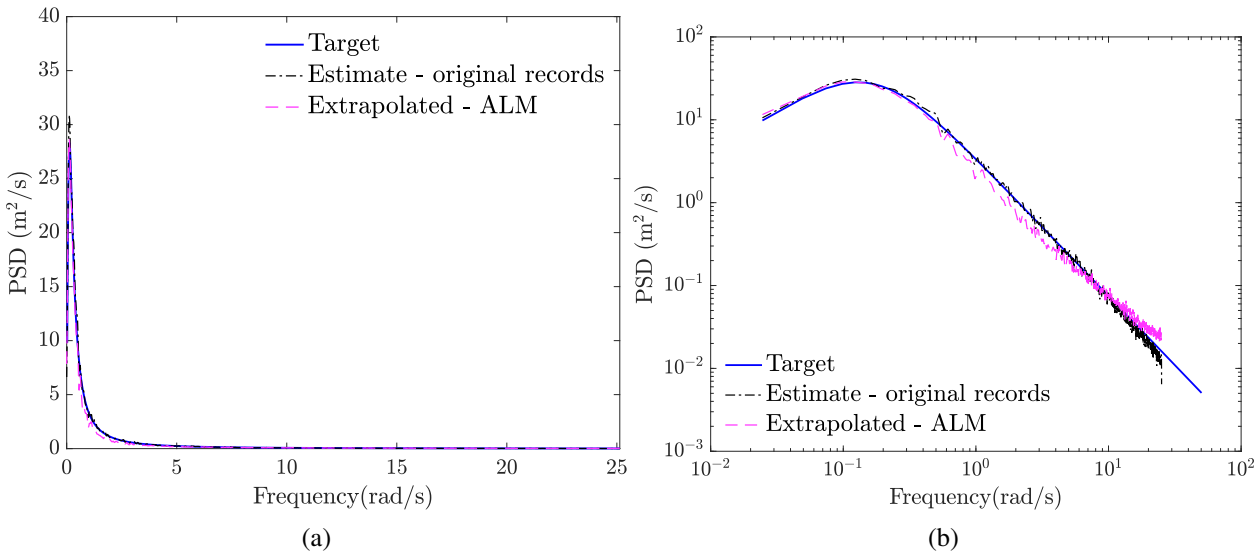

Fig. 4.14: Estimated PSD corresponding to point P_2 as shown in Fig. (4.12) based on the ensemble average of ALM-based extrapolated time-histories; (a) linear scale and (b) logarithmic scale.

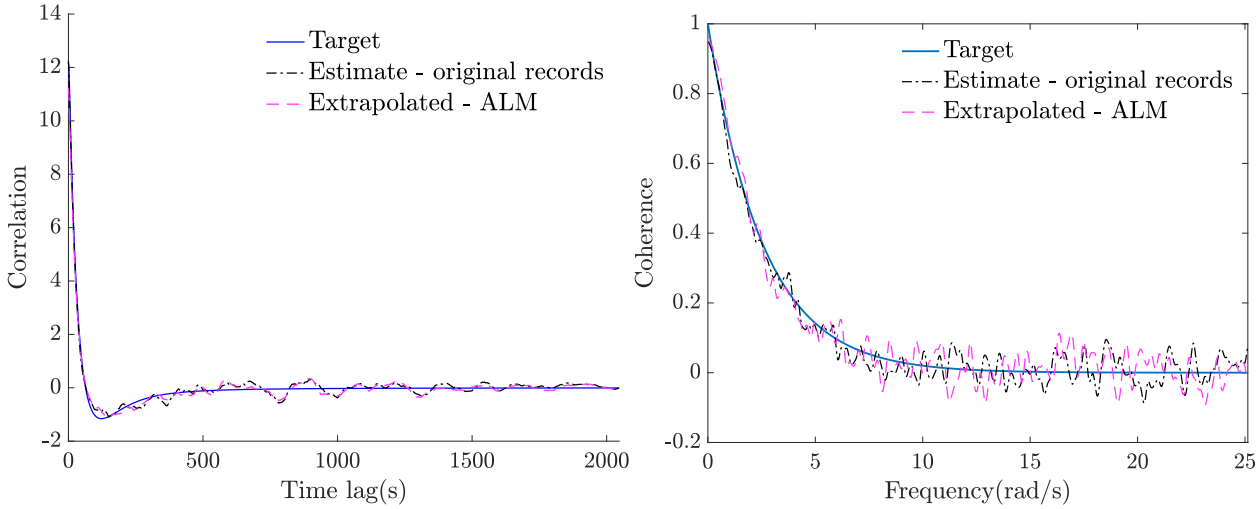

(a) (b)

Fig. 4.15: (a) Cross-correlation and (b) coherence function between the ALM-based extrapolated time histories of points P_1 and P_3 as shown in Fig. (4.12).

have been considered for demonstrating the reliability of the proposed methodologies regarding reconstruction and extrapolation of wind field data compatible with a joint wavenumber-frequency PSD. It has been shown that the methodologies exhibit a relatively high degree of accuracy in estimating relevant statistics of the underlying stochastic field based on the ensemble of the reconstructed/extrapolated realizations, even for a large percentage of missing data. However, as anticipated, the accuracy degree in estimating coherence values decreases for increasing distance between the considered locations in the spatial domain. Finally, it is worth noting that the developed methodologies can be used potentially for environmental hazard modeling within the context of performance-based design optimization of structural systems.

CRediT authorship contribution statement

George Pasparakis: Conceptualization, Methodology, Software, Writing - original draft, Visualization, Validation. Ketson dos Santos: Conceptualization, Methodology. Ioannis A. Kougioumtzoglou: Conceptualization, Methodology, Writing - review & editing, Supervision, Project admin-

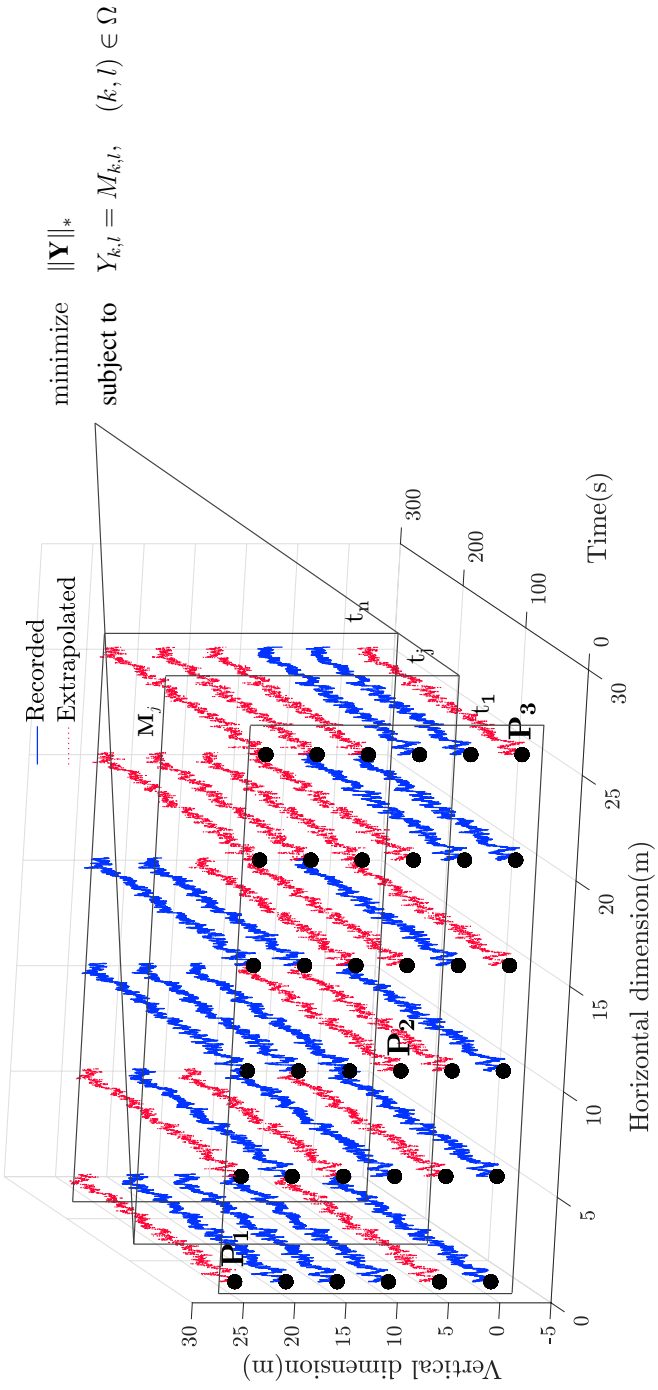

Fig. 4.16: Schematic representation of the extrapolation scheme in two dimensions via nuclear norm minimization; extrapolating to 18 grid points based on 18 measurement locations.

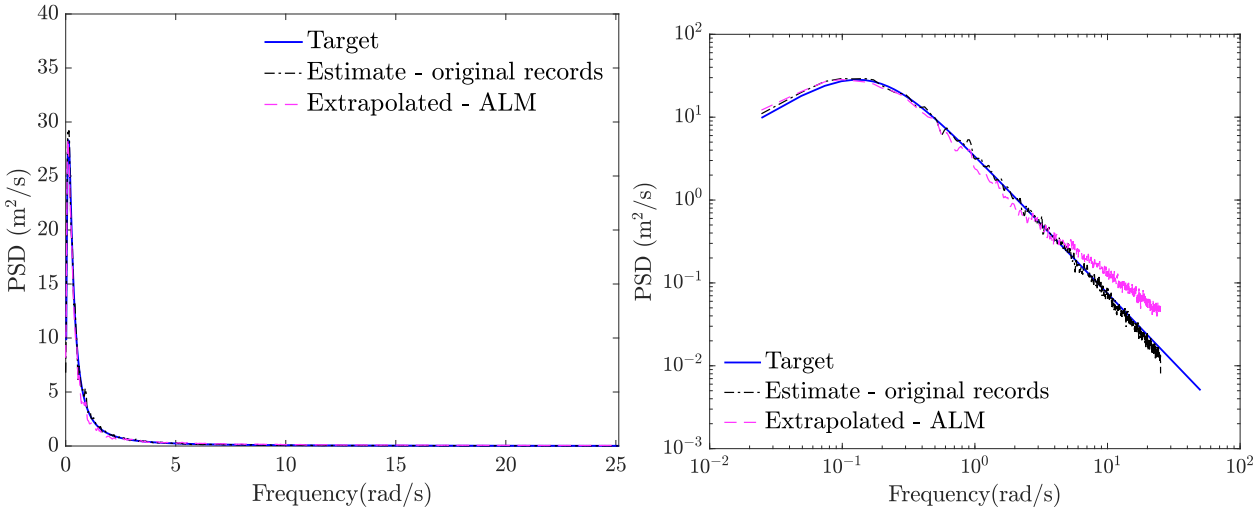

Fig. 4.17: Estimated PSD corresponding to point P_1 as shown in Fig. (4.16) based on the ensemble average of ALM-based extrapolated time-histories; (a) linear scale and (b) logarithmic scale.

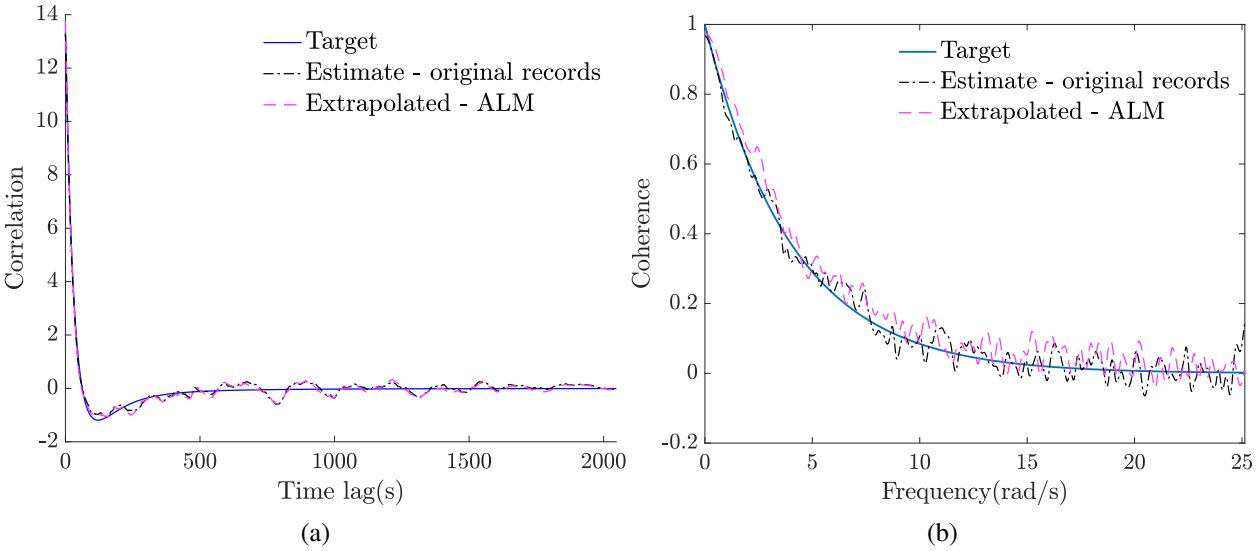

Fig. 4.18: (a) Cross-correlation and (b) coherence function between the ALM-based extrapolated time histories of points P_1 and P_2 as shown in Fig. (4.16).

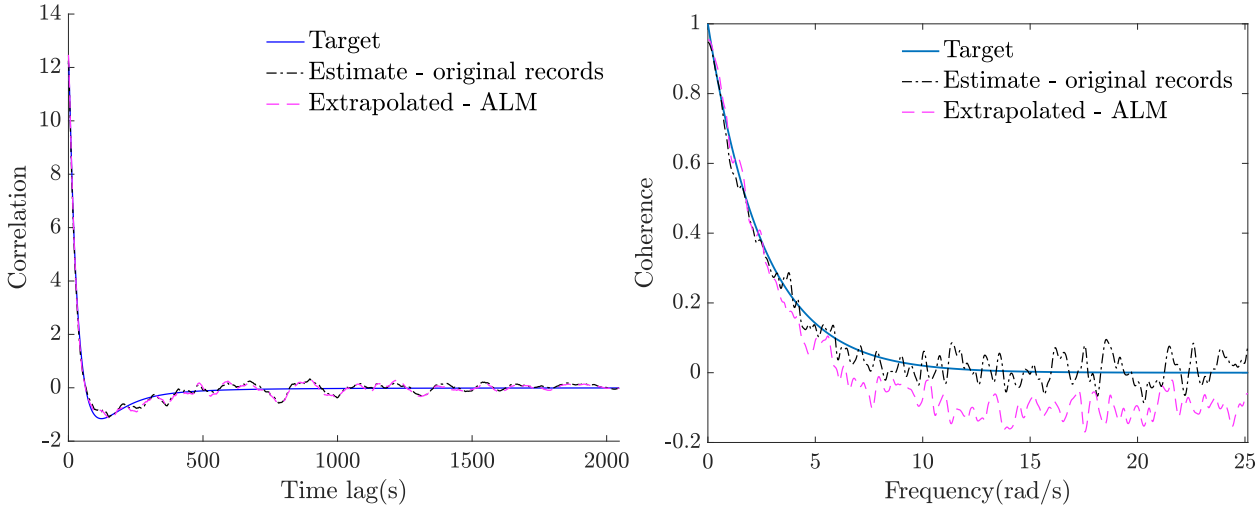

Fig. 4.19: (a) Cross-correlation and (b) coherence function between the ALM-based extrapolated time histories of points P_1 and P_3 as shown in Fig. (4.16).

istration, Funding acquisition. Michael Beer: Supervision, Funding acquisition.

Declaration of Competing Interest

The authors declare that they have no known competing financial interests or personal relationships that could have appeared to influence the work reported in this paper.

Acknowledgement

G. D. Pasparakis and M. Beer gratefully acknowledge the support and funding from the European Union's Horizon 2020 research and innovation programme under the Marie Skłodowska-Curie grant agreement No 764547.

I. A. Kougioumtzoglou gratefully acknowledges the support by the CMMI Division of the National Science Foundation, USA (Award number: 1724930).

Chapter 5

Research article 4: Discovering nonlinear structural system dynamics based on compressive sampling concepts and tools

Discovering nonlinear structural system dynamics based on compressive sampling concepts and tools

George D. Pasparakis[a], V. C. Fragkoulis[a], I. A. Kougioumtzoglou[b,*], M. Beer[a,c,d]

[a]*Institute for Risk and Reliability, Leibniz Universität Hannover, Callinstr. 34, 30167 Hannover, Germany*

[b]*Department of Civil Engineering and Engineering Mechanics, Columbia University*

[c]*Institute for Risk and Uncertainty and School of Engineering, University of Liverpool, Liverpool L69 7ZF, UK*

[d]*International Joint Research Center for Engineering Reliability and Stochastic Mechanics, Tongji University, Shanghai, China*

Abstract: A data-driven technique based on compressive sampling concepts and tools is developed for discovering the governing equations of stochastically excited structural systems exhibiting diverse nonlinear behaviors and/or following a fractional derivative modeling. This is done by relying on measured data and by utilizing a state-variable formulation of the system governing equations. Further, considering an expansion basis for approximating the nonlinear system dynamics leads to either an over- or an under-determined system of equations. This is solved based on sparsity-promoting numerical techniques for determining the active coefficients in the expansion basis. Note that the uncertainty associated with the model estimate is also quantified based on a Bayesian formulation of the technique. An indicative numerical example pertaining to a nonlinear electromechanical energy harvester with fractional derivative elements is considered for demonstrating the reliability of the technique, even in cases of highly limited/incomplete measured data.

Keywords: Wind data; Stochastic field; Sparse representations; Compressive sampling; Low-rank matrix.

*Corresponding author

E-mail addresses: george.pasparakis@irz.uni-hannover.de (G. D. Pasparakis), ketson.santos@epfl.ch (Ketson R.M. dos Santos), ikougioum@columbia.edu (I. A. Kougioumtzoglou), beer@irz.uni-hannover.de (M.Beer).

5.1 Introduction

A novel paradigm of data-driven model discovery has emerged in recent years (e.g., Brunton and Kutz (2022)). This framework can readily account for arbitrary nonlinear and time-variant behaviors, and is motivated primarily by the fact that in many problems a purely physics-based modeling of the governing dynamics by resorting to first-principles may be untenable. However, it can be argued that, for data-driven modeling to be efficacious, the identified model should exhibit sparsity in the sense that the fewest possible terms are considered for the description of the system dynamics. The rationale relates to the fact that the dynamics of most physical systems can be described accurately by considering only very few relevant terms in an appropriate expansion basis; thus, rendering the governing equations sparse in a high-dimensional nonlinear function space.

In this regard, approaches for sparse identification of nonlinear dynamics based on standard compressive sampling concepts and tools have been proposed recently (e.g., Schaeffer et al. (2013); Brunton et al. (2016); Champion et al. (2019); Brunton and Kutz (2022)). Note, however, that alternative advanced compressive sampling tools can be employed that exploit additional information in the data and enhance solution sparsity. These include l_p-norm, $0 < p < 1$, minimization formulations and iterative re-weighting solution schemes, Bayesian approaches, as well as structured sparsity and dictionary learning strategies; see Kougioumtzoglou et al. (2020) for a broad perspective.

Specifically, a data-driven technique based on Bayesian compressive sampling is developed in this paper for discovering the governing equations of stochastically excited structural systems exhibiting diverse nonlinear behaviors and/or following a fractional derivative modeling. This is done by relying on measured data and by utilizing a state-variable formulation of the system governing equations. Compared to alternative state-of-the-art schemes that yield deterministic estimates for the expansion coefficient vector (e.g., Champion et al. (2019), Brunton and Kutz (2022)), the

herein developed technique is capable also of quantifying the uncertainty associated with the model estimate; thus, providing a measurable confidence degree when employing the technique as a prediction tool. An indicative numerical example pertaining to a nonlinear electromechanical energy harvester with fractional derivative elements is considered for demonstrating the reliability of the technique, even in cases of highly limited/incomplete measured data.

5.2 Mathematical formulation

5.2.1 Sparse representation of governing equations

Consider the general form of governing equations

$$\dot{\mathbf{x}} = \mathbf{f}(\mathbf{X}, \boldsymbol{\eta}) \tag{5.1}$$

where a dot above a variable denotes differentiation with respect to time; $\mathbf{f}(\cdot)$ is an operator (nonlinear, differential, etc) to be identified; and $\mathbf{X}$ and $\boldsymbol{\eta}$ are the vectors corresponding to the states of the dynamical system and the excitation, respectively. In the following, attention is directed to structural systems that can be represented by Eq. (5.1) based on a state-variable formulation, where $\mathbf{X} = [\mathbf{X_1}; \mathbf{X_2}]^{\mathrm{T}}$ with $\mathbf{X_1}$ and $\mathbf{X_2}$ denoting the response displacement and velocity, respectively.

Next, relying on measured data $\mathbf{X}$, Eq. (5.1) is approximated by

$$\dot{\mathbf{x}} = \boldsymbol{\Theta}(\mathbf{X})\boldsymbol{\Xi}, \tag{5.2}$$

where $\boldsymbol{\Theta}(\mathbf{X})$ is a library of candidate (nonlinear) functions, and $\boldsymbol{\Xi}$ denotes the coefficient vector to be determined. Note that Eq. (5.2) can represent a non-square linear system of algebraic equations for various reasons. For example, it can be an under-determined system due to missing entries in the measured data (incomplete data). Also it can be an over-determined system due to considering long

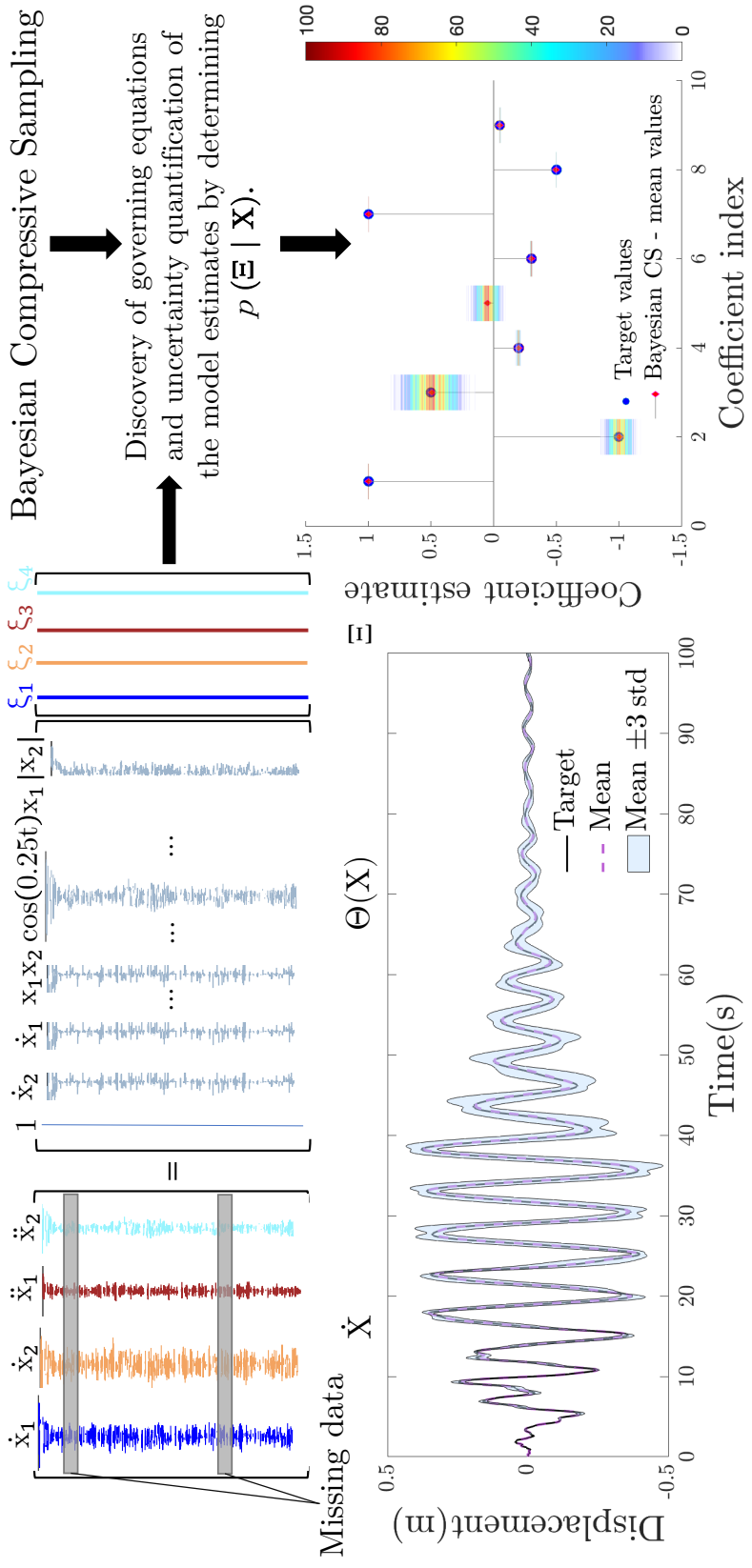

Fig. 5.1: Schematic representation of the Bayesian Compressive Sampling scheme for discovering governing equations of nonlinear dynamical systems, even when endowed with fractional derivative elements and subject to incomplete measured data.

time-series data. To derive a parsimonious model and to promote a sparse coefficient vector $\boldsymbol{\Xi}$ with only few non-zero entries, compressive sampling theory can be used and l_p-norm minimization can be applied for solving Eq. (5.2), i.e.,

$$\min \mid\mid \dot{\mathbf{x}} - \boldsymbol{\Theta}(\mathbf{X})\boldsymbol{\Xi} \mid\mid_2 + \lambda \mid\mid \boldsymbol{\Xi} \mid\mid_p \tag{5.3}$$

where $\mid\mid \cdot \mid\mid_p$ denotes the p-norm, $0 \leq p \leq 1$, and λ is a penalization factor; see also Kougioumtzoglou et al. (2020) for a broad perspective.

Regarding alternative solution schemes for treating Eq. (5.2), Brunton et al. (2016) utilized a sequentially Thresholded Least Squares (STLS) algorithm. However, this optimization scheme relies heavily on the selection of the thresholding level, which, in many cases, can be arbitrary and sub-optimal. Further, the algorithm yields a unique solution based on the Moore-Penrose pseudo-inverse only under the assumption that $\boldsymbol{\Theta}(\mathbf{X})$ has full column rank, i.e., the system of Eq. (5.2) is overdetermined. Furthermore, Champion et al. (2019) utilized an l_1-norm minimization approach for solving Eq. (5.2), which is a special case of the solution treatment proposed in Eq. (5.3). Clearly, as demonstrated in various diverse applications in engineering dynamics (e.g., Zhang et al. 2018), employing an l_p-norm minimization with $p < 1$ is anticipated to promote solution sparsity further and yield an even sparser representation of system dynamics.

Nevertheless, even the solution treatment in Eq. (5.3) yields a deterministic estimate for the coefficient vector $\boldsymbol{\Xi}$. In other words, there is no quantification of the uncertainty associated with the accuracy degree of the identified sparse model. To address this limitation, and provide with a measurable confidence degree when employing the technique as a prediction tool, a Bayesian formulation is developed in the following section. This provides a posterior probability density function (PDF) $p(\boldsymbol{\Xi} \mid \mathbf{X})$ which quantifies the uncertainty of the coefficient vector estimate $\boldsymbol{\Xi}$ given the data $\mathbf{X}$.

5.2.2 Bayesian compressive sampling

Following Ji et al. (2008), consider a signal $\mathbf{g}$ expanded in a basis $\mathbf{\Phi}$ as

$$\mathbf{g} = \mathbf{\Phi}\mathbf{w} + \epsilon, \tag{5.4}$$

where $\mathbf{w}$ is the coeffiicient vector and ϵ is an error vector of identically distributed Gaussian random variables with zero mean variance σ_ϵ^2. Comparing Eqs. (5.2) and (5.4), it is seen that $\mathbf{g} = \text{vec}\,(\dot{\mathbf{x}})$, $\mathbf{\Phi} = \mathbf{I} \otimes \mathbf{\Theta}(\mathbf{X})$ and $\mathbf{w} = \text{vec}\,(\Xi)$, where "vec" represents the vectorization operator, "$\otimes$" is the Kronecker product and $\mathbf{I}$ is the identity matrix. Next, a zero mean Gaussian prior PDF is considered for the coefficients $\mathbf{w}$ in the form

$$p\left(\mathbf{w} \mid \sigma_{\mathbf{w}}\right) = \prod_i N\left(w_i \mid 0, \sigma_{w_i}^2\right) \tag{5.5}$$

where $\mathbf{w}, \sigma_{\mathbf{w}}, \sigma_\epsilon$ are unknowns. Further, the conditional PDF of the unknowns is given by

$$p\left(\mathbf{w}, \sigma_{\mathbf{w}}, \sigma_\epsilon^2 \mid \mathbf{g}\right) = p\left(\mathbf{w} \mid \mathbf{g}, \sigma_{\mathbf{w}}, \sigma_\epsilon^2\right) p\left(\sigma_{\mathbf{w}}, \sigma_\epsilon^2 \mid \mathbf{g}\right) \tag{5.6}$$

and the first term on the right hand side of Eq. (5.6) is expressed based on the Bayes' theorem as

$$p\left(\mathbf{w} \mid \mathbf{g}, \sigma_{\mathbf{w}}, \sigma_\epsilon^2\right) = \frac{p\left(\mathbf{g} \mid \mathbf{w}, \sigma_\epsilon^2\right) p\left(\mathbf{w} \mid \sigma_{\mathbf{w}}\right)}{p\left(\mathbf{g} \mid \sigma_{\mathbf{w}}, \sigma_\epsilon^2\right)} \tag{5.7}$$

Furthermore, considering the Gaussian assumption for the error in Eq. (5.4), the likelihood $p\left(\mathbf{g} \mid \mathbf{w}, \sigma_\epsilon^2\right)$ in Eq. (5.7) is also Gaussian. In this regard, taking into account also Eq. (5.6), the posterior distribution takes a multivariate Gaussian form, i.e., $p\left(\mathbf{w} \mid \mathbf{g}, \sigma_{\mathbf{w}}, \sigma_\epsilon^2\right) = N(\mu, \mathbf{\Sigma})$ with mean vector and covariance matrix

$$\mu = \sigma_\epsilon^{-2}\mathbf{\Sigma}\mathbf{\Phi}^{\mathrm{T}} \text{ and } \mathbf{\Sigma} = \left(\mathbf{A} + \sigma_\epsilon^{-2}\mathbf{\Phi}^{\mathrm{T}}\mathbf{\Phi}\right)^{-1}, \tag{5.8}$$

respectively, with $\mathbf{A} = \text{diag}\left(\sigma_{w_1}^{-2}, \sigma_{w_2}^{-2}, \dots\right)$. Further, the optimal values for $\sigma_{\mathbf{w}}$ and σ_{ϵ} are computed based on a type-II maximum likelihood estimation (MLE) scheme (e.g. MacKay (1992))

Obviously, the uncertainty of the estimated coefficient vector $\boldsymbol{\Xi}$ in Eq. (5.2) is quantified herein based on the multivariate Gaussian PDF $p(\boldsymbol{\Xi} \mid \mathbf{X})$ with mean vector and covariance matrix given by Eq. (5.8). The mechanization of the herein developed technique is provided in Fig. 5.1.

5.3 Numerical example

Following Petromichelakis et al. (2018), consider next a nonlinear electromechanical energy harvester governed by the coupled equations

$$\begin{aligned} &\ddot{x} + 2\zeta\left(\mathbf{D}^{\gamma}x\right)(t) + x + \delta x^2 + \beta x^3 - \lambda y = f(t) \\ &\dot{y} + \alpha y + k\dot{x} = 0 \end{aligned} \tag{5.9}$$

where q denotes the displacement of the beam and y the induced voltage. The applied excitation $f(t)$ is modeled as a Gaussian, zero-mean white noise process with a power spectrum value $S_0 = 0.05$. Further, the parameter values used next are: $\zeta = 0.15$, $\gamma = 0.5$, $\beta = 0.05$, $\delta = 0.2$, $\lambda = 0.5$, $\alpha = 0.05$, $k = 0.5$, whereas the response vector $\mathbf{x}^{\mathrm{T}} = [x\ \dot{x}\ y]$ is obtained by solving numerically Eq. (5.9). Next, Eq. (5.2) is constructed by considering the quite general library of functions

$$\boldsymbol{\Theta}(\mathbf{X}) = \left[\mathbf{1},\ \mathbf{x},\ \mathbf{x}^{P_i},\ |\ \mathbf{x}\ |,\ \mathbf{D}^{\gamma_k}\mathbf{x},\ \text{sgn}(\mathbf{x}),\ f(t)\right], \tag{5.10}$$

where P_i is the polynomial order for different values of i and "$\circ$" denotes the Hadamard product. Also, a 90% randomly missing data scenario is considered. Applying the developed technique in section 5.2 yields the coefficient vector $\boldsymbol{\Xi}$ Gaussian PDF estimates described by Eq. (5.8). They are plotted in Fig. 5.2 and compared with the target deterministic values. It is seen that the mean values of the coefficients are in excellent agreement with the target values. Coefficient vector estimates

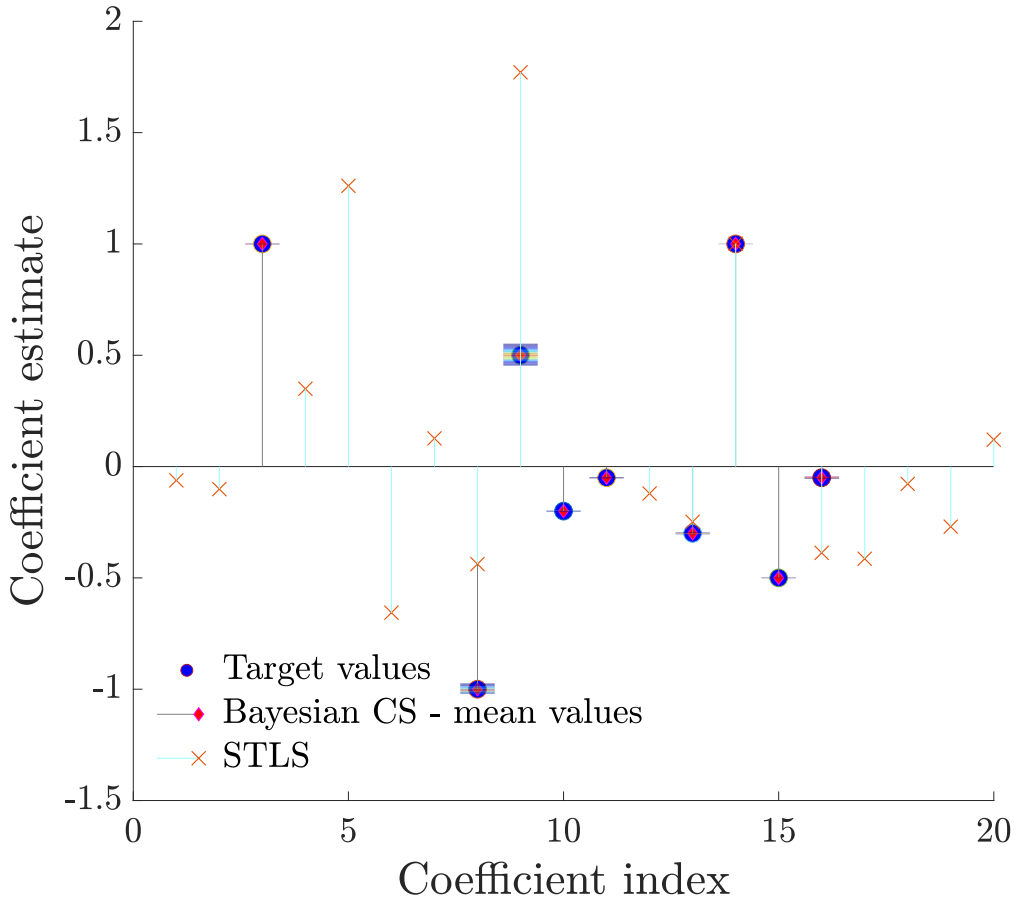

Fig. 5.2: Uncertainty quantification of the estimated coefficient vector corresponding to the system of Eq. (5.9) subject to measured time-histories with 90% missing data.

based on the STLS algorithm Brunton et al. (2016) are included as well. Clearly, however, the STLS-based scheme fails to yield a sparse, parsimonious solution. Further, a Monte Carlo simulation is performed (1000 samples) by using Eq. (5.2) and considering the PDF of the coefficient vector given by Eq. (5.8). In this regard, Fig. 5.3 shows the predicted response voltage time-history along with the quantified uncertainty.

5.4 Concluding remarks

A data-driven technique based on Bayesian compressive sampling has been developed for discovering the governing equations of stochastically excited structural systems exhibiting diverse nonlinear

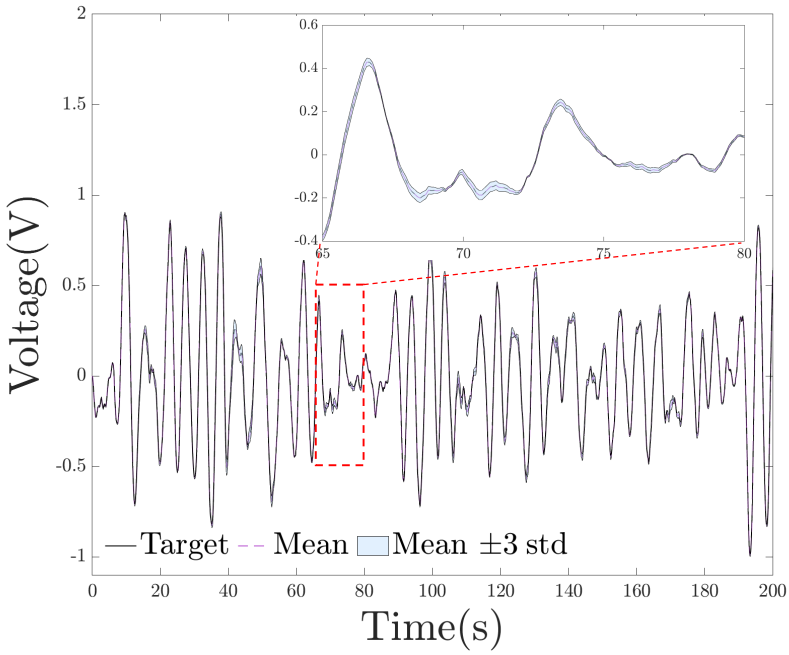

Fig. 5.3: Uncertainty quantification of the estimated response of the system of Eq. (5.9).

behaviors and/or following a fractional derivative modeling. A significant advantage of the technique relates to the fact that the uncertainty associated with the model estimate is also quantified. Further, the technique has exhibited robust performance even in cases of highly limited/incomplete data.

Acknowledgement

G. D. Pasparakis and M. Beer gratefully acknowledge the support and funding from the European Union's Horizon 2020 research and innovation programme under the Marie Skłodowska-Curie grant agreement No 764547.

I. A. Kougioumtzoglou gratefully acknowledges the support by the CMMI Division of the National Science Foundation, USA (Award number: 1724930).

Chapter 6
Concluding Remarks

In this chapter, the main conclusions regarding the contributions of the present thesis are reviewed and some future research paths are discussed.

Chapter 1 serves as an introductory part and summarizes key challenges in Random Vibration. These pertain to stochastic response determination of systems with singular matrices, probabilistic modeling of stochastic processes in the presence of missing data and data-driven system identification. Further, state-of-the-art frameworks are briefly discussed and potential solution frameworks are introduced to address some of the associated limitations.

In chapter 2 approximate analytical expressions have been derived for determining the response evolutionary power spectrum of MDOF systems with singular matrices subject to non-stationary excitation. The aim of the proposed formulation is geared towards generalizing earlier results in stochastic dynamics to systems with singular matrices. The main focus is concentrated on the treatment of complex multi-body systems whose governing equations of motion are derived by utilizing non-generalized coordinate modeling approaches. This is motivated by the fact that unconventional modeling schemes that employ additional DOFs are associated with enhanced flexibility and facilitate the derivation of cost-effective solution methodologies, especially with increasing model complexity and numbers of DOF. The proposed solution is derived by augmenting the constraints equations in the system parameter matrices and by expanding the response on a GHW basis. Exploiting the orthogonality properties of the latter yields an input-output relationship by means of a generalized M-P harmonic wavelet frequency response function. The proposed methodology is applied to nonlinear systems with singular matrices by employing the SLM which enables the def-

inition of a new, equivalent linear system. The envisaged computational accuracy for both linear and nonlinear systems is displayed by comparing results from a generalized and a non-generalized coordinate modeling scheme.

In chapter 3 the stochastic response determination problem of chapter 2 has been cast into an alternative solution framework which is geared towards improving the versatility of the technique. Considering the fact that GHWs do not form an orthogonal basis in a finite time interval, a periodization procedure has been carried out and a set of connection wavelet coefficients has been derived. The merit of this approach is twofold. First, it bypasses the restriction of "local stationarity" which is inherent in the previous implementation. Secondly, it allows for a convenient expansion of the response process permitting the energy transfer between different scales and translation levels. An additional contribution in chapter 3 pertains to the fact that the proposed technique treats general forms of system constraints, which renders the technique applicable to a broader class of engineering systems. This is supported by comparing obtained results with MCS estimates. Future research directions include coupling of the method presented in chapter 3 with the statistical linearization method in order to account for nonlinear systems. It is noted that the M-P matrix inverse, which is employed in this work, is based on l_2-norm minimization. In view of this, exploring the potential of alternative algorithms, such as the l_1-norm minimization is identified as a future research direction.

In chapter 4 a sparse representation framework has been developed for the statistical estimation of wind field models in the presence of missing data and/or limited observations. Specifically, a sparse representation scheme has been employed for treating incomplete (in temporal and spatial domains) wind speed measurements. Within this context, the wind time histories are projected on an appropriately constructed and sufficiently sparse Fourier basis whose coefficients are found via a sparsity promoting l_1-weighted norm minimization algorithm. The extrapolation scheme is extended to two spatial dimensions via a "matrix-reshape" nuclear norm minimization scheme which greatly reduces the associated computational overheads. The reported statistical accuracy and robustness of

the the method (even in the presence of high degree of missing data) poses as a promising tool for calibrating probabilistic models from field measurements. Further, application of the method to non-stationary, multi-dimensional data in the context of response reliability assessment is also identified as future work.

In chapter 5 a novel technique has been proposed for sparse identification of nonlinear dynamical systems utilizing exclusively input/output measurements. The methodology relies on the fact that most physical system dynamics can be captured by a few possible terms in an appropriately constructed expansion basis. In light of this, a BCS treatment has been developed for determining the governing equations of stochastically excited structural systems. This builds upon previous research efforts in the field of sparsity-based system identification. In this work, utilizing a BCS implementation further promotes sparsity and renders the method more robust to missing data configurations. Further, it enables quantifying the uncertainty associated with the model estimate as well as assessing the confidence degree in future predictions. The reliability of the method in identifying systems following fractional derivative modeling has also been investigated. Future research directions include coupling of the proposed technique with dimensionality reduction approaches. This will potentially yield a parsimonious, physically interpretable model in the reduced space which can be utilized as a prediction tool for high-dimensional complex systems.

List of publications

In preparation

- Pasparakis, G.D., Fragkoulis, V.C., Kougioumtzoglou, I.A. and Beer, M et al. 2022. Discovering nonlinear structural system dynamics via compressive sampling and dimensionality reduction approach.

Peer-Reviewed International Journals

- Pasparakis, G. D., dos Santos, K. R. M., Kougioumtzoglou, I.A. and Beer, M., 2022. Wind data extrapolation and stochastic field statistics estimation via compressive sampling and low rank matrix recovery methods. *Mechanical Systems and Signal Processing, 162*, p.107975.
- Pasparakis, G. D., Kougioumtzoglou, I. A., Fragkoulis, V. C., Kong, F. and Beer, M., 2022. Excitation–response relationships for linear structural systems with singular parameter matrices: A periodized harmonic wavelet perspective. *Mechanical Systems and Signal Processing, 169,* p.108701
- Pasparakis, G. D., Fragkoulis, V. C. and Beer, M., 2021. Harmonic wavelets based response evolutionary power spectrum determination of linear and nonlinear structural systems with singular matrices. *Mechanical Systems and Signal Processing, 149*, p.107203.

Peer-Reviewed Conference Proceedings (Papers)

- Pasparakis, G. D., Fragkoulis, V. C., Kong, F. and Beer, M. 2022. Stochastic response analysis of a piezoelectric harvesting device subjected to non-stationary wind loading. *Proceedings of the* 8^{th} *International Symposium on Reliability Engineering and Risk Management (ISRERM 2022), Hannover, Germany, September* $4^{th} - 7^{th}$ *2022*, Research Publishing (S) Pte Ltd.

References

Addison, P. S. (2017). *The illustrated wavelet transform handbook: introductory theory and applications in science, engineering, medicine and finance*. CRC press.

Adhikari, S., Friswell, M., and Inman, D. (2009). Piezoelectric energy harvesting from broadband random vibrations. *Smart Materials and Structures*, 18(11):115005.

Antoniou, E. N., Pantelous, A. A., Kougioumtzoglou, I. A., and Pirrotta, A. (2017a). Response determination of linear dynamical systems with singular matrices: A polynomial matrix theory approach. *Applied Mathematical Modelling*, 42:423–440.

Antoniou, E. N., Pantelous, A. A., Kougioumtzoglou, I. A., and Pirrotta, A. (2017b). Response determination of linear dynamical systems with singular matrices: A polynomial matrix theory approach. *Applied Mathematical Modelling*, 42:423–440.

Azam, S., Chatzi, E., and Papadimitriou, C. (2015). A dual kalman filter approach for state estimation via output-only acceleration measurements. *Mechanical Systems and Signal Processing*, 60:866–886.

Balakrishnan, A. V. (1996). Vibrating systems with singular mass-inertia matrices. In *Nonlinear Problems in Aviation and Aerospace*.

Basu, B. and Gupta, V. K. (1997). Non-stationary seismic response of mdof systems by wavelet transform. *Earthquake Engineering & Structural Dynamics*, 26(12):1243–1258.

Basu, B. and Gupta, V. K. (1998). Seismic response of sdof systems by wavelet modeling of nonstationary processes. *Journal of Engineering Mechanics*, 124(10):1142–1150.

Basu, B., Nagarajaiah, S., and Chakraborty, A. (2008). Online identification of linear time-varying stiffness of structural systems by wavelet analysis. *Structural Health Monitoring*, 7(1):21–36.

Bathe, K. (2006). *Finite element procedures*. Klaus-Jurgen Bathe.

Beck, J. L. and Papadimitriou, C. (1993). Moving resonance in nonlinear response to fully nonstationary stochastic ground motion. *Probabilistic Engineering Mechanics*, 8(3-4):157–167.

Ben-Israel, A. and Greville, T. N. E. (2003). *Generalized inverses: theory and applications*, volume 15. Springer Science & Business Media.

Bendat, J. S. and Turin, G. L. (1959). Principles and applications of random noise theory. *Physics Today*, 12(4):46–49.

Benowitz, B. A. and Deodatis, G. (2015). Simulation of wind velocities on long span structures: A novel stochastic wave based model. *Journal of Wind Engineering and Industrial Aerodynamics*, 147:154–163.

Beylkin, G. (1992). On the representation of operators in bases of compactly supported wavelets. *SIAM Journal on Numerical Analysis*, 29(6):1716–1740.

Bouc, R. (1971). Modèle mathématique d'hystérésis. *Acustica*, 21:16–25.

Brunton, S. L. and Kutz, J. N. (2022). *Data-driven science and engineering: Machine learning, dynamical systems, and control*. Cambridge University Press.

Brunton, S. L., Proctor, J. L., and Kutz, J. N. (2016). Discovering governing equations from data by sparse identification of nonlinear dynamical systems. *Proceedings of the National Academy of Sciences*, 113(15):3932–3937.

Cai, G. Q. and Lin, Y. K. (1988). A new approximate solution technique for randomly excited non-linear oscillators. *International Journal of Non-Linear Mechanics*, 23(5-6):409–420.

Cai, J., Candès, E. J., and Shen, Z. (2010). A singular value thresholding algorithm for matrix completion. *SIAM Journal on Optimization*, 20(4):1956–1982.

Campbell, S. and Meyer, C. (2009). *Generalized inverses of linear transformations*. SIAM.

Candès, E. J. and Recht, B. (2009). Exact matrix completion via convex optimization. *Foundations of Computational Mathematics*, 9(6):717.

Candes, E. J., Romberg, J. K., and Tao, T. (2006). Stable signal recovery from incomplete and inaccurate measurements. *Communications on Pure and Applied Mathematics: A Journal Issued by the Courant Institute of Mathematical Sciences*, 59(8):1207–1223.

Candès, E. J. and Wakin, M. B. (2008). An introduction to compressive sampling. *IEEE Signal Processing Magazine*, 25(2):21–30.

Caputo, M. (1967). Linear models of dissipation whose q is almost frequency independent—ii. *Geophysical Journal International*, 13(5):529–539.

Carassale, L. and Solari, G. (2006). Monte Carlo simulation of wind velocity fields on complex structures. *Journal of Wind Engineering and Industrial Aerodynamics*, 94(5):323–339.

Cattani, C. (2005). Harmonic wavelets towards the solution of nonlinear PDE. *Computers & Mathematics with Applications*, 50(8-9):1191–1210.

Champion, K., Lusch, B., Kutz, J. N., and Brunton, S. L. (2019). Data-driven discovery of coordinates and governing equations. *Proceedings of the National Academy of Sciences*, 116(45):22445–22451.

Chen, J., Song, Y., Peng, Y., and Spanos, P. D. (2018). Simulation of homogeneous fluctuating wind field in two spatial dimensions via a joint wave number–frequency power spectrum. *Journal of Engineering Mechanics*, 144(11):04018100.

Chen, J., Sun, W., Li, J., and Xu, J. (2013). Stochastic harmonic function representation of stochastic processes. *Journal of Applied Mechanics*, 80(1).

Chen, M., Hwang, C., and Shih, Y. (1996). The computation of wavelet-Galerkin approximation on a bounded interval. *International Journal for Numerical Methods in Engineering*, 39(17):2921–2944.

Chen, S. S., Donoho, D. L., and Saunders, M. A. (2001). Atomic decomposition by basis pursuit. *SIAM Review*, 43(1):129–159.

Cline, R. (1964). Representations for the generalized inverse of a partitioned matrix. *Journal of the Society for Industrial and Applied Mathematics*, 12(3):588–600.

Cohen, L. (1995). *Time-frequency analysis*, volume 778. Prentice hall New Jersey.

Comerford, L. A., Beer, M., and Kougioumtzoglou, I. A. (2014). Compressive sensing based power spectrum estimation from incomplete records by utilizing an adaptive basis. In *2014 IEEE Symposium on Computational Intelligence for Engineering Solutions (CIES)*, pages 117–124.

Comerford, L. A., Jensen, H. A., Mayorga, F., Beer, M., and Kougioumtzoglou, I. A. (2017). Compressive sensing with an adaptive wavelet basis for structural system response and reliability analysis under missing data. *Computers & Structures*, 182:26–40.

Comerford, L. A., Kougioumtzoglou, I. A., and Beer, M. (2016). Compressive sensing based stochastic process power spectrum estimation subject to missing data. *Probabilistic Engineering Mechanics*, 44:66–76.

Cortiella, A., Park, K., and Doostan, A. (2021). Sparse identification of nonlinear dynamical systems via reweighted l_1-regularized least squares. *Computer Methods in Applied Mechanics and Engineering*, 376:113620.

Craig, R. R. and Kurdila, A. J. (2006). *Fundamentals of structural dynamics*. John Wiley & Sons.

Crandall, S. H. (1958). *Notes for the MIT Special Summer Program on Random Vibration*, volume 1. Technology Press of the Massachusetts Institute of Technology.

Crandall, S. H. and Mark, W. D. (2014). *Random vibration in mechanical systems*. Academic Press.

Critchley, J. and Anderson, K. S. (2003). A generalized recursive coordinate reduction method for multibody system dynamics. *International Journal for Multiscale Computational Engineering*, 1(2&3).

Daqaq, M. F., Masana, R., Erturk, A., and Dane, Q. D. (2014). On the role of nonlinearities in vibratory energy harvesting: a critical review and discussion. *Applied Mechanics Reviews*, 66(4).

Daubechies, I. (1988). Orthonormal bases of compactly supported wavelets. *Communications on Pure and Applied Mathematics*, 41(7):909–996.

Daubechies, I. (1992). *Ten lectures on wavelets*. SIAM.

Davenport, A. G. (1961). The spectrum of horizontal gustiness near the ground in high winds. *Quarterly Journal of the Royal Meteorological Society*, 87(372):194–211.

de Falco, D., Pennestri, E., and Vita, L. (2005). The udwadia-kalaba formulation: A report on its numerical efficiency in multibody dynamics simulations and on its teaching effectiveness. *Multibody Dynamics*, 2005:21–24.

Deodatis, G. and Shinozuka, M. (1989). Simulation of seismic ground motion using stochastic waves. *Journal of Engineering Mechanics*, 115(12):2723–2737.

Dérian, P., Mauzey, C. F., and Mayor, S. D. (2015). Wavelet-based optical flow for two-component wind field estimation from single aerosol lidar data. *Journal of Atmospheric and Oceanic Technology*, 32(10):1759–1778.

Di Matteo, A., Kougioumtzoglou, I. A., Pirrotta, A., Spanos, P. D., and Di Paola, M. (2014).

Stochastic response determination of nonlinear oscillators with fractional derivatives elements via the Wiener path integral. *Probabilistic Engineering Mechanics*, 38:127–135.

Di Paola, M., Failla, G., Pirrotta, A., Sofi, A., and Zingales, M. (2013). The mechanically based non-local elasticity: an overview of main results and future challenges. *Philosophical Transactions of the Royal Society A: Mathematical, Physical and Engineering Sciences*, 371(1993):20120433.

Di Paola, M., Pirrotta, A., and Valenza, A. (2011). Visco-elastic behavior through fractional calculus: an easier method for best fitting experimental results. *Mechanics of materials*, 43(12):799–806.

Di Paola, M. and Zingales, M. (2000). Digital simulation of multivariate earthquake ground motions. *Earthquake Engineering & Structural Dynamics*, 29(7):1011–1027.

Donoho, D. L. (2006). Compressed sensing. *IEEE Transactions on Information Theory*, 52(4):1289–1306.

dos Santos, K. R. M., Brudastova, O., and Kougioumtzoglou, I. A. (2020). Spectral identification of nonlinear multi-degree-of-freedom structural systems with fractional derivative terms based on incomplete non-stationary data. *Structural Safety*, 86:101975.

dos Santos, K. R. M., Kougioumtzoglou, I. A., and Spanos, P. D. (2019). Hilbert transform–based stochastic averaging technique for determining the survival probability of nonlinear oscillators. *Journal of Engineering Mechanics*, 145(10):04019079.

Einstein, A. (1905). On the motion of small particles suspended in liquids at rest required by the molecular-kinetic theory of heat. *Annalen der physik*, 17(549-560):208.

Eldar, Y. C. and Kutyniok, G. (2012). *Compressed sensing: theory and applications*. Cambridge university press.

Elishakoff, I. (1999). *Probabilistic theory of structures*. Courier Corporation.

Elishakoff, I., Andriamasy, L., and Dolley, M. (2009). Application and extension of the stochastic linearization by anh and di paola. *Acta Mechanica*, 204(1):89–98.

Farhat, C., Bos, A., Avery, P., and Soize, C. (2018). Modeling and quantification of model-form uncertainties in eigenvalue computations using a stochastic reduced model. *AIAA Journal*, 56(3):1198–1210.

Featherstone, R. (1984). *Robot dynamics algorithms*. Springer Science+Business Media New York USA.

Fokker, A. D. (1913). *Over Brown'sche bewegingen in het stralingsveld: en waar-schijnlijkheids-beschouwingen in de stralingstheorie...* J. Enschedë en zonen.

Fragkoulis, V. C. (2017). *Random vibration of systems with singular matrices*. The University of Liverpool (United Kingdom).

Fragkoulis, V. C., Kougioumtzoglou, I. A., and Pantelous, A. A. (2016a). Linear random vibration of structural systems with singular matrices. *Journal of Engineering Mechanics*, 142(2):04015081.

Fragkoulis, V. C., Kougioumtzoglou, I. A., and Pantelous, A. A. (2016b). Statistical linearization of nonlinear structural systems with singular matrices. *Journal of Engineering Mechanics*, 142(9):04016063.

Fragkoulis, V. C., Kougioumtzoglou, I. A., Pantelous, A. A., and Beer, M. (2019). Non-stationary response statistics of nonlinear oscillators with fractional derivative elements under evolutionary stochastic excitation. *Nonlinear Dynamics*, 97(4):2291–2303.

Fragkoulis, V. C., Kougioumtzoglou, I. A., Pantelous, A. A., and Beer, M. (2022). Joint statistics of natural frequencies corresponding to structural systems with singular random parameter matrices. *Journal of Engineering Mechanics*, pages 10.1061/(ASCE)EM.1943–7889.0002081.

Fragkoulis, V. C., Kougioumtzoglou, I. A., Pantelous, A. A., and Pirrotta, A. (2015). Higher order

matrix differential equations with singular coefficient matrices. In *AIP Conference Proceedings*, volume 1648, page 340002. AIP Publishing LLC.

Frehlich, R., Hannon, S. M., and Henderson, S. W. (1998). Coherent doppler lidar measurements of wind field statistics. *Boundary-Layer Meteorology*, 86(2):233–256.

Friedland, S. and Lim, L.-H. (2018). Nuclear norm of higher-order tensors. *Mathematics of Computation*, 87(311):1255–1281.

Gallego, G., Yezzi, A., Fedele, F., and Benetazzo, A. (2011). A variational stereo method for the three-dimensional reconstruction of ocean waves. *IEEE Transactions on Geoscience and Remote Sensing*, 49(11):4445–4457.

Gemant, A. (1936). A method of analyzing experimental results obtained from elasto-viscous bodies. *Physics*, 7(8):311–317.

Gersch, W., Taoka, G. T., and Liu, R. (1976). Structural system parameter estimation by two-stage least squares method. *Journal of the Engineering Mechanics Division*, 102(5):883–899.

Ghanem, R. and Ghosh, D. (2007). Efficient characterization of the random eigenvalue problem in a polynomial chaos decomposition. *International Journal for Numerical Methods in Engineering*, 72(4):486–504.

Ghanem, R. and Romeo, F. (2000). A wavelet-based approach for the identification of linear time-varying dynamical systems. *Journal of Sound and Vibration*, 234(4):555–576.

Ghanem, R. G. and Spanos, P. D. (2003). *Stochastic finite elements: a spectral approach*. Courier Corporation.

Ginsberg, J. (2008). *Engineering dynamics*, volume 10. Cambridge University Press.

Goswami, J. C. and Chan, A. K. (2011). *Fundamentals of wavelets: theory, algorithms, and applications*. John Wiley & Sons.

Grigoriu, M. (2013). *Stochastic calculus: applications in science and engineering*. Springer Science & Business Media.

Grossmann, A. and Morlet, J. (1984). Decomposition of hardy functions into square integrable wavelets of constant shape. *SIAM Journal on Mathematical Analysis*, 15(4):723–736.

Grover, A. and Lall, B. (2021). A recursive method for estimating missing data in spatio-temporal applications. *IEEE Transactions on Industrial Informatics*, 18(4):2714–2723.

Hansen, P. C. (1998). *Rank-deficient and discrete ill-posed problems: numerical aspects of linear inversion*. SIAM.

Harris, M., Hand, M., and Wright, A. (2006). Lidar for turbine control. *National Renewable Energy Laboratory, Golden, CO, Report No. NREL/TP-500-39154*.

Harris, R. I. (1968). *On the spectrum and auto-correlation function of gustiness in high winds*. Electrical Research Association.

He, Z. C., Zhang, Z., and Li, E. (2019). Multi-source random excitation identification for stochastic structures based on matrix perturbation and modified regularization method. *Mechanical Systems and Signal Processing*, 119:266–292.

Hestenes, M. R. (1969). Multiplier and gradient methods. *Journal of Optimization Theory and Applications*, 4(5):303–320.

Housner, G. W. and Jennings, P. C. (1964). Generation of artificial earthquakes. *Journal of the Engineering Mechanics Division*, 90(1):113–150.

Ibrahim, R. A. (2008). *Parametric random vibration*. Courier Dover Publications.

Ismail, M., Ikhouane, F., and Rodellar, J. (2009). The hysteresis bouc-wen model, a survey. *Archives of Computational Methods in Engineering*, 16(2):161–188.

Karageorgos, A. D., Moysis, L., Fragkoulis, V. C., Kougioumtzoglou, I. A., and Pantelous, A. A.

(2021). Random vibration of linear systems with singular matrices based on Kronecker canonical forms of matrix pencils. *Mechanical Systems and Signal Processing*, 161:107896.

Kareem, A. (2008). Numerical simulation of wind effects: a probabilistic perspective. *Journal of Wind Engineering and Industrial Aerodynamics*, 96(10-11):1472–1497.

Kareem, A. and Kijewski, T. (2002). Time-frequency analysis of wind effects on structures. *Journal of Wind Engineering and Industrial Aerodynamics*, 90(12-15):1435–1452.

Kareem, A. and Wu, T. (2013). Wind-induced effects on bluff bodies in turbulent flows: Nonstationary, non-Gaussian and nonlinear features. *Journal of Wind Engineering and Industrial Aerodynamics*, 122:21–37.

Katsidoniotaki, M. I., Psaros, A. F., and Kougioumtzoglou, I. A. (2022). Uncertainty quantification of nonlinear system stochastic response estimates based on the wiener path integral technique: A bayesian compressive sampling treatment. *Probabilistic Engineering Mechanics*, 67:103193.

Khintchine, A. (1934). Korrelationstheorie der stationären stochastischen prozesse. *Mathematische Annalen*, 109(1):604–615.

Kijewski, T. and Kareem, A. (2002). On the presence of end effects and their melioration in wavelet-based analysis. *Journal of Sound and Vibration*, 256(5):980–988.

Kijewski, T. and Kareem, A. (2003). Wavelet transforms for system identification in civil engineering. *Computer-Aided Civil and Infrastructure Engineering*, 18(5):339–355.

Koh, C. G. and Kelly, J. M. (1990). Application of fractional derivatives to seismic analysis of base-isolated models. *Earthquake Engineering & Structural Dynamics*, 19(2):229–241.

Kolmogoroff, A. (1931). On analytical methods in the theory of probability. *Mathematische Annalen*, 104:415–458.

Kong, F., Han, R., Li, S., and He, W. (2022a). Non-stationary approximate response of non-

linear multi-degree-of-freedom systems subjected to combined periodic and stochastic excitation. *Mechanical Systems and Signal Processing*, 166:108420.

Kong, F., Kougioumtzoglou, I. A., Spanos, P. D., and Li, S. (2016). Nonlinear system response evolutionary power spectral density determination via a harmonic wavelets based Galerkin technique. *International Journal for Multiscale Computational Engineering*, 14(3).

Kong, F. and Li, J. (2015). Wavelet-expansion-based stochastic response of chain-like mdof structures. *Journal of Sound and Vibration*, 359:136–153.

Kong, F., Li, S., and Zhou, W. (2014a). Wavelet-Galerkin approach for power spectrum determination of nonlinear oscillators. *Mechanical Systems and Signal Processing*, 48(1-2):300–324.

Kong, F., Spanos, P. D., Li, J., and Kougioumtzoglou, I. A. (2014b). Response evolutionary power spectrum determination of chain-like mdof non-linear structural systems via harmonic wavelets. *International Journal of Non-Linear Mechanics*, 66:3–17.

Kong, F., Zhang, Y., and Zhang, Y. (2022b). Non-stationary response power spectrum determination of linear/non-linear systems endowed with fractional derivative elements via harmonic wavelet. *Mechanical Systems and Signal Processing*, 162:108024.

Kougioumtzoglou, I. A. (2013). Stochastic joint time–frequency response analysis of nonlinear structural systems. *Journal of Sound and Vibration*, 332(26):7153–7173.

Kougioumtzoglou, I. A., Di Matteo, A., Spanos, P. D., Pirrotta, A., and Di Paola, M. (2015). An efficient Wiener path integral technique formulation for stochastic response determination of nonlinear mdof systems. *Journal of Applied Mechanics*, 82(10).

Kougioumtzoglou, I. A., dos Santos, K. R. M., and Comerford, L. A. (2017a). Incomplete data based parameter identification of nonlinear and time-variant oscillators with fractional derivative elements. *Mechanical Systems and Signal Processing*, 94:279–296.

Kougioumtzoglou, I. A., Fragkoulis, V. C., Pantelous, A. A., and Pirrotta, A. (2017b). Random vibration of linear and nonlinear structural systems with singular matrices: A frequency domain approach. *Journal of Sound and Vibration*, 404:84–101.

Kougioumtzoglou, I. A., Ni, P., Mitseas, I. P., Fragkoulis, V. C., and Beer, M. (2022). An approximate stochastic dynamics approach for design spectrum based response analysis of nonlinear structural systems with fractional derivative elements. *International Journal of Non-Linear Mechanics*, 146:104178.

Kougioumtzoglou, I. A., Petromichelakis, I., and Psaros, A. F. (2020). Sparse representations and compressive sampling approaches in engineering mechanics: A review of theoretical concepts and diverse applications. *Probabilistic Engineering Mechanics*, 61:103082.

Kougioumtzoglou, I. A. and Spanos, P. D. (2013a). An identification approach for linear and nonlinear time-variant structural systems via harmonic wavelets. *Mechanical Systems and Signal Processing*, 37(1-2):338–352.

Kougioumtzoglou, I. A. and Spanos, P. D. (2013b). Response and first-passage statistics of nonlinear oscillators via a numerical path integral approach. *Journal of Engineering Mechanics*, 139(9):1207–1217.

Kougioumtzoglou, I. A. and Spanos, P. D. (2014). Nonstationary stochastic response determination of nonlinear systems: A Wiener path integral formalism. *Journal of Engineering Mechanics*, 140(9):04014064.

Kougioumtzoglou, I. A. and Spanos, P. D. (2016). Harmonic wavelets based response evolutionary power spectrum determination of linear and non-linear oscillators with fractional derivative elements. *International Journal of Non-Linear Mechanics*, 80:66–75.

Laface, V., Kougioumtzoglou, I. A., Malara, G., and Arena, F. (2017). Efficient processing of water

wave records via compressive sensing and joint time-frequency analysis via harmonic wavelets. *Applied Ocean Research*, 69:1–9.

Lagos-Varas, M., Movilla-Quesada, D., Arenas, J., Raposeiras, A., Castro-Fresno, D., Calzada-Pérez, M., Vega-Zamanillo, A., and Maturana, J. (2019). Study of the mechanical behavior of asphalt mixtures using fractional rheology to model their viscoelasticity. *Construction and Building Materials*, 200:124–134.

Lai, Z., Mylonas, C., Nagarajaiah, S., and Chatzi, E. (2021). Structural identification with physics-informed neural ordinary differential equations. *Journal of Sound and Vibration*, 508:116196.

Lai, Z. and Nagarajaiah, S. (2019). Sparse structural system identification method for nonlinear dynamic systems with hysteresis/inelastic behavior. *Mechanical Systems and Signal Processing*, 117:813–842.

Li, J. and Chen, J. (2009). *Stochastic dynamics of structures*. John Wiley & Sons.

Liang, J., Chaudhuri, S. R., and Shinozuka, M. (2007). Simulation of nonstationary stochastic processes by spectral representation. *Journal of Engineering Mechanics*, 133(6):616–627.

Lin, H. and Yim, S. (1996). Nonlinear rocking motions. ii: Overturning under random excitations. *Journal of Engineering Mechanics*, 122(8):728–735.

Lin, Q. and Li, C. (2020). Kriging based sequence interpolation and probability distribution correction for Gaussian wind field data reconstruction. *Journal of Wind Engineering and Industrial Aerodynamics*, 205:104340.

Lin, Y.-K. (1967). *Probabilistic theory of structural dynamics*. McGraw-Hill.

Lin, Y.-K. and Yong, Y. (1987). Evolutionary Kanai-Tajimi type earthquake models. In *Stochastic Approaches in Earthquake Engineering*, pages 174–203. Springer.

Lin, Z., Chen, M., and Ma, Y. (2010). The augmented lagrange multiplier method for exact recovery of corrupted low-rank matrices. *arXiv preprint arXiv:1009.5055*.

Liu, W. K., Belytschko, T., and Mani, A. (1986). Probabilistic finite elements for nonlinear structural dynamics. *Computer Methods in Applied Mechanics and Engineering*, 56(1):61–81.

Maciejewski, A. A. (1990). Dealing with the ill-conditioned equations of motion for articulated figures. *IEEE Computer Graphics and Applications*, 10(3):63–71.

MacKay, D. J. (1992). Bayesian interpolation. *Neural computation*, 4(3):415–447.

Malara, G., Kougioumtzoglou, I. A., and Arena, F. (2018). Extrapolation of random wave field data via compressive sampling. *Ocean Engineering*, 157:87 – 95.

Mallat, S. (1999). *A wavelet tour of signal processing*. Elsevier.

Mallat, S. G. (1988). *Multiresolution representations and wavelets*. University of Pennsylvania.

Mariti, L., Belfiore, N., Pennestri, E., and Valentini, P. P. (2011). Comparison of solution strategies for multibody dynamics equations. *International Journal for Numerical Methods in Engineering*, 88(7):637–656.

Meyer, C. D. (2000). *Matrix analysis and applied linear algebra*, volume 71. Siam.

Mignolet, M. P., Przekop, A., Rizzi, S. A., and Spottswood, S. M. (2013). A review of indirect/non-intrusive reduced order modeling of nonlinear geometric structures. *Journal of Sound and Vibration*, 332(10):2437–2460.

Mitseas, I. P., Kougioumtzoglou, I. A., and Beer, M. (2016). An approximate stochastic dynamics approach for nonlinear structural system performance-based multi-objective optimum design. *Structural Safety*, 60:67–76.

Moens, D. and Vandepitte, D. (2006). Recent dvances in non-probabilistic approaches for non-

deterministic dynamic finite element analysis. *Archives of Computational Methods in Engineering*, 13(3):389–464.

Mohandes, M. A. and Rehman, S. (2018). Wind speed extrapolation using machine learning methods and lidar measurements. *IEEE Access*, 6:77634–77642.

Morison, J. R., Johnson, J. W., and Schaaf, S. A. (1950). The force exerted by surface waves on piles. *Journal of Petroleum Technology*, 2(05):149–154.

Morlet, J., Arens, G., Fourgeau, E., and Glard, D. (1982). Wave propagation and sampling theory—part i: Complex signal and scattering in multilayered media. *Geophysics*, 47(2):203–221.

Naess, A. and Johnsen, J. M. (1993). Response statistics of nonlinear, compliant offshore structures by the path integral solution method. *Probabilistic Engineering Mechanics*, 8(2):91–106.

Nason, G. P., Von Sachs, R., and Kroisandt, G. (2000). Wavelet processes and adaptive estimation of the evolutionary wavelet spectrum. *Journal of the Royal Statistical Society: Series B (Statistical Methodology)*, 62(2):271–292.

Nayfeh, A. H. and Mook, D. T. (2008). *Nonlinear oscillations*. John Wiley & Sons.

Newland, D. E. (1993). Harmonic wavelet analysis. *Proceedings of the Royal Society of London. Series A: Mathematical and Physical Sciences*, 443(1917):203–225.

Newland, D. E. (1994). Harmonic and musical wavelets. *Proceedings of the Royal Society of London. Series A: Mathematical and Physical Sciences*, 444(1922):605–620.

Newland, D. E. (1999). Ridge and phase identification in the frequency analysis of transient signals by harmonic wavelets.

Ni, P., Fragkoulis, V. C., Kong, F., Mitseas, I. P., and Beer, M. (2021). Response determination of nonlinear systems with singular matrices subject to combined stochastic and deterministic ex-

citations. *ASCE-ASME Journal of Risk and Uncertainty in Engineering Systems, Part A: Civil Engineering*, 7(4):04021049.

Ni, Y. and Li, M. (2016). Wind pressure data reconstruction using neural network techniques: A comparison between bpnn and grnn. *Measurement*, 88:468–476.

Ornstein, L. (1927). Zur theorie der brown schen bewegung für systeme, worin mehrere temperaturen vorkommen. *Zeitschrift für Physik*, 41(4):848–856.

Pantelous, A. A. and Pirrotta, A. (2017). Modal analysis of multi-degrees-of-freedom systems with singular matrices: Analytical dynamics approach. *Journal of Engineering Mechanics*, 143(6):06017005.

Pappalardo, C. M. and Guida, D. (2018a). A comparative study of the principal methods for the analytical formulation and the numerical solution of the equations of motion of rigid multibody systems. *Archive of Applied Mechanics*, 88(12):2153–2177.

Pappalardo, C. M. and Guida, D. (2018b). On the lagrange multipliers of the intrinsic constraint equations of rigid multibody mechanical systems. *Archive of Applied Mechanics*, 88(3):419–451.

Pasparakis, G. D., dos Santos, K. R., Kougioumtzoglou, I. A., and Beer, M. (2022a). Wind data extrapolation and stochastic field statistics estimation via compressive sampling and low rank matrix recovery methods. *Mechanical Systems and Signal Processing*, 162:107975.

Pasparakis, G. D., Fragkoulis, V. C., and Beer, M. (2021). Harmonic wavelets based response evolutionary power spectrum determination of linear and nonlinear structural systems with singular matrices. *Mechanical Systems and Signal Processing*, 149:107203.

Pasparakis, G. D., Kougioumtzoglou, I. A., Fragkoulis, V. C., Kong, F., and Beer, M. (2022b). Excitation–response relationships for linear structural systems with singular parameter matrices: A periodized harmonic wavelet perspective. *Mechanical Systems and Signal Processing*, 169:108701.

Peeters, B. and De Roeck, G. (1999). Reference-based stochastic subspace identification for output-only modal analysis. *Mechanical Systems and Signal Processing*, 13(6):855–878.

Petromichelakis, I. and Kougioumtzoglou, I. A. (2020). Addressing the curse of dimensionality in stochastic dynamics: a Wiener path integral variational formulation with free boundaries. *Proceedings of the Royal Society A*, 476(2243):20200385.

Petromichelakis, I., Psaros, A. F., and Kougioumtzoglou, I. A. (2018). Stochastic response determination and optimization of a class of nonlinear electromechanical energy harvesters: A Wiener path integral approach. *Probabilistic Engineering Mechanics*, 53:116–125.

Petromichelakis, I., Psaros, A. F., and Kougioumtzoglou, I. A. (2020). Stochastic response determination of nonlinear structural systems with singular diffusion matrices: A Wiener path integral variational formulation with constraints. *Probabilistic Engineering Mechanics*, 60:103044 1–15.

Petromichelakis, I., Psaros, A. F., and Kougioumtzoglou, I. A. (2021). Stochastic response analysis and reliability-based design optimization of nonlinear electromechanical energy harvesters with fractional derivative elements. *ASCE-ASME Journal of Risk and Uncertainty in Engineering Systems, Part B: Mechanical Engineering*, 7(1):010901.

Pi, Y. L. and Mickleborough, N. C. (1989). Modal identification of vibrating structures using arma model. *Journal of Engineering Mechanics*, 115(10):2232–2250.

Pirrotta, A., Kougioumtzoglou, I. A., Di Matteo, A., Fragkoulis, V. C., Pantelous, A. A., and Adam, C. (2021). Deterministic and random vibration of linear systems with singular parameter matrices and fractional derivative terms. *Journal of Engineering Mechanics*, 147(6):04021031.

Pirrotta, A., Kougioumtzoglou, I. A., and Pantelous, A. A. (2019). Stochastic response determination of structural systems modeled via dependent coordinates: a frequency domain treatment based on generalized modal analysis. *Meccanica*, 54(9):1421–1431.

Podlubny, I. (1999). Fractional differential equations, mathematics in science and engineering.

Pourhabib, A., Huang, J. Z., and Ding, Y. (2016). Short-term wind speed forecast using measurements from multiple turbines in a wind farm. *Technometrics*, 58(1):138–147.

Powell, M. J. D. (1978). A fast algorithm for nonlinearly constrained optimization calculations. In *Numerical analysis*, pages 144–157. Springer.

Priestley, M. B. (1965). Evolutionary spectra and non-stationary processes. *Journal of the Royal Statistical Society: Series B (Methodological)*, 27(2):204–229.

Psaros, A. F., Brudastova, O., Malara, G., and Kougioumtzoglou, I. A. (2018). Wiener path integral based response determination of nonlinear systems subject to non-white, non-Gaussian, and non-stationary stochastic excitation. *Journal of Sound and Vibration*, 433:314–333.

Psaros, A. F., Petromichelakis, I., and Kougioumtzoglou, I. A. (2019a). Wiener path integrals and multi-dimensional global bases for non-stationary stochastic response determination of structural systems. *Mechanical Systems and Signal Processing*, 128:551–571.

Psaros, A. F., Petromichelakis, I., and Kougioumtzoglou, I. A. (2019b). Wiener path integrals and multi-dimensional global bases for non-stationary stochastic response determination of structural systems. *Mechanical Systems and Signal Processing*, 128:551 – 571.

Qin, L., Liu, S., Long, T., Shahzad, M. A., Schlaberg, H. I., and Yan, S. A. (2018). Wind field reconstruction using dimension-reduction of cfd data with experimental validation. *Energy*, 151:272–288.

Qu, F., Liu, J., Ma, Y., Zang, D., and Fu, M. (2020). A novel wind turbine data imputation method with multiple optimizations based on gans. *Mechanical Systems and Signal Processing*, 139:106610.

Raissi, M., Perdikaris, P., and Karniadakis, G. E. (2019). Physics-informed neural networks: A deep learning framework for solving forward and inverse problems involving nonlinear partial differential equations. *Journal of Computational Physics*, 378:686–707.

Ranieri, J., Chebira, A., and Vetterli, M. (2014). Near-optimal sensor placement for linear inverse problems. *IEEE Transactions on Signal Processing*, 62(5):1135–1146.

Rice, S. O. (1944). Mathematical analysis of random noise. *The Bell System Technical Journal*, 23(3):282–332.

Roberts, J. and Spanos, P. D. (2003). *Random vibration and statistical linearization*. Courier Corporation.

Roberts, J. B. and Spanos, P. D. (1986). Stochastic averaging: an approximate method of solving random vibration problems. *International Journal of Non-Linear Mechanics*, 21(2):111–134.

Rockafellar, R. T. (1973). The multiplier method of hestenes and powell applied to convex programming. *Journal of Optimization Theory and Applications*, 12(6):555–562.

Rubinstein, R. Y. (1981). Simulation and monte carlo method. new york: John & wiley & sons.

Rüdinger, F. (2006). Tuned mass damper with fractional derivative damping. *Engineering Structures*, 28(13):1774–1779.

Safaei, M., Sodano, H. A., and Anton, S. R. (2019). A review of energy harvesting using piezoelectric materials: state-of-the-art a decade later (2008–2018). *Smart Materials and Structures*, 28(11):113001.

Santos, R. A. (2007). *Damage mitigating control for wind turbines*. PhD thesis, University of Colorado at Boulder.

Schaeffer, H., Caflisch, R., Hauck, C. D., and Osher, S. (2013). Sparse dynamics for partial differential equations. *Proceedings of the National Academy of Sciences*, 110(17):6634–6639.

Schmidt, M. and Lipson, H. (2009). Distilling free-form natural laws from experimental data. *Science*, 324(5923):81–85.

Schutte, A. and Udwadia, F. (2011). New approach to the modeling of complex multibody dynamical systems. *Journal of Applied Mechanics*, 78(2):021018.

Scialò, A., Malara, G., Kougioumtzoglou, I. A., and Arena, F. (2022). Stochastic response determination of u-owc energy harvesters: a statistical linearization solution treatment accounting for intermittent wave excitation. *Nonlinear Dynamics*, 109(4):2281–2295.

Shen, K. L. and Soong, T. T. (1995). Modeling of viscoelastic dampers for structural applications. *Journal of Engineering Mechanics*, 121(6):694–701.

Shinozuka, M. and Astill, C. J. (1972). Random eigenvalue problems in structural analysis. *AIAA journal*, 10(4):456–462.

Shinozuka, M. and Deodatis, G. (1996). Simulation of multi-dimensional Gaussian stochastic fields by spectral representation. *Applied Mechanics Reviews*, 49(1):29–53.

Shinozuka, M. and Jan, C. (1972). Digital simulation of random processes and its applications. *Journal of Sound and Vibration*, 25(1):111–128.

Simiu, E. and Scanlan, R. H. (1996). Wind effects on structures: fundamentals and applications to design.

Socha, L. (2007). *Linearization methods for stochastic dynamic systems*, volume 730. Springer Science & Business Media.

Spanos, P. D. and Evangelatos, G. I. (2010). Response of a non-linear system with restoring forces governed by fractional derivatives—time domain simulation and statistical linearization solution. *Soil Dynamics and Earthquake Engineering*, 30(9):811–821.

Spanos, P. D. and Failla, G. (2004). Evolutionary spectra estimation using wavelets. *Journal of Engineering Mechanics*, 130(8):952–960.

Spanos, P. D. and Failla, G. (2005). Wavelets: Theoretical concepts and vibrations related applications. *The Shock and Vibration Digest*, 37(5):359–376.

Spanos, P. D., Failla, G., Santini, A., and Pappatico, M. (2006). Damage detection in euler–bernoulli beams via spatial wavelet analysis. *Structural Control and Cealth Monitoring: The Official Journal of the International Association for Structural Control and Monitoring and of the European Association for the Control of Structures*, 13(1):472–487.

Spanos, P. D., Giaralis, A., Politis, N. P., and Roesset, J. M. (2007). Numerical treatment of seismic accelerograms and of inelastic seismic structural responses using harmonic wavelets. *Computer-Aided Civil and Infrastructure Engineering*, 22(4):254–264.

Spanos, P. D., Kong, F., Li, J., and Kougioumtzoglou, I. A. (2016). Harmonic wavelets based excitation–response relationships for linear systems: A critical perspective. *Probabilistic Engineering Mechanics*, 44:163–173.

Spanos, P. D. and Kougioumtzoglou, I. A. (2012). Harmonic wavelets based statistical linearization for response evolutionary power spectrum determination. *Probabilistic Engineering Mechanics*, 27(1):57–68.

Spanos, P. D. and Malara, G. (2014). Nonlinear random vibrations of beams with fractional derivative elements. *Journal of Engineering Mechanics*, 140(9):04014069.

Spanos, P. D. and Solomos, G. P. (1983). Markov approximation to transient vibration. *Journal of Engineering Mechanics*, 109(4):1134–1150.

Spanos, P. D., Strati, F. M., Malara, G., and Arena, F. (2018). An approach for non-linear stochastic analysis of u-shaped owc wave energy converters. *Probabilistic Engineering Mechanics*, 54:44–52. ISM 2016.

Spanos, P. D., Tezcan, J., and Tratskas, P. (2005). Stochastic processes evolutionary spectrum

estimation via harmonic wavelets. *Computer Methods in Applied Mechanics and Engineering*, 194(12-16):1367–1383.

Staszewski, W. (1997). Identification of damping in mdof systems using time-scale decomposition. *Journal of Sound and Vibration*, 203(2):283–305.

Stefanou, G. (2009). The stochastic finite element method: Past, present and future. *Computer Methods in Applied Mechanics and Engineering*, 198(9):1031–1051.

Sun, S., Liu, S., Chen, M., and Guo, H. (2019a). An optimized sensing arrangement in wind field reconstruction using cfd and pod. *IEEE Transactions on Sustainable Energy*, 11(4):2449–2456.

Sun, S., Liu, S., Liu, J., and Schlaberg, H. I. (2019b). Wind field reconstruction using inverse process with optimal sensor placement. *IEEE Transactions on Sustainable Energy*, 10(3):1290–1299.

Tarasov, V. E. (2017). Fractional mechanics of elastic solids: Continuum aspects. *Journal of Engineering Mechanics*, 143(5):D4016001.

Tascikaraoglu, A., Sanandaji, B. M., Poolla, K., and Varaiya, P. (2016). Exploiting sparsity of interconnections in spatio-temporal wind speed forecasting using wavelet transform. *Applied Energy*, 165:735–747.

Tikhonov, A. N. and Arsenin, V. I. (1977). *Solutions of Ill-posed Problems: Andrey N. Tikhonov and Vasiliy Y. Arsenin. Translation Editor Fritz John*. Wiley.

Towers, P. and Jones, B. L. (2016). Real-time wind field reconstruction from lidar measurements using a dynamic wind model and state estimation. *Wind Energy*, 19(1):133–150.

Tratskas, P. and Spanos, P. D. (2003). Linear multi-degree-of-freedom system stochastic response by using the harmonic wavelet transform. *J. Appl. Mech.*, 70(5):724–731.

Tubaldi, E. and Kougioumtzoglou, I. A. (2015). Nonstationary stochastic response of structural

systems equipped with nonlinear viscous dampers under seismic excitation. *Earthquake Engineering & Structural Dynamics*, 44(1):121–138.

Udwadia, F. and Kalaba, R. (2001). Explicit equations of motion for mechanical systems with nonideal constraints. *Journal of Applied Mechanics*, 68(3):462–467.

Udwadia, F. and Phohomsiri, P. (2006). Explicit equations of motion for constrained mechanical systems with singular mass matrices and applications to multi-body dynamics. *Proceedings of the Royal Society A: Mathematical, Physical and Engineering Sciences*, 462(2071):2097–2117.

Udwadia, F. and Wanichanon, T. (2013). On general nonlinear constrained mechanical systems. *Numer. Algebra Control Optim*, 3(3):425–443.

Udwadia, F. E. and Kalaba, R. E. (1992). A new perspective on constrained motion. *Proceedings: Mathematical and Physical Sciences*, pages 407–410.

Udwadia, F. E. and Kalaba, R. E. (2007). *Analytical dynamics: a new approach*. Cambridge University Press.

Van Den Berg, E. and Friedlander, M. P. (2009). Probing the pareto frontier for basis pursuit solutions. *SIAM Journal on Scientific Computing*, 31(2):890–912.

Wang, D., Yu, F., Kong, F., and Xu, J. (2022). Simulation of fully nonstationary random processes using generalized harmonic wavelets. *Mechanical Systems and Signal Processing*, 181:109468.

Wang, Y., Zhao, T., and Phoon, K. K. (2019). Statistical inference of random field auto-correlation structure from multiple sets of incomplete and sparse measurements using bayesian compressive sampling-based bootstrapping. *Mechanical Systems and Signal Processing*, 124:217–236.

Wiener, N. (1930). Generalized harmonic analysis. *Acta mathematica*, 55(1):117–258.

Xiao, X., Zhang, Y., Shen, W., and Kong, F. (2021). A stochastic analysis method of transient

responses using harmonic wavelets, part 1: Time-invariant structural systems. *Mechanical Systems and Signal Processing*, 160:107870.

Yang, X., Venturi, D., Chen, C., Chryssostomidis, C., and Karniadakis, G. E. (2010). EOF-based constrained sensor placement and field reconstruction from noisy ocean measurements: Application to nantucket sound. *Journal of Geophysical Research: Oceans*, 115(C12).

Yang, Y. and Nagarajaiah, S. (2013). Time-frequency blind source separation using independent component analysis for output-only modal identification of highly damped structures. *Journal of Structural Engineering*, 10(1061):1780–1793.

Yang, Y. and Nagarajaiah, S. (2016). Harnessing data structure for recovery of randomly missing structural vibration responses time history: Sparse representation versus low-rank structure. *Mechanical Systems and Signal Processing*, 74:165–182.

Yang, Y., Nagarajaiah, S., and Ni, Y.-Q. (2015). Data compression of very large-scale structural seismic and typhoon responses by low-rank representation with matrix reshape. *Structural Control and Health Monitoring*, 22(8):1119–1131.

Zerva, A. (1992). Seismic ground motion simulations from a class of spatial variability models. *Earthquake Engineering & Structural Dynamics*, 21(4):351–361.

Zhang, Y., Comerford, L. A., Kougioumtzoglou, I. A., and Beer, M. (2018). Lp-norm minimization for stochastic process power spectrum estimation subject to incomplete data. *Mechanical Systems and Signal Processing*, 101:361 – 376.